

INFORMATION TO USERS

This manuscript has been reproduced from the microfilm master. UMI films the text directly from the original or copy submitted. Thus, some thesis and dissertation copies are in typewriter face, while others may be from any type of computer printer.

The quality of this reproduction is dependent upon the quality of the copy submitted. Broken or indistinct print, colored or poor quality illustrations and photographs, print bleedthrough, substandard margins, and improper alignment can adversely affect reproduction.

In the unlikely event that the author did not send UMI a complete manuscript and there are missing pages, these will be noted. Also, if unauthorized copyright material had to be removed, a note will indicate the deletion.

Oversize materials (e.g., maps, drawings, charts) are reproduced by sectioning the original, beginning at the upper left-hand corner and continuing from left to right in equal sections with small overlaps.

Photographs included in the original manuscript have been reproduced xerographically in this copy. Higher quality 6" x 9" black and white photographic prints are available for any photographs or illustrations appearing in this copy for an additional charge. Contact UMI directly to order.

ProQuest Information and Learning
300 North Zeeb Road, Ann Arbor, MI 48106-1346 USA
800-521-0600

UMI[®]

UNIVERSITY OF OKLAHOMA

GRADUATE COLLEGE

ESTIMATION OF DOPPLER AND POLARIMETRIC VARIABLES
FOR WEATHER RADARS

A Dissertation

SUBMITTED TO THE GRADUATE FACULTY

in partial fulfillment of the requirements for the

degree of

Doctor of Philosophy

By

SEBASTIAN MARIANO TORRES

Norman, Oklahoma

2001

UMI Number: 3023443



UMI Microform 3023443

Copyright 2001 by Bell & Howell Information and Learning Company.

All rights reserved. This microform edition is protected against
unauthorized copying under Title 17, United States Code.


Bell & Howell Information and Learning Company
300 North Zeeb Road
P.O. Box 1346
Ann Arbor, MI 48106-1346

© Copyright by SEBASTIAN MARIANO TORRES 2001
All Rights Reserved.

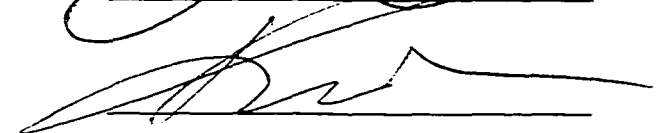
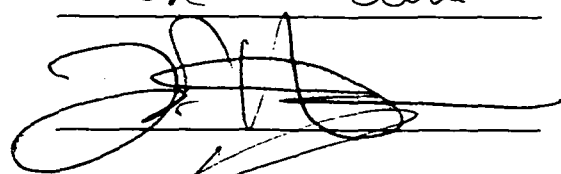
ESTIMATION OF DOPPLER AND POLARIMETRIC VARIABLES
FOR WEATHER RADARS

A Dissertation APPROVED FOR THE
SCHOOL OF ELECTRICAL AND COMPUTER ENGINEERING

BY



Edward Cline



*To my parents,
who taught me integrity, ethics, and raised me up to be the man that I am today.*

ACKNOWLEDGEMENTS

I would like to express my profound gratitude to my mentor Dr. Dusan Zrníc. He brought me into one of the best weather radar research and development groups in the world at the National Severe Storms Laboratory (NSSL). He encouraged me to pursue my Ph.D. studies, and he led me through this journey with wisdom and humbleness. I admire him and I have learned tremendously from him.

I am especially thankful to my adviser, Dr. J. R. Cruz, for believing in me, for challenging me with new ideas, and for patiently encouraging me. Also, I would like to thank the other members of my committee: Dr. Joseph Havlicek, Dr. John Cheung, and Dr. Ed Cline for their valuable help and excellent instruction during my years as a student at OU.

I am deeply grateful to my good friend and colleague Chris Curtis at NSSL with whom I had many lengthy discussions on my research work. His insight was at times an invaluable aid in the quest towards my Ph.D.

I wish to thank Allen Zahrai at NSSL for his continuous support and flexible work schedule that allowed me to attend classes. I would also like to acknowledge the Cooperative Institute for Mesoscale Meteorological Studies (CIMMS) and NSSL for their financial assistance through tuition reimbursement programs; I feel fortunate to be part of such fantastic organizations.

Finally, I am grateful for the unconditional love and support from my wife Lorena and for the encouragement from my friends. Thank you for making me feel that no goal is out of reach.

TABLE OF CONTENTS

1. Introduction	1
1.1. Polarimetric Doppler Weather Radars	1
1.2. Weather Radar Signals	6
1.3. Weather Signal Processing	13
1.4. Problem Statement	20
2. Whitening Transformation of Oversampled Range Data	22
2.1. Motivation	22
2.2. Previous Work	25
2.3. Significance	27
2.4. Implementation	28
2.5. Performance Analysis	32
3. Spectral Moment Estimation	38
3.1. Estimation of Signal Power	38
3.1.1. Noiseless Case	38
3.1.1.1 Correlated Samples	38
3.1.1.2 Whitened Samples	41
3.1.1.3 Comparison	42
3.1.2. Noisy Case	44
3.1.2.1 Correlated Samples	44
3.1.2.2 Whitened Samples	47
3.1.2.3 Comparison	52
3.2. Estimation of Mean Doppler Velocity	54
3.2.1. Correlated Samples	54
3.2.2. Whitened Samples	57
3.2.3. Comparison	59
3.3. Estimation of Doppler Spectrum Width	61
3.3.1. Correlated Samples	61
3.3.2. Whitened Samples	64
3.3.3. Comparison	65
3.4. Estimation of Doppler Spectrum	68

3.5. Results	70
4. Polarimetric Variable Estimation	72
4.1. Estimation of Differential Reflectivity.....	72
4.1.1. Correlated Samples.....	73
4.1.2. Whitened Samples.....	76
4.1.3. Comparison	78
4.2. Estimation of Differential Phase	79
4.2.1. Correlated Samples.....	80
4.2.2. Whitened Samples.....	82
4.2.3. Comparison	84
4.3. Estimation of the Magnitude of the Cross-Correlation Coefficient	85
4.3.1. Correlated Samples.....	86
4.3.2. Whitened Samples.....	89
4.3.3. Comparison	92
4.4. Results	93
5. The Whitening Transformation in Perspective	95
5.1. Alternatives to the Whitening Transformation.....	95
5.1.1. Regular Pulse with Averaging in Range	98
5.1.2. Short Pulse with Averaging in Range	100
5.1.3. Pulse Compression	102
5.1.4. Regular Pulse with Whitening in Range	105
5.1.5. Comparison	107
5.2. Modifications of the Whitening Transformation	109
5.2.1. Minimum Mean-Square Error Equalization.....	110
5.2.2. Pseudo Whitening Transformation.....	112
5.2.3. Whitening of Correlation Estimates	115
5.2.4. Whitening of Spectral Coefficient Estimates	116
6. Practical Effects and Implementation Issues	119
6.1. Effects of Transmitted Pulse Shape	119
6.2. Effects of Receiver Filter Characteristics.....	123
6.3. Effects of Reflectivity Gradients within the Resolution Volume.....	125
6.4. Implementation Issues.....	128

7. Conclusions and Future Work.....	134
Appendix A. Simulation of Oversampled Weather Radar Signals	145
A.1. Autocorrelation of Samples along Range Time	145
A.2. Autocorrelation of Samples along Sample Time	149
A.3. Cross-correlation of Horizontally- and Vertically-Polarized Echoes	151
A.4. Additive Noise.....	153
A.5. Reflectivity Gradients.....	153
A.6. Simulation Procedure	154
A.7. Simulation Results	156

LIST OF TABLES

Table 1.1. Summary of specifications for the National Weather Service WSR-88D weather surveillance radar (also known as NEXRAD).....	5
Table 5.1. Comparison of methods that use range samples to reduce the variance of estimates.....	108

LIST OF FIGURES

- Figure 1.1. The resolution volume in a pulsed radar is approximately shaped as a frustum of a cone. The location of its center in space is given by (r_0, θ_0, ϕ_0) and its extent by (r_1, θ_1, ϕ_1) (related to the pulse duration and the antenna beamwidth)..... 2
- Figure 1.2. Simplified block diagram of a polarimetric Doppler weather radar. A Klystron pulse modulated by a radio-frequency (RF) signal is transmitted by the antenna with vertical and horizontal polarization at periodic time intervals. During the “listening periods”, weather echoes are received (a tilde indicates signals at RF). Coherent down-conversion (synchronous detection) controlled by a stable local oscillator (“stalo”) produces base-band complex envelopes $V_H = I_H + jQ_H$ and $V_V = I_V + jQ_V$ for the horizontal and vertical channels, respectively. After digitalization, I and Q signals are used for the estimation of spectral moments and polarimetric variables. . 4
- Figure 1.3. Depiction of sample time and range time in a polarimetric Doppler radar. Pulses of width τ are transmitted every T_s seconds. During reception between pulses, echoes are sampled at times τ_s (range time). Samples at a fixed range location are spaced by T_s and give origin to the sample time. 6
- Figure 1.4. Contributions to weather signals from hydrometeors in a resolution volume. Signal samples are denoted by $V(l\tau)$, and their corresponding range, r_l , is given by $cl\tau/2$, where l is a positive integer. In this example, as in the WSR-88D radar, range gate sampling times are given as $l\tau$, where τ is the transmitted pulse width..... 7
- Figure 1.5. Weather echo amplitude for a point scatterer at range r_1 after the receiver filter and the synchronous detector. The contribution of each hydrometeor is determined by the weighting function $W(\tau_s)$. τ_r is the radar delay, and τ_{s1} is the sampling time (from Doviak and Zrnic 1993). 7
- Figure 1.6. Decomposition of the resolution volume into L independent shells, each contributing a differential voltage dV weighted by the transmitted pulse shape. Weights of elemental shell contributions to $V(\tau_{s1})$ and $V(\tau_{s1}+m\tau_o)$ are shown in solid and dashed lines, respectively. 9
- Figure 2.1. Effects of whitening on the noise power level. The noise enhancing effect of the whitening transformation is plotted for oversampling factors from 2 to 10. The result of (2.26) is included to show the agreement between theory and simulations. 36
- Figure 2.2. Noise power of correlated (top) and whitened (bottom) observations along range time. Dashed lines are at the mean power levels for each case. The predicted enhancement factor of 9.0909 ($L = 10$) is verified through simulations. 37
- Figure 3.1. Fractional standard deviation for correlated and whitened data as a function of the oversampling factor L for the ideal case. The number of samples M is 32, the normalized spectrum width σ_{vn} is 0.08, and the SNR is very large. Both theoretical results (dashed line) and simulation results (solid line) are plotted. 43

Figure 3.2. Normalized standard error for the power estimates on correlated data versus the normalized spectrum width σ_{vn} with the SNR as a parameter for the ideal case. The oversampling factor L is 8. Both theoretical results (dashed line) and simulation results (solid line) are plotted.	47
Figure 3.3. Normalized standard error for the power estimates on whitened data versus the normalized spectrum width σ_{vn} with the signal-to-noise ratio (SNR) as a parameter for the ideal case. The oversampling factor L is 8. Both theoretical results (dashed line) and simulation results (solid line) are plotted.	50
Figure 3.4. (Top) Standard deviation for the power estimator on both correlated and whitened data as a function of the signal-to-noise ratio (SNR) for the ideal case. The oversampling factor L is 8, the normalized spectrum width σ_{vn} is 0.08. (Bottom) Variance reduction factor for the same parameters. Theoretical results (dashed line) and simulation results (solid line) are plotted in both cases.	51
Figure 3.5. Crossover signal-to-noise ratio SNR_c versus the normalized spectrum width for the power estimator in an ideal system. The oversampling factor L is 8.	53
Figure 3.6. Normalized standard deviation of Doppler velocity estimates on correlated data versus the normalized spectrum width with the SNR as a parameter for the ideal case. The oversampling factor L is 8. Both theoretical results (dashed line) and simulation results (solid line) are plotted.	57
Figure 3.7. Normalized standard deviation of Doppler velocity estimates on whitened data versus the normalized spectrum width with the SNR as a parameter for the ideal case. The oversampling factor L is 8. Both theoretical results (dashed line) and simulation results (solid line) are plotted.	59
Figure 3.8. Crossover signal-to-noise ratio SNR_c versus the normalized spectrum width for the mean Doppler velocity estimator and an ideal system. The oversampling factor L is 8.	60
Figure 3.9. Normalized standard deviation of Doppler spectrum width estimates on correlated data versus the normalized spectrum width with the SNR as a parameter for the ideal case. The oversampling factor L is 8. Both theoretical results (dashed line) and simulation results (solid line) are plotted.	64
Figure 3.10. Normalized standard deviation Doppler spectrum width estimates on whitened data versus the normalized spectrum width with the SNR as a parameter for the ideal case. The oversampling factor L is 8. Both theoretical results (dashed line) and simulation results (solid line) are plotted.	66
Figure 3.11. Crossover signal-to-noise ratio SNR_c versus the normalized spectrum width for the Doppler spectrum width estimator and an ideal system. The oversampling factor L is 8.	67

- Figure 4.1. Normalized standard deviation of differential reflectivity estimates on correlated data versus the normalized spectrum width with the correlation coefficient $|\rho_{HV}(0)|$ as a parameter for the ideal case. The oversampling factor L is 8 and the SNR is very large. Both theoretical results (dashed line) and simulation results (solid line) are plotted..... 75
- Figure 4.2. Normalized standard deviation of differential reflectivity estimates on whitened data versus the normalized spectrum width with the correlation coefficient $|\rho_{HV}(0)|$ as a parameter for the ideal case. The oversampling factor L is 8 and the SNR is very large. Both theoretical results (dashed line) and simulation results (solid line) are plotted..... 77
- Figure 4.3. Crossover signal-to-noise ratio SNR_c versus the normalized spectrum width for the differential reflectivity estimator and an ideal system using the actual differential reflectivity (Z_{DR}) as a parameter. The oversampling factor L is 8 and the magnitude of the cross-correlation coefficient $|\rho_{HV}(0)|$ is 0.98..... 78
- Figure 4.4. Normalized standard deviation of differential phase estimates on correlated data versus the normalized spectrum width with the correlation coefficient $|\rho_{HV}(0)|$ as a parameter for the ideal case. The oversampling factor L is 8 and the SNR is very large. Both theoretical results (dashed line) and simulation results (solid line) are plotted..... 82
- Figure 4.5. Normalized standard deviation of differential phase estimates on whitened data versus the normalized spectrum width with the correlation coefficient $|\rho_{HV}(0)|$ as a parameter for the ideal case. The oversampling factor L is 8 and the SNR is very large. Both theoretical results (dashed line) and simulation results (solid line) are plotted..... 84
- Figure 4.6. Crossover signal-to-noise ratio SNR_c versus the normalized spectrum width for the differential phase estimator and an ideal system using the differential reflectivity (Z_{DR}) as a parameter. The oversampling factor L is 8 and the magnitude of the cross-correlation coefficient $|\rho_{HV}(0)|$ is 0.98. 85
- Figure 4.7. Normalized standard deviation of cross-correlation coefficient estimates on correlated data versus the normalized spectrum width with the actual correlation coefficient $|\rho_{HV}(0)|$ as a parameter for the ideal case. The oversampling factor L is 8 and the SNR is very large. Both theoretical results (dashed line) and simulation results (solid line) are plotted. 89
- Figure 4.8. Normalized standard deviation of cross-correlation coefficient estimates on whitened data versus the normalized spectrum width with the actual correlation coefficient $|\rho_{HV}(0)|$ as a parameter for the ideal case. The oversampling factor L is 8 and the SNR is very large. Both theoretical results (dashed line) and simulation results (solid line) are plotted. 92

Figure 4.9. Crossover signal-to-noise ratio SNR_c versus the normalized spectrum width for the cross-correlation coefficient estimator and an ideal system using the differential reflectivity (Z_{DR}) as a parameter. The oversampling factor L is 8 and the magnitude of the cross-correlation coefficient $ \rho_{HV}(0) $ is 0.98.....	93
Figure 5.1. Hydrometeors in each resolution volume are represented by their equivalent scatterer center, spaced by $c\tau/2L$ along range. Returns at the receiver front end are weighted by the transmitted pulse envelope.....	97
Figure 5.2. Simplified block diagram of a digital-receiver-based weather radar for the estimation of reflectivity.....	98
Figure 5.3. Processing for the estimation of reflectivity in the case of regular pulse with averaging in range.	99
Figure 5.4. Processing and estimation for the case of short pulse with averaging in range.	100
Figure 5.5. Processing and estimation for the case of pulse compression.	102
Figure 5.6. Processing and estimation for the case of regular pulse with whitening in range.	106
Figure 5.7. Normalized standard deviation for power estimates from correlated, whitened, and pseudo-whitened data as a function of the signal-to-noise ratio (SNR) for the ideal case. The oversampling factor L is 8, the normalized spectrum width σ_{vn} is 0.08. The pseudo-whitening transformation is based on a sharpening filter with parameter $p = 3$	115
Figure 5.8. Block diagram depicting the process involving whitening of correlation estimates.	116
Figure 5.9. Block diagram depicting the process involving whitening of Fourier coefficients.	118
Figure 6.1. Transmitter pulse shape approximated with sigmoid functions for different values of γ . The ideal pulse is obtained as $\gamma \rightarrow \infty$. A pulse with a rise time of 10% of the pulse width (as the one in the WSR-88D weather radar) corresponds to $\gamma = 44$	121
Figure 6.2. Effects of the transmitter pulse shape on the performance of the whitening transformation. (Top) Variance reduction factor vs. the pulse smoothness parameter γ , and (bottom) noise enhancement vs. the pulse smoothness parameter γ . In both cases the receiver filter is ideal and the oversampling factor L is 8.	122
Figure 6.3. Effects of the receiver filter bandwidth on the performance of the whitening transformation. (Top) Variance reduction factor vs. the receiver-bandwidth pulse-width product $B_0\tau$, and (bottom) noise enhancement vs. the receiver-bandwidth pulse-width product. In both cases the transmitted pulse is ideal and the oversampling factor L is 8.	125

Figure 6.4. Effects of reflectivity gradients on the performance of the whitening transformation. (Top) Variance reduction factor vs. the normalized reflectivity gradient gL , and (bottom) normalized bias of power estimates vs. the normalized reflectivity gradient gL . In both cases, the reflectivity profile is linear on decibel scale and gL indicates the total reflectivity variation on a range interval of $c\tau/2$ meters.	128
Figure 6.5. Depiction of sampling in range and processing of the signals. (a) Samples in range with spacing equal to the pulse length; standard processing to obtain the Doppler spectrum and its moments is indicated. (b) Oversampling in range. (c) Zoomed presentation of range locations (oversampled) at which meteorological variables (including spectra) are estimated. Range samples that are to be whitened are indicated. (d) Processing of whitened samples to obtain estimates of spectra, spectral moments, and polarimetric variables in range.	130
Figure 6.6. Schematic of the proposed processing that also retains the advantages of the traditional processing.	131
Figure 6.7. Performance of WTB estimators on real weather data. (Top) Total power estimates and (bottom) mean Doppler velocity estimates vs. range for whitened (solid line), correlated (dotted line), and non-oversampled data (dashed line). Data was acquired with a digital receiver and a stationary antenna. The oversampling factor is $L = 3$. Recorded data streams were processed off-line by the procedure described in Section 2.4 (see Figure 6.5). Results corroborate the accuracy of WTB estimators.	132
Figure A.1. Basic elements involved in the simulation of oversampled weather signals.	147
Figure A.2. Dual-polarized weather signal simulation. (Left column) Theoretical and simulated sample-time power spectral density (PSD) for both channels. (Right column) Theoretical and simulated range-time autocorrelation for both channels.	157
Figure A.3. Dual-polarized weather signal simulation. (Left column) Time-series on a sample-time axis for both channels. (Right column) Theoretical and simulated cross-power spectral density (PSD).	158

ABSTRACT

A method for estimation of Doppler spectrum and its moments as well as several polarimetric variables on pulsed weather radars is presented. This scheme operates on oversampled echoes in range, that is samples of in-phase and quadrature phase components are taken at a rate several times larger than the reciprocal of the transmitted pulse length. The aforementioned radar variables are estimated by suitably combining weighted averages of these oversampled signals in range with usual processing of samples (spaced at pulse repetition time) at a fixed range location. The weights in range are derived from a whitening transformation, hence, the oversampled signals become uncorrelated and consequently the variance of the estimates decreases significantly. Because the estimates' errors are inversely proportional to the volume scanning times, it follows that storms can be surveyed much faster than is possible with current processing methods, or equivalently, for the current volume scanning time, accuracy of the estimates can be greatly improved. This massive improvement is achievable at large signal-to-noise ratios (approximately greater than 15 dB).

1. INTRODUCTION

This introductory chapter presents the basics behind the problem of estimating meteorological variables using a whitening transformation where the fields of digital signal processing and remote sensing, particularly in the area of radar meteorology, are brought together. First, the principles of operation of polarimetric Doppler weather radars are reviewed, and meteorological parameters of interest obtained by these remote-sensing devices are presented. Next, weather signals are described both conceptually and mathematically. Processing of these signals to obtain meteorological variables, which is usually referred to as weather signal processing, is then presented. Autocovariance methods are generally preferred due to their computational efficiency and acceptable accuracy; however, the performance of these estimation techniques is not optimum, leaving room for a much needed improvement. Finally, the problem of obtaining better meteorological parameter estimates without sacrificing range resolution or antenna rotation speed is recognized, and the remainder of this dissertation focuses on a novel method for its efficient solution.

1.1. Polarimetric Doppler Weather Radars

Polarimetric Doppler weather radars have a unique ability to survey storms due to the capability of microwaves to penetrate clouds and rain, which does not exist on other meteorological instruments. These observations enable forecasters to provide timely warnings and researchers to understand some of the complex dynamics of meteorological phenomena (Doviak and Zrnic 1993).

Pulsed weather radars broadcast a brief intense pulse of energy followed by a relatively long “listening period” during which energy reflected from scatterers is received and processed. The time delay between transmitted and reflected signals determines the distance (range) to the scatterers and the strength of the backscattered signal is measured to gain information about the scatterers. Doppler radars, additionally, can measure the radial velocities of scatterers in the electromagnetic beam path of the radar because of the Doppler effect. The electromagnetic pulse is restricted in azimuth and elevation by the antenna illumination pattern $f(\theta, \phi)$ and in time (or range) by a finite transmission time (pulse) of duration τ . The space from which the electromagnetic pulse returns echoes to the receiver such that contributions from individual scatterers arrive at the same time to the receiver is called the resolution volume (see Figure 1.1).

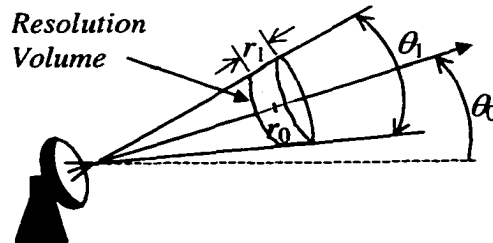


Figure 1.1. The resolution volume in a pulsed radar is approximately shaped as a frustum of a cone. The location of its center in space is given by (r_0, θ_0, ϕ_0) and its extent by (r_1, θ_1, ϕ_1) (related to the pulse duration and the antenna beamwidth).

Doppler radars sample the atmosphere using the resolution volume as the “sampling unit.” That is, for the collection of all scatterers in each resolution volume, the radar supplies three parameters of interest: (a) the total reflected power, P , which is related to the liquid water content or precipitation rate; (b) the composite Doppler radial velocity, \bar{v} , which is essentially mean radial motion of scatterers towards or away from the radar;

and (c) the Doppler spectrum width, σ_v , which is an indication of shear or turbulence from the scatterers associated with a given resolution volume (Zrníc 1979).

Doppler radars capable of transmitting two electromagnetic beams with different polarization provide several additional parameters of interest. Dual polarization measurements are based on the fact that raindrops, particularly larger ones, are not spherical, so they will respond differently to vertically and horizontally polarized electromagnetic waves. When the information can be retrieved with sufficient accuracy, polarimetry allows better precipitation measurements, classification of hydrometeors, identification of electrically active storms, and distinction of biological scatterers as shown in recent experiments (Zrníc and Ryzhkov 1999).

A simplified block diagram of a polarimetric Doppler weather radar like the one planned as an improvement to the national network of weather radars WSR-88D (NEXRAD) is depicted in Figure 1.2 (Zahrai and Zrníc 1997). The radar transmits and receives simultaneous horizontal and vertical polarizations with the aid of two receivers and just one transmitter. A novel arrangement of switches distributes each signal to its corresponding receiver. After demodulation and synchronous detection, in-phase (I) and quadrature (Q) components are digitized and routed to the processing subsystem for parameter estimation and display.

As a reference, some of the parameters of the WSR-88D radar operated by the National Weather Service are presented in Table 1.1.

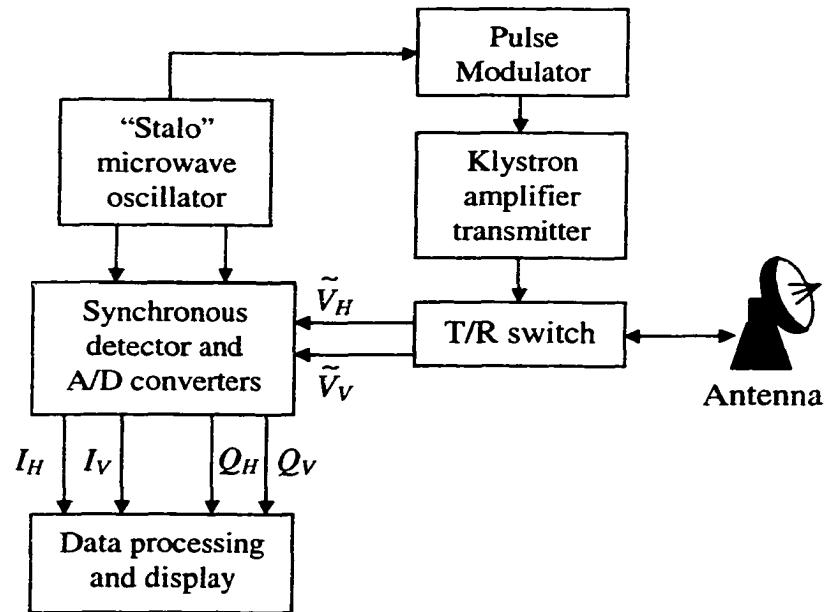


Figure 1.2. Simplified block diagram of a polarimetric Doppler weather radar. A Klystron pulse modulated by a radio-frequency (RF) signal is transmitted by the antenna with vertical and horizontal polarization at periodic time intervals. During the “listening periods”, weather echoes are received (a tilde indicates signals at RF). Coherent down-conversion (synchronous detection) controlled by a stable local oscillator (“stalo”) produces base-band complex envelopes $V_H = I_H + jQ_H$ and $V_V = I_V + jQ_V$ for the horizontal and vertical channels, respectively. After digitalization, I and Q signals are used for the estimation of spectral moments and polarimetric variables.

Antenna Subsystem	
<i>Pedestal</i>	
Maximum scanning rates	$30^{\circ} \text{ s}^{-1}$
Acceleration	$15^{\circ} \text{ s}^{-2}$
Mechanical limits	-1° to $+60^{\circ}$ in elevation
<i>Reflector</i>	
Type	Paraboloid of revolution
Polarization	Linear
Diameter	8.54 m
Gain	44.5 dB
Beam width	1°
First sidelobe level	-26 dB (with radome)
Transmitter and Receiver Subsystem	
<i>Transmitter</i>	
Frequency	2700 MHz to 3000 MHz
Pulse peak power	700 kW
Pulse widths, 6 dB	1.57 μs and 4.71 μs
Pulse repetition frequencies (PRF)	Eight selectable in the range from
Short pulse	320 Hz to 1300 Hz
Long pulse	320 Hz and 450 Hz
<i>Receiver</i>	
Type	Linear
Dynamic range	93 dB
Intermediate frequency	57.6 MHz
Bandwidth, 3 dB	630 kHz
Signal Processor Subsystem	
Intensity calculation	Linear return power average
Velocity calculation	Pulse-pair
Spectrum width calculation	Pulse pair logarithm
Number of pulses in Doppler modes	40 to 280
Number of pulses in Surveillance	16 to 65

Table 1.1. Summary of specifications for the National Weather Service WSR-88D weather surveillance radar (also known as NEXRAD).

1.2. Weather Radar Signals

Weather radar signals are a composite of echoes from a very large number of individual hydrometeors or from refractive index irregularities in clear air. These signals are sampled at discrete time delays τ_s , where the corresponding range (or distance from the radar) is given by $r = c\tau_s/2$ (c is the speed of light). The “range time” τ_s is the time it takes a transmitted pulse to make a round trip to a distance r . Pulses of a radio-frequency (RF) sine wave of width τ are sent every T_s seconds; this gives origin to the sample time, or time between samples for a fixed location in range (Figure 1.3).

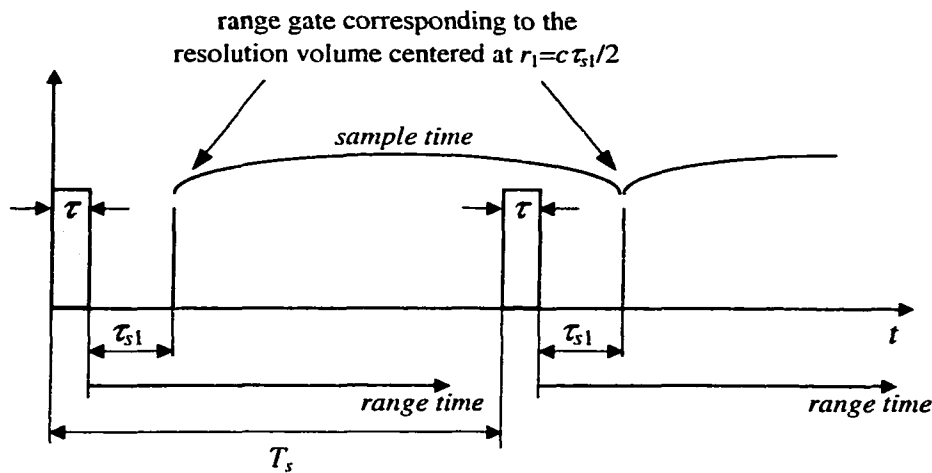


Figure 1.3. Depiction of sample time and range time in a polarimetric Doppler radar. Pulses of width τ are transmitted every T_s seconds. During reception between pulses, echoes are sampled at times τ_s (range time). Samples at a fixed range location are spaced by T_s and give origin to the sample time.

For each sample value there is an associated resolution volume in space with the hydrometeors that contribute the most to that sample. A weighting function that depends on the antenna radiation pattern, the transmitted pulse shape, and the receiver-filter transfer function determines how each sample contributes to the composite signal (Zrnic

and Doviak 1978). Figure 1.4 shows contributions from spaced resolution volumes as seen by the antenna. Figure 1.5 shows the corresponding signal from the receiver's point of view.

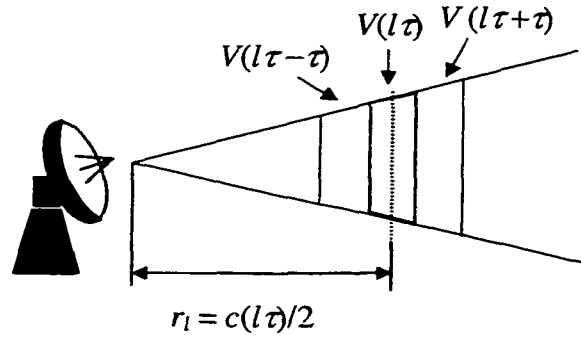


Figure 1.4. Contributions to weather signals from hydrometeors in a resolution volume. Signal samples are denoted by $V(l\tau)$, and their corresponding range, r_l , is given by $cl\tau/2$, where l is a positive integer. In this example, as in the WSR-88D radar, range gate sampling times are given as $l\tau$, where τ is the transmitted pulse width.

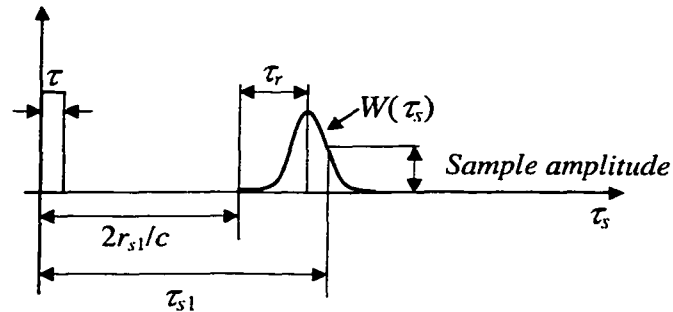


Figure 1.5. Weather echo amplitude for a point scatterer at range r_1 after the receiver filter and the synchronous detector. The contribution of each hydrometeor is determined by the weighting function $W(\tau_s)$. τ_r is the radar delay, and τ_{s1} is the sampling time (from Doviak and Zrnic 1993).

It was mentioned before that weather echoes contribute to produce a complex voltage sample $V = I + jQ$, where I and Q are the in-phase and quadrature components, respectively. The random size and location of scatterers cause I and Q to be random

variables. By the central limit theorem, I and Q have Gaussian probability density function (pdf) with zero mean and variance σ^2 (Zrnic 1975). The pdf of the magnitude of V is Rayleigh, and the one of the phase is uniform in the interval $[0, 2\pi)$ (Papoulis 1984). Although I and Q are uncorrelated random variables, the correlation between successive samples is not zero. The correlation between two successive samples will be appreciably different from zero if the distribution of Doppler velocities for the scatterers in the resolution volume is “narrow” compared to the range of unambiguous velocities. A narrow distribution of velocities corresponds to a more “coherent” process; this explains an appreciable correlation between samples.

For Doppler measurements the radar is pulsed at a sufficiently high rate so that the atmospheric phenomena produce correlated signal samples. The sample-time correlation of weather signals $R_V^{(T)}(mT_s)$ is a Gabor function (it is Gaussian for zero Doppler velocity) and given by (Doviak and Zrnic 1993)

$$R_V^{(T)}(mT_s) = S \exp[-8(\pi\sigma_v mT_s / \lambda)^2] e^{-j4\pi\bar{v}mT_s / \lambda}, \quad (1.1)$$

where the superscript (T) denotes “sample time,” S is the weather signal mean power, \bar{v} the mean Doppler velocity of scatterers, and σ_v the associated spectrum width. In addition, λ is the radar wavelength which is linked to the RF frequency f through the relation $\lambda = c/f$.

Under certain assumptions, the correlation of samples along range time can be derived exactly. If the scatterers are uniformly distributed in space and the transmitter pulse has a finite duration of τ seconds, we can decompose the contribution of all hydrometeors in

the resolution volume to the signal V sampled at time τ_s as a sum of L contributions dV from contiguous elemental shells in the range interval $c\tau/2$. Each elemental shell has a depth in range given by $r_o = c\tau/2L = c\tau_o/2$, where the sampling time τ_o is defined as τ/L . For simplicity, let us represent all the scatterers in each elemental shell by an equivalent “aggregate scatterer”. These equivalent scatterers are located at ranges $r_o, 2r_o, 3r_o$, etc. Here we assume that the scatterers are frozen although they have random placement. This is a good approximation because the little reshuffling that occurs during the separation time between echoes from overlapping range intervals can be neglected (τ is on the order of microseconds). Figure 1.6 depicts the decomposition of the resolution volume into elemental shells and the weighting on each shell’s contribution by the transmitted pulse shape along the sample-time (range) axis.

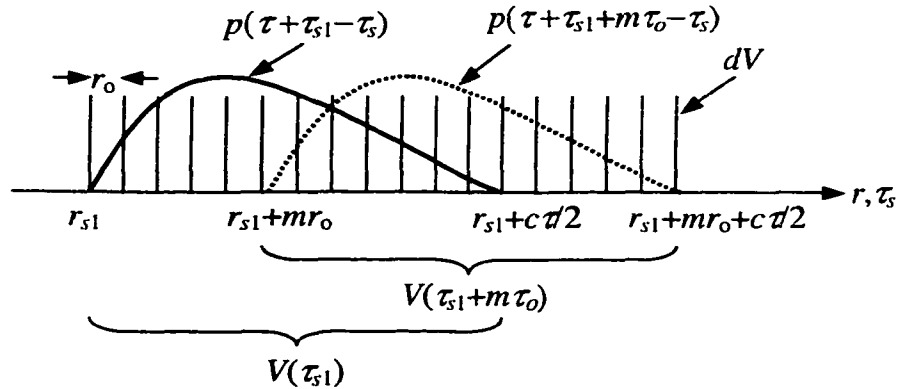


Figure 1.6. Decomposition of the resolution volume into L independent shells, each contributing a differential voltage dV weighted by the transmitted pulse shape. Weights of elemental shell contributions to $V(\tau_{s1})$ and $V(\tau_{s1} + m\tau_o)$ are shown in solid and dashed lines, respectively.

Thus, the contribution dV at sample time τ_s from the i -th shell in the resolution volume corresponding to range r_s at the receiver front end is given by

$$d\tilde{V}_{r_s}(\tau_s, i) = A(r_s + ir_o) \exp \left[j2\pi f \tau_s - j \frac{4\pi(r_s + ir_o)}{\lambda} + j\psi_i \right] p \left[\tau + \tau_s - \frac{2(r_s + ir_o)}{c} \right], \quad (1.2)$$

where p is the transmitter pulse envelope, $A(r_s)$ is the backscattered signal (amplitude and phase) corresponding to the shell at range r_s , and the corresponding phase includes temporal ($2\pi f \tau_s$), propagation ($4\pi r_s / \lambda$), and initial transmitter (ψ_i) phase terms. In (1.2) the tilde indicates that signals have not been down-converted to base band. The composite weather signal at a fixed sampling time τ_{s1} can be expressed as the sum of elemental contributions as

$$\tilde{V}(\tau_{s1}) = \sum_{i=0}^{L-1} d\tilde{V}_{r_{s1}}(\tau_{s1}, i). \quad (1.3)$$

Using (1.3), the correlation of samples along range time before the receiver filter (equivalent to having an ideal, infinite-bandwidth receiver filter) can be written as

$$\begin{aligned} R_{\tilde{V}_{ideal}}^{(R)}(m\tau_o) &= E[\tilde{V}^*(\tau_{s1})\tilde{V}(\tau_{s1} + m\tau_o)] = \\ &= E \left[\sum_{i=0}^{L-1} d\tilde{V}_{r_{s1}}^*(\tau_{s1}, i) \sum_{k=0}^{L-1} d\tilde{V}_{r_{s1}+mr_o}(\tau_{s1} + m\tau_o, k) \right], \end{aligned} \quad (1.4)$$

where the superscript (R) denotes “range time” and the subscript *ideal* refers to the receiver filter characteristics. Taking the expectation operation inside the summations in (1.4) produces

$$R_{\tilde{V}_{ideal}}^{(R)}(m\tau_o) = \sum_{i=0}^{L-1} \sum_{k=0}^{L-1} E[d\tilde{V}_{r_{s1}}^*(\tau_{s1}, i) d\tilde{V}_{r_{s1}+mr_o}(\tau_{s1} + m\tau_o, k)]. \quad (1.5)$$

The expected value inside (1.5) can be computed as

$$\begin{aligned}
E[d\tilde{V}_{r_{s1}}^*(\tau_{s1}, i)d\tilde{V}_{r_{s1}+mr_o}(\tau_{s1}+m\tau_o, k)] &= \\
&= E\{A^*(r_{s1}+ir_o)e^{-j[2\pi f\tau_{s1}-4\pi(r_{s1}+ir_o)/\lambda+\psi_i]}p[\tau+\tau_{s1}-2(r_{s1}+ir_o)/c] \\
&\quad A(r_{s1}+mr_o+kr_o)e^{j[2\pi f(\tau_{s1}+m\tau_o)-4\pi(r_{s1}+mr_o+kr_o)/\lambda+\psi_i]}p[\tau+\tau_{s1}+m\tau_o-2(r_{s1}+mr_o+kr_o)/c]\} \\
&= E[A^*(r_{s1}+ir_o)A(r_{s1}+mr_o+kr_o)]e^{j2\pi fm\tau_o}e^{j4\pi(i-m-k)r_o/\lambda} \\
&\quad p[\tau+\tau_{s1}-2(r_{s1}+ir_o)/c]p[\tau+\tau_{s1}+m\tau_o-2(r_{s1}+mr_o+kr_o)/c]. \tag{1.6}
\end{aligned}$$

If the wavelength λ is small compared to the size of each elemental shell, the contributions from different shells are independent random variables because non-overlapping shells have no scatterers in common. Therefore,

$$E[A^*(r_{s1}+ir_o)A(r_{s1}+mr_o+kr_o)] = \sigma_s^2(r_{s1}+ir_o)\delta(i-m-k), \tag{1.7}$$

where δ is the usual discrete-time Krönecker delta, and $\sigma_s^2(r)$ is the backscattered power contribution of each shell ($E[|dV|^2]$), which was assumed to be uniform so $\sigma_s^2(r) = \sigma_s^2$.

Introducing (1.7) into (1.6) and using the fact that $\tau_{s1} = 2r_{s1}/c$ (1.5) becomes

$$R_{\tilde{V}_{ideal}}^{(R)}(m\tau_o) = \sigma_s^2 e^{j2\pi mf\tau_o} \sum_{i=0}^{L-1} p(\tau-i\tau_o)p[\tau-(m-i)\tau_o]. \tag{1.8}$$

Letting $k = L - i$ so that $i = L - k$, and using the fact that $\tau = L\tau_o$, (1.8) becomes

$$R_{\tilde{V}_{ideal}}^{(R)}(m\tau_o) = \sigma_s^2 e^{j2\pi mf\tau_o} \sum_{k=0}^{L-1} p(k\tau_o)p[(k-m)\tau_o]. \tag{1.9}$$

Finally, recognizing that the summation in the previous equation is the convolution of $p(m\tau_o)$ with $p(-m\tau_o)$,

$$R_{\tilde{V}_{ideal}}^{(R)}(m\tau_o) = \sigma_s^2 [p(m\tau_o) * p^*(-m\tau_o)] e^{j2\pi mf\tau_o}. \tag{1.10}$$

For a non-ideal receiver filter, i.e. a receiver with a finite bandwidth, the correlation of

samples in range time can be determined as (Doviak and Zrnic 1979)

$$R_{\tilde{V}}^{(R)}(m\tau_o) = R_{\tilde{V}_{ideal}}^{(R)}(m\tau_o) * h(m\tau_o) * h^*(-m\tau_o), \quad (1.11)$$

where h is the impulse response of the receiver filter. Using the commutative and associative properties of the convolution, we can define the “modified” pulse envelope

$$p_m(m\tau_o) = p(m\tau_o) * h(m\tau_o), \quad (1.12)$$

so the correlation of samples in range time after the receiver filter can be written in an analogous fashion as in (1.10) to obtain

$$R_{\tilde{V}}^{(R)}(m\tau_o) = \sigma_s^2 [p_m(m\tau_o) * p_m^*(-m\tau_o)] e^{j2\pi m f \tau_o}. \quad (1.13)$$

The linear phase term of (1.13) is inherent to the propagation of the electromagnetic wave and has been overlooked in derivations that consider the signal at base band (e.g., Doviak and Zrnic 1979).

After the synchronous detector, the correlation of range samples can be found by recognizing that V at base band can be obtained from \tilde{V} at RF (radio frequency) via the down-conversion process as

$$V(\tau_{s1}) = \tilde{V}(\tau_{s1}) e^{-j2\pi f \tau_{s1}}; \quad (1.14)$$

therefore,

$$\begin{aligned} R_{\tilde{V}_{ideal}}^{(R)}(m\tau_o) &= E[V^*(\tau_{s1})V(\tau_{s1} + m\tau_o)] = \\ &= E[\tilde{V}^*(\tau_{s1})\tilde{V}(\tau_{s1} + m\tau_o)] e^{-j2\pi m f \tau_o} = R_{\tilde{V}_{ideal}}^{(R)}(m\tau_o) e^{-j2\pi m f \tau_o}. \end{aligned} \quad (1.15)$$

Finally,

$$R_V^{(R)}(m\tau_o) = \sigma_s^2 [p_m(m\tau_o) * p_m^*(-m\tau_o)]. \quad (1.16)$$

Although the theoretical result in (1.16) predicts a real autocorrelation for samples along range time, practical effects such as amplitude modulation-to-phase modulation (AM-to-PM) conversion within the pulse were not accounted for in the analysis. In fact, the complex nature of $R_V^{(R)}$ was recently exposed after analyzing practical measurements performed on oversampled (in range) weather signals acquired with a digital receiver on the WSR-88D (Ivic 2001). Nevertheless, the analysis in the following chapters can readily accommodate the linear phase terms in $R_V^{(R)}$ like the ones observed by Ivic (2001).

As a final comment in this section, note that the expression for the correlation coefficient [dividing (1.16) by $\sigma_s^2 \sum_i |p_m(i\tau_o)|^2$] along range time depends solely on parameters that are known (or can be measured) and therefore allows for its exact determination. This important observation will be exploited later.

1.3. Weather Signal Processing

The principal purpose of radar signal processing is the accurate, efficient extraction of information from radar echoes. Modern atmospheric polarimetric Doppler radars can sample an entire volume of a weather event in just a few minutes. Therefore, a very large amount of data must be processed to give the user compact, comprehensible information (spectral moments and polarimetric variables). Note that signal processing for weather radars is primarily used as an estimation procedure. Target detection is not the goal of these remote sensing devices.

The output of a polarimetric radar receiver consists of two complex signals (see Figure 1.2),

$$V_H(kT_s) = I_H(kT_s) + jQ_H(kT_s) = s_H(kT_s) \exp(j\omega_d kT_s) + n_H(kT_s), \quad (1.17)$$

and

$$V_V(kT_s) = I_V(kT_s) + jQ_V(kT_s) = s_V(kT_s) \exp(j\omega_d kT_s) + n_V(kT_s), \quad (1.18)$$

where the subscripts H and V stand for horizontal and vertical polarizations (channels), s and n represent the signal and noise component of the weather echo, ω_d is the Doppler shift, and T_s the pulse repetition time (PRT) or time between pulses. These time series in raw form convey little useful information about the weather, but their second order moments are well defined and contain the essential information. Therefore, further processing is needed to retrieve these statistical quantities and to provide significant information to meteorologists.

As previously mentioned, V is usually characterized by a Gaussian correlation in sample time and therefore the auto- and cross-correlation functions for the polarimetric signals are:

$$R_{V_H}^{(T)}(mT_s) = S_H \rho(mT_s) e^{-j4\pi \tilde{\nu} mT_s / \lambda} + N_H \delta(mT_s), \quad (1.19)$$

$$R_{V_V}^{(T)}(mT_s) = S_V \rho(mT_s) e^{-j4\pi \tilde{\nu} mT_s / \lambda} + N_V \delta(mT_s), \quad (1.20)$$

$$R_{V_H V_V}^{(T)}(mT_s) = \sqrt{S_H S_V} \rho_{HV}(mT_s) e^{-j4\pi \tilde{\nu} mT_s / \lambda}, \quad (1.21)$$

where $\rho(mT_s) = \exp[-8(\pi \sigma_v mT_s / \lambda)^2]$ is the signal correlation coefficient, $\rho_{HV}(mT_s) = \rho_{HV}(0) \rho(mT_s)$ the cross-correlation coefficient, S and N are the signal and

noise power respectively, and λ is the transmitter wavelength. The notation for $\rho_{v_H v_V}$ is simplified to ρ_{HV} for the sake of consistency with the notation found in the literature. Note that in (1.21) it was assumed that the cross-coupling between horizontal and vertical channels is negligible, hence the cross-correlation between the noise in the horizontal and vertical channels is zero.

Expressions (1.19) to (1.21) correspond to a power spectral density (also called Doppler spectrum) of the form:

$$S_{v_H, v_V}(v) = \frac{S_{H,V}}{\sqrt{2\pi}\sigma_v} \exp\left[-(v - \bar{v})^2 / 2\sigma_v^2\right] + \frac{2N_{H,V}T_s}{\lambda}, \quad (1.22)$$

where the subscripts H, V indicate that the same expression applies for either horizontally- or vertically-polarized signals. Parameters S , \bar{v} and σ_v are related to precipitation and kinematic fields and thus contain meaningful information if they are accurately estimated. Spectral moment estimation methods make use of known statistical properties of weather signals, and a considerable number of such methods have been introduced in the literature. However, throughout this work special stress will be given to the properties of those spectral moment estimation methods implemented in the WSR-88D radar.

The total power in the weather echo, $P = S + N$, is estimated with the formula

$$\hat{P}_{H,V} = \frac{1}{M} \sum_{k=0}^{M-1} P_{H,V}(k) = \frac{1}{M} \sum_{k=0}^{M-1} |V_{H,V}(kT_s)|^2, \quad (1.23)$$

where M is the number of samples available for processing. This estimator is unbiased and its variance is given by

$$\text{Var}(\hat{P}) = \frac{1}{M^2} \sum_{k=0}^{M-1} \sum_{l=0}^{M-1} E\left\{|V(kT_s)V(lT_s)|^2\right\} - P^2. \quad (1.24)$$

The expectation inside the double summation can be simplified for Gaussian processes as follows (Reed 1962):

$$\begin{aligned} E\left\{|V(kT_s)V(lT_s)|^2\right\} &= E\{V(kT_s)V^*(kT_s)V(lT_s)V^*(lT_s)\} \\ &= E\{V(kT_s)V^*(kT_s)\}E\{V(lT_s)V^*(lT_s)\} + \\ &\quad + E\{V(kT_s)V^*(lT_s)\}E\{V(lT_s)V^*(kT_s)\} \\ &= P^2 + |R[(k-l)T_s]|^2. \end{aligned} \quad (1.25)$$

Finally,

$$\text{Var}(\hat{P}) = \sum_{m=-M+1}^{M-1} \frac{M-|m|}{M^2} |R[(mT_s)]|^2, \quad (1.26)$$

which gives

$$\text{Var}(\hat{P}) = S^2 \sum_{m=-M+1}^{M-1} \frac{M-|m|}{M^2} \rho^2(mT_s) + \frac{N^2 + 2SN}{M}. \quad (1.27)$$

Hence, errors in mean power estimates can be reduced by increasing the available number of samples M or by reducing the noise power, both of which may be parameters out of the user's control.

An important result arises from the noiseless case. If there is no noise (1.27) becomes

$$\text{Var}(\hat{P}) = S^2 \sum_{m=-M+1}^{M-1} \frac{M-|m|}{M^2} \rho^2(mT_s). \quad (1.28)$$

This leads to the definition of the equivalent number of independent samples (Walker et

al. 1980) as the ratio of the variance of a single sample to the variance of the sampled mean:

$$M_I = \frac{Var(P_k)}{Var(\hat{P})} = \left(\sum_{m=-M+1}^{M-1} \frac{M-|m|}{M^2} \rho^2(mT_s) \right)^{-1}, \quad (1.29)$$

where P_k is the mean power of each sample used in the average, i.e. $P_k = E\{|V_{H,V}(kT_s)|^2\}$, so $Var(P_k) = S^2$. In other words, the equivalent number of independent samples is the number of uncorrelated samples that achieve the same variance reduction as a given set of correlated samples.

One of the simplest methods for the estimation of the first and second spectral moments is the autocovariance or pulse-pair processing (Sirmans and Bumgarner 1975). Using this technique, the mean Doppler velocity \bar{v} and the spectrum width σ_v can be estimated with the following formulas (Doviak and Zrnic 1993):

$$\hat{v} = -\frac{\lambda}{4\pi T_s} \arg\{\hat{R}(T_s)\}, \quad (1.30)$$

$$\hat{\sigma}_v = \frac{\lambda}{2\pi T_s \sqrt{2}} \left| \ln \left(\frac{\hat{S}}{|\hat{R}(T_s)|} \right) \right|^{\frac{1}{2}} \operatorname{sgn} \left[\ln \left(\frac{\hat{S}}{|\hat{R}(T_s)|} \right) \right], \quad (1.31)$$

where

$$\hat{S} = \hat{P} - N, \quad (1.32)$$

is the weather signal power estimator based on (1.23), and

$$\hat{R}(T_s) = \frac{1}{M-1} \sum_{m=0}^{M-2} V^*(mT_s) V(mT_s + T_s) \quad (1.33)$$

is the asymptotically-unbiased estimator of the autocorrelation of V for lag one.

Zmic (1977) derived expressions for the variances of these estimators for high signal-to-noise ratio (SNR) and small spectrum width as

$$Var(\hat{v}) \approx \frac{\sigma_v \lambda}{8MT_s \sqrt{\pi}}, \quad (1.34)$$

and

$$Var(\hat{\sigma}_v) \approx \frac{3\sigma_v \lambda}{64MT_s \sqrt{\pi}}. \quad (1.35)$$

As before, variance reduction is achieved by increasing the number of available samples M in (1.33).

It was mentioned earlier that polarimetric variables supply additional parameters related to precipitation type and amount. Here, I will concentrate on three of these, namely the differential reflectivity Z_{DR} , the total differential phase Φ_{DP} , and the magnitude of the cross-correlation coefficient at lag zero $|\rho_{HV}(0)|$. The differential reflectivity Z_{DR} (in dB) is used for accurate rainfall estimation and hydrometeor identification. It may be estimated using the formula

$$\hat{Z}_{DR} = 10 \log_{10} \left(\frac{\hat{S}_H}{\hat{S}_V} \right), \quad (1.36)$$

where \hat{S} (for horizontal or vertical co-polar signals) is computed from the mean power estimate in (1.32) as $\hat{S}_{H,V} = \hat{P}_{H,V} - \hat{N}_{H,V}$. Another polarimetric variable that enhances the classification and quantification of precipitation is the correlation between the two co-

polar signals. One co-polar signal is for vertical polarization of transmitted and received waves whereas the other is for horizontal polarization of these waves. This correlation is obtained as

$$\rho_{HV}(0) = \frac{\sum_{k=0}^{M-1} V_H^*(kT_s) V_V(kT_s)}{\sqrt{\sum_{k=0}^{M-1} |V_H(kT_s)|^2} \sqrt{\sum_{k=0}^{M-1} |V_V(kT_s)|^2}}, \quad (1.37)$$

and the argument of (1.37) gives the total differential phase Φ_{DP} . As with the spectral moments, it can be shown that the variances of the estimators in (1.36) and (1.37) are inversely proportional to the number of samples M (Sachidananda and Zrnic 1985, Ryzhkov and Zrnic 1988, Liu et al. 1994).

To obtain meaningful estimates that allow efficient quantification of weather phenomena, estimation errors must be kept below maximum allowable limits. WSR-88D specifications call for a nominal error in Doppler velocity and spectrum width of 1 m s^{-1} and a fractional error of 1 dB is allowed for the estimation of mean power. Similar constraints are established for the polarimetric variables to obtain accurate meteorological fields. The only parameter we can adjust to accommodate these requirements is the number of samples used in the estimation process. More samples are required to lower error magnitudes, which in turn implies a slower antenna rotation rate and an overall increase in acquisition time. With longer times between scans, the probing of weather phenomena is performed less frequently and important storm developments could be missed. The statistical estimation framework becomes of particular significance when the goal is to scan a phenomenon quickly and accurately, since the random-process nature of

weather signals will demand a certain amount of averaging if a desired accuracy is to be achieved. This is a trade-off in all polarimetric Doppler radar systems.

1.4. Problem Statement

Polarimetric weather radars probe the atmosphere and retrieve spectral moments and polarimetric variables for each resolution volume in the surrounding space. To reduce the statistical uncertainty of estimates of spectral moments and polarimetric variables for each resolution volume it is customary to average signals from many pulses. The variance reduction of averaged estimates is inversely proportional to the equivalent number of independent samples (1.29), which depends on the correlation between samples and the total number of samples averaged. The number of samples available for averaging is determined by the pulse repetition time T_s and the dwell time, which is usually determined by the required azimuthal resolution. In addition to averaging along sample time, some radars average a few samples along range time to further reduce the estimates' errors. However, this process degrades the range resolution of the system, diminishing its effectiveness for sampling small-scale phenomena.

On one side, large estimation errors restrict the applicability of weather surveillance radars for precise quantification and identification of weather phenomena. On the other hand, the need for faster updates between volume scans calls for faster antenna rotation rates, which limits the number of samples available for each resolution volume, which as shown before, is inversely related to the variance of estimates. These are conflicting requirements.

A technique that increased the number of independent samples by keeping the dwell time constant without degrading the range resolution would help solve either one of these problems. More independent samples would reduce the estimates' errors at the same antenna rotation rate, or would speed up volume scans while keeping the errors at previous levels; in both cases no or little degradation in the range resolution of estimates is required.

A well-known method to reduce the acquisition time without sacrificing range resolution is the pulse compression technique (Nathanson 1969, Mudukutore et al. 1998). Pulse compression can be applied to increase the number of independent samples by averaging high-resolution estimates in range. However, most ground-based weather radars do not use pulse compression due to the so-called range sidelobes and the need to increase the transmission bandwidth.

The remaining chapters of this dissertation are devoted to a detailed study of a novel method that increases the equivalent number of independent samples available for the estimation of meteorological variables without requiring a larger transmission bandwidth. It will be shown that it is possible to utilize the weather signal samples efficiently so that the variance of the estimates is considerably reduced with little sacrifice in range resolution or antenna rotation speed.

2. WHITENING TRANSFORMATION OF OVERSAMPLED RANGE DATA

Chapter 1 presented the problem of obtaining more accurate estimates without decreasing the antenna rotation speed or degrading the range resolution considerably. This chapter is devoted to introducing a practical and efficient answer to the aforementioned problem where the proposed solution involves the use of a whitening transformation on oversampled data along range time. The study of theoretical estimation performance limits and the conditions under which these limits are attained motivate the use of a whitening transformation. Other approaches aiming to solve similar problems found in the literature are reviewed and disqualified as candidate solutions for different reasons. Next, the goals and implications of this research work are stated. Finally, the last two sections of this chapter are devoted to studying the implementation of the whitening transformation on oversampled range data and its performance in environments with and without additive noise. The application of this technique to the construction of efficient estimators of Doppler spectral moments and polarimetric variables is addressed in Chapters 3 and 4.

2.1. Motivation

The current implementation of spectral moment and polarimetric variable estimators uses a simple method of averaging samples in range at the expense of degradation in range resolution. Simple averaging, however, does not yield the best performance when the observations are correlated [see (1.28)].

What is the best performance that could be reached? The Cramer-Rao Lower Bound (CRLB) provides the theoretical ideal performance of an unbiased estimator of a set of signal parameters. An unbiased estimator that attains the CRLB is said to be efficient in that it efficiently uses the data. The expression for the bound is (Kay 1993)

$$\text{var}(\hat{\theta}_i) \geq [\mathbf{I}^{-1}(\boldsymbol{\theta})]_{ii}; \quad i = 1, 2, \dots, p, \quad (2.1)$$

where $\boldsymbol{\theta} = [\theta_1 \ \theta_2 \ \dots \ \theta_p]^T$ is the vector of parameters to be estimated and $\mathbf{I}(\boldsymbol{\theta})$ is the p -by- p Fisher information matrix. For the general case, the Fisher information matrix is defined as

$$[\mathbf{I}(\boldsymbol{\theta})]_{ij} = -E \left[\frac{\partial^2 \ln p(\mathbf{x}; \boldsymbol{\theta})}{\partial \theta_i \partial \theta_j} \right]; \quad i, j = 1, 2, \dots, p; \quad (2.2)$$

where $p(\mathbf{x}; \boldsymbol{\theta})$ is the probability density function of the observations \mathbf{x} parameterized by the unknown vector of parameters $\boldsymbol{\theta}$. For zero-mean, complex Gaussian observations with covariance matrix \mathbf{C} , the expression for $\mathbf{I}(\boldsymbol{\theta})$ is simplified as [(15.52) of Kay (1993)]

$$[\mathbf{I}(\boldsymbol{\theta})]_{ij} = \text{tr} \left[\mathbf{C}^{-1}(\boldsymbol{\theta}) \frac{\partial \mathbf{C}(\boldsymbol{\theta})}{\partial \theta_i} \mathbf{C}^{-1}(\boldsymbol{\theta}) \frac{\partial \mathbf{C}(\boldsymbol{\theta})}{\partial \theta_j} \right]. \quad (2.3)$$

Let us compute the CRLB of the power estimator¹ of complex, zero-mean Gaussian data with correlation matrix given by $\mathbf{C} = S\rho$. Here S is the signal mean power, and ρ is the normalized correlation matrix of the complex samples used in the estimation process. In this case, it is straightforward to see that $I(S) = \text{tr} \{ [\mathbf{C}^{-1}(S) \frac{d\mathbf{C}(S)}{dS}]^2 \} = \frac{M}{S^2}$ and consequently

¹ For a more detailed analysis of the CRLB for Gaussian random processes in the context of weather radars refer to Frehlich (1993).

$$Var(\hat{S}) \geq \frac{S^2}{M}. \quad (2.4)$$

Based on the previous equation, the CRLB does not depend on the correlation structure of the observations, and it can be inferred that it is not the correlation between observations that limits the accuracy of a given estimator, but the way those observations are used to compute the estimates. Therefore, it is reasonable to think that knowledge of the correlation coefficient $\rho(mT_s)$ could be used to formulate estimators that attain the CRLB (Schulz and Kostinski 1997).

It is known from estimation theory that classical estimators of the mean and variance of white (i.e. uncorrelated) Gaussian observations attain the CRLB. Therefore, one would like to derive a transformation on the original data based on their correlation such that the resulting samples would be uncorrelated (or white). Still, this transformation would have to preserve the same properties that are of interest in the original data set. If the underlying samples have zero mean such transformation exists and it is usually termed as “whitening” (Van Trees 1968) or decorrelation transformation. The whitening transformation has been applied to solve a variety of signal processing problems (Sosulin and Kostrov 1998, Mohamed and Schwarz 1998, Izquierdo et al. 2000, Bruniquel et al. 1996) and in this research work it will be exploited for the transformation of oversampled range data to generate efficient estimates of meteorological variables.

2.2. Previous Work

The problem of obtaining more efficient spectral moment and polarimetric variable estimates is not new, and several solutions have been proposed to reduce output product errors in weather radars. In the quest for finding better estimators of spectral moments, Zmic (1979) showed that maximum likelihood (ML) estimators yield errors one order of magnitude less than those obtained with conventional autocovariance methods. Later, Frehlich (1993) improved Zmic's results and derived simplified expressions to test new estimators based on the ML approach. Due to the complexity of ML estimators, researchers focused on ways to simplify spectral moment estimators by assuming knowledge of some of the underlying parameters of the weather signal. Bamler (1991) computed the CRLB for Doppler frequency estimates assuming both the correlation (or spectrum) of samples and SNR are known. Frehlich (1993) analyzed the performance of approximate ML estimators under analogous assumptions. Later, Chornoboy (1993) obtained an optimal estimator for Doppler velocity that is simpler than ML formulations, but again, the SNR and the spectrum width were assumed to be known. Using the whitening approach, Frehlich (1999) investigated the performance of ML estimators of spectral moments under the same assumptions of previous works. Summarizing, compared to classical estimators (Zmic 1979), ML estimators provide better accuracy for high SNR and are moderately complex if the spectrum width is known a priori. However, this last assumption restricts the application of these estimators, because the correlation coefficient of $V(kT_s)$ is not known and must be estimated. That is, for processing spectral moments, the joint estimate of S , \bar{v} , and σ_v would need to be calculated, which turns out to be computationally very intensive.

Koivunen and Kostinski (1999) took a step further. They suggested that knowledge of the correlation coefficient could improve the variance of spectral moments estimates. By means of the whitening transformation, they devised improved estimators that theoretically can achieve the CRLB. Nevertheless, this attempt fails again because the correlation of weather signals along sample time must be estimated and Gaussian sample-covariance matrices are ill conditioned (Kostinski and Koivunen 2000).

Alternatively, Rodríguez González (1999) acknowledged that the variance of estimates could be reduced by averaging a number of samples along range, and that this number of samples depends on the range correlation function, which is known exactly in the case of range samples (1.13). However, in this work the author merely computes the number of independent samples for a given set of radar parameters, and no effort is being made to obtain better spectral moment estimates by using the knowledge of those parameters.

More recently, Fjørtoft and Lopès (2001) proposed a method for estimating the reflectivity on synthetic aperture radar (SAR) images with correlated samples (pixels). The method is based on a modified whitening transformation (Novak and Burl 1990) that exhibits a low computational complexity and is suitable for oversampled data. Although they did not extend this approach to the estimation of other spectral moments or the polarimetric variables, this work shows one of the first successful attempts at using a whitening transformation in the pursuit of improved estimators for remote sensing devices.

It will be shown later that in contrast to most of the previous work, the whitening transformation on oversampled data along range time results in an efficient and practical method of obtaining better estimates of spectral moments and polarimetric variables.

2.3. Significance

The purpose of this work is to provide a method whereby the abovementioned deficiencies of the previous work are overcome. The proposed processing increases the number of independent samples in a simple manner while the sacrifice in range resolution is minimal and the transmission bandwidth is not broadened. It is somewhat surprising that previous works overlooked the fact that while the correlation of samples separated by T_s needs to be estimated for each particular case (it depends on the meteorological conditions being observed), samples spaced in range exhibit a correlation coefficient that allows its exact computation a priori; the underlying assumption here is that the mean echo power changes very little over the average interval in range. By exactly knowing the correlation coefficient, it is possible to apply the whitening transformation without worrying about the pitfalls originating from an estimated quantity. As a result, we obtain $M_I = M$ [see (1.29)], and the variance reduction through averaging is maximized.

Maximization of the equivalent number of independent samples lead to the following implications:

- For the same uncertainty as the one obtained with correlated samples, faster scan rates are possible, as the total number M of samples for a resolution volume is determined by the pulse repetition time (PRT) and the dwell time.

- For the same scanning rates, lower uncertainties can be obtained, making the use of polarimetric variables feasible for accurate rainfall estimation and hydrometeor identification.

With the advent of digital receivers (Brunkow 1999), oversampling is indeed feasible. Therefore, it is possible to maintain the same current radar capabilities (involving no oversampling or whitening) while adding, in parallel, a set of more reliable estimates obtained from whitened oversampled range data.

2.4. Implementation

The procedure starts with oversampling in range so that there are L samples during the pulse duration τ (that is oversampling by a factor of L). Assume that the range of depth $c\tau/2$ (where c is the speed of light) is uniformly filled with scatterers. For relatively short pulses this is a common occurrence. For convenience, the contribution from the resolution volume to the sampled complex voltage $V(nT_s) = I(nT_s) + jQ(nT_s)$ at a fixed time delay nT_s , can be decomposed into sub contributions $s(l\tau_0, nT_s)$ from L contiguous elemental shells or “slabs” each $c\tau/2L$ thick, as shown in Chapter 1. For simplicity τ_0 and T_s are dropped hereafter so the indexes l and n indicate times at sampling-time (range-time) increments τ_0 and at pulse-repetition (sample-time) increments T_s , respectively. The voltages $s(l, n)$ are identically distributed complex Gaussian random variables, the real and imaginary parts, $\text{Re}\{s(l, n)\}$ and $\text{Im}\{s(l, n)\}$, have variances σ^2 , and the average power of $s(l, n)$ is $\sigma_s^2 = 2\sigma^2$. Pulse of an arbitrary shape $p(l)$ (index l indicates time increments of τ_0 within the transmitted pulse which correspond to a decreasing index in range, see

(4.17) in Doviak and Zrnic 1993) induces weighting to the contributions from contiguous “slabs” such that the composite voltage is

$$V(l, n) = I(l, n) + jQ(l, n) = \left[\sum_{i=0}^{L-1} s(l+i, n) p(L-1-i) \right] * h(l), \quad (2.5)$$

where $h(l)$ is the impulse response of the receiver filter. Then, as shown in Chapter 1

$$R_V^{(R)}(m) = \sigma_s^2 [p_m(m) * p_m^*(-m)], \quad (2.6)$$

where the modified pulse envelope p_m is given by

$$p_m(m) = p(m) * h(m). \quad (2.7)$$

Hence, the correlation coefficient of range samples $\rho_V^{(R)}$ is

$$\rho_V^{(R)}(m) = \frac{R_V^{(R)}(m)}{R_V^{(R)}(0)} = \frac{p_m(m) * p_m^*(-m)}{\sum_{l=0}^{L-1} p_m^2(l)}. \quad (2.8)$$

If the transmitted pulse envelope has a rectangular shape (ideal transmitter) and the receiver has infinite bandwidth, the correlation coefficient of samples along range time simplifies to

$$\rho_V^{(R)}(m) = \begin{cases} \frac{L-|m|}{L} & |m| < L \\ 0 & \text{otherwise.} \end{cases} \quad (2.9)$$

For other pulse shapes and band-limited receivers $\rho_V^{(R)}$ can be evaluated by attenuating the transmitted pulse, injecting it directly into the receiver, and oversampling the result to obtain the modified pulse envelope p_m . Introducing p_m into (2.8) produces $\rho_V^{(R)}$; this is done only once for a given pulse shape and receiver bandwidth.

The procedure for implementing the whitening transformation is as follows. Define the Toeplitz Hermitian normalized correlation matrix \mathbf{C}_V as

$$\mathbf{C}_V = \begin{bmatrix} 1 & \rho_V^{(R)}(1) & \cdots & \rho_V^{(R)}(L-1) \\ \rho_V^{(R)}(1)^* & 1 & \cdots & \rho_V^{(R)}(L-2) \\ \vdots & \vdots & \ddots & \vdots \\ \rho_V^{(R)}(L-1)^* & \rho_V^{(R)}(L-2)^* & \cdots & 1 \end{bmatrix}. \quad (2.10)$$

Because this matrix is positive semidefinite (Therrien 1992), it can be decomposed into a product of a matrix \mathbf{H} and its conjugate transpose (or adjoint) as

$$\mathbf{C}_V = \mathbf{H} \mathbf{H}^{*T}, \quad (2.11)$$

where the superscript T indicates matrix transpose. Any \mathbf{H} that satisfies (2.11) is called a square root of \mathbf{C}_V (Faddeev and Faddeeva 1963) and is the inverse of a whitening transformation matrix

$$\mathbf{W} = \mathbf{H}^{-1}, \quad (2.12)$$

which if applied to the range samples produces L uncorrelated random variables with identical variance (Kay 1993). Strictly speaking, this is an isotropic transformation (Manolakis et al, 2000) because it produces unit-variance uncorrelated vectors.

Denote with $X(l,n)$ the sequence of time samples spaced T_s seconds apart each of which is obtained as

$$\mathbf{X}_n = \mathbf{W} \mathbf{V}_n, \quad (2.13)$$

where $\mathbf{V}_n = [V(0,n), V(1,n), \dots, V(L-1,n)]^T$ and $\mathbf{X}_n = [X(0,n), X(1,n), \dots, X(L-1,n)]^T$. In general, the orthogonalization is not unique and many well-known methods could be applied to generate different whitened sequences. Two prominent methods to generate

whitened sequences are the eigenvalue decomposition (Therrien 1992) and triangular decomposition, which is equivalent to Gram-Schmidt orthogonalization (Therrien 1992, Papoulis 1984).

In the eigenvalue decomposition method the eigenvalues λ_i of the correlation matrix \mathbf{C}_v are computed first and \mathbf{C}_v is represented as $\mathbf{C}_v = \mathbf{U} \mathbf{\Lambda} \mathbf{U}^{*T}$, where $\mathbf{\Lambda}$ is a diagonal matrix of eigenvalues, and \mathbf{U} is the unitary transformation matrix whose columns are the eigenvectors of \mathbf{C}_v . Then, to obtain \mathbf{W} , a diagonal matrix \mathbf{D} with elements on the diagonal equal to $\lambda_i^{-1/2}$ is constructed and

$$\mathbf{W} = \mathbf{H}^{-1} = \mathbf{D} \mathbf{U}^{*T}. \quad (2.14)$$

The transformation in (2.14) is the Mahalanobis transformation (Tong 1995).

Triangular (or Cholesky) decomposition is identical to Gram-Schmidt orthogonalization (Papoulis 1984). In this case, the correlation matrix decomposes as $\mathbf{C}_v = \mathbf{H} \mathbf{H}^{*T}$, where the matrix \mathbf{H} is a lower triangular matrix; hence, the whitening matrix (2.12) is also lower triangular. A possible advantage of triangular \mathbf{H} matrices is that whitening can proceed in a pipeline manner; that is, computations can start as soon as the first sample is taken and progress through subsequent samples. Non-triangular \mathbf{H} matrices require presence of all data before computations can start.

Regardless of the method selected to compute \mathbf{W} , the application of the whitening transformation to a set of oversampled data (fixed n) is given by (2.13), or explicitly as

$$X(l, n) = \sum_{j=0}^{L-1} w_{l,j} V(j, n); \quad l = 0, 1, \dots, L-1, \quad (2.15)$$

where $w_{l,j}$ are the entries of $\mathbf{W} = \mathbf{H}^{-1}$.

2.5. Performance Analysis

To prove the whitening property of the transformation defined by (2.12), let us apply the transformation matrix to the data as in (2.13) and compute the correlation for the random vector \mathbf{X}_n as

$$\mathbf{R}_x = E[\mathbf{X}_n \mathbf{X}_n^{*T}] = \mathbf{W} E[\mathbf{V}_n \mathbf{V}_n^{*T}] \mathbf{W}^{*T}. \quad (2.16)$$

Now, the correlation matrix of \mathbf{V}_n is given by $P\mathbf{C}_v$, where $P = \sigma_s^2 \left[\sum_{l=0}^{L-1} p_m^2(l) \right]$ [see (2.6)

and (2.8)] and $\mathbf{W} = \mathbf{H}^{-1}$, then

$$\mathbf{R}_x = \mathbf{H}^{-1} [P\mathbf{C}_v] (\mathbf{H}^{-1})^{*T} = P [\mathbf{H}^{-1} \mathbf{H}] [\mathbf{H}^{*T} (\mathbf{H}^{*T})^{-1}] = P\mathbf{I}, \quad (2.17)$$

where \mathbf{I} is the L -by- L identity matrix.

By definition, \mathbf{X}_n is white because its correlation is a diagonal matrix. Additionally, all components have identical variance because \mathbf{R}_x is a scalar multiple of the identity matrix (\mathbf{I}). In other words, $R_x^{(R)}(l) = P\delta(l)$. Furthermore, as discussed before, the signals have Gaussian distributions hence the variables $X(l,n)$ are independent for a fixed n . In conclusion, by applying the whitening transformation given by \mathbf{W} to the oversampled weather signal V , we obtained a vector with uncorrelated components, each with the same mean power (P) as V .

The presence of noise is inherent to every radar system, so it is of concern to analyze the performance of the whitening transformation under noisy conditions. Let $V = V_S + V_N$, where the subscripts 'S' and 'N' stand for signal and noise components, respectively. When applying the whitening transformation, both signal and noise are evenly affected,

therefore

$$\mathbf{X} = \mathbf{WV} = \mathbf{WV}_s + \mathbf{WV}_N. \quad (2.18)$$

For simplicity, we dropped the subscript “n” that is used to indicate sample time. From (2.18), we can see that the signal is whitened and the noise, which was white prior to the whitening transformation, becomes colored. To gain more insight into this process, it is useful to decompose $\mathbf{C}_{\mathbf{v}_s}$ using eigenvalue decomposition. With this decomposition, the whitening transformation is given by (2.14). Then, the correlation matrix of \mathbf{X} is

$$\begin{aligned} \mathbf{R}_x &= E[\mathbf{X}\mathbf{X}^{*T}] \\ &= \mathbf{D}\mathbf{U}^{*T} E[\mathbf{V}\mathbf{V}^{*T}] \mathbf{U}\mathbf{D}^{*T} \\ &= \mathbf{D}\mathbf{U}^{*T} (S\mathbf{C}_{\mathbf{v}_s} + N\mathbf{I}) \mathbf{U}\mathbf{D} \\ &= \mathbf{D}\mathbf{U}^{*T} (S\mathbf{U}\mathbf{\Lambda}\mathbf{U}^{*T} + N\mathbf{I}) \mathbf{U}\mathbf{D} \\ &= S\mathbf{I} + N\mathbf{\Lambda}^{-1}, \end{aligned} \quad (2.19)$$

where we used the fact that $\mathbf{X}=\mathbf{WV}$, $\mathbf{W}=\mathbf{D}\mathbf{U}^{*T}$, $\mathbf{U}^{*T}\mathbf{U} = \mathbf{I}$ (since \mathbf{U} is unitary), and by definition \mathbf{D} is real, $\mathbf{D}\mathbf{D} = \mathbf{\Lambda}^{-1}$, and $\mathbf{D}\mathbf{\Lambda}\mathbf{D} = \mathbf{I}$. The signal-to-noise ratio (SNR) for the l -th component of \mathbf{X}_n is

$$SNR_l = \frac{S}{N} \lambda_l; \quad l = 0, 1, \dots, L-1, \quad (2.20)$$

where λ_l is the l -th eigenvalue of $\mathbf{C}_{\mathbf{v}_s}$. The partial SNR defined in (2.20) makes sense because the eigenvalues of a positive-definite, symmetric matrix are real and positive. Equation (2.20) indicates that the SNR for each component changes from the original SNR according to the magnitude of the corresponding eigenvalue. For $\lambda_l > 1$, the SNR of the whitened signal increases; otherwise, the noise gets enhanced. To quantify this noise-

enhancing effect, compute the total average noise power as

$$N_w = \frac{1}{L} \sum_{l=0}^{L-1} N_l = \frac{1}{L} \sum_{l=0}^{L-1} \frac{N}{\lambda_l} = \frac{N}{L} \sum_{l=0}^{L-1} \lambda_l^{-1}. \quad (2.21)$$

It is a well-known fact that if $\{\lambda_l\}_{l=0}^{L-1}$ are the eigenvalues of \mathbf{A} , then $\{\lambda_l^{-1}\}_{l=0}^{L-1}$ are the eigenvalues of \mathbf{A}^{-1} (Lütkepohl 1996). In addition, the trace of \mathbf{A} satisfies the relationship $\text{tr}\{\mathbf{A}\} = \sum_{l=0}^{L-1} \lambda_l$; therefore, to compute $\sum_{l=0}^{L-1} \lambda_l^{-1}$ we could invert $\mathbf{C}_{\mathbf{v}_s}$ and then compute its trace so

$$N_w = N \frac{\text{tr}\{\mathbf{C}_{\mathbf{v}_s}^{-1}\}}{L} = N(NEF), \quad (2.22)$$

where $\text{tr}\{\mathbf{C}_{\mathbf{v}_s}^{-1}\} / L$ is defined as the noise-enhancement factor NEF .

For a correlation matrix corresponding to (2.9) it is not very difficult to find a closed-form solution for the previous equation. For this ideal case, the correlation matrix is

$$\mathbf{C}_{\mathbf{v}_s} = \begin{bmatrix} 1 & \frac{L-1}{L} & \dots & \frac{1}{L} \\ \frac{L-1}{L} & 1 & \dots & \frac{2}{L} \\ \vdots & \vdots & \ddots & \vdots \\ \frac{1}{L} & \frac{2}{L} & \dots & 1 \end{bmatrix}, \quad (2.23)$$

and it can be verified that

$$\mathbf{C}_{\mathbf{v}_s}^{-1} = \begin{bmatrix} \frac{L(L+2)}{2L+2} & -\frac{L}{2} & 0 & \dots & 0 & \frac{L}{2L+2} \\ -\frac{L}{2} & L & -\frac{L}{2} & \ddots & & 0 \\ 0 & -\frac{L}{2} & \ddots & \ddots & \ddots & \vdots \\ \vdots & \ddots & \ddots & \ddots & \ddots & 0 \\ 0 & & \ddots & \ddots & L & -\frac{L}{2} \\ \frac{L}{2L+2} & 0 & \dots & 0 & -\frac{L}{2} & \frac{L(L+2)}{2L+2} \end{bmatrix}. \quad (2.24)$$

Then,

$$\frac{\text{tr}\{\mathbf{C}_{\mathbf{v}_s}^{-1}\}}{L} = \frac{L^2}{L+1}, \quad (2.25)$$

and thus (2.21) becomes

$$N_w = N \frac{L^2}{L+1}. \quad (2.26)$$

The previous equation shows that the noise is enhanced for $L > 1$ (which is always the case if there is oversampling). Therefore, for relatively small SNR, the variance reduction achieved by increasing L will be masked by a corresponding noise power boost.

Figure 2.1 shows the noise enhancement factor in (2.26) obtained through simulations by measuring the power of white noise before and after the application of the whitening transformation. Figure 2.2 shows the noise power for whitened and correlated observations along the range-time axis. As expected, in the case of correlated samples the noise power is uniform and equal to the simulated noise power. On the other hand, the whitening transformation enhances the mean noise power by a factor of 9.0909, as predicted by (2.26). Observe that the noise power is redistributed (colored) in range so that the enhancement is different for each range component. Note, however, that this redistribution of noise along the range-time axis does not affect the spectral shape of the noise in the sample-time domain. That is, the noise is still white along sample time but its total power is a function of range.

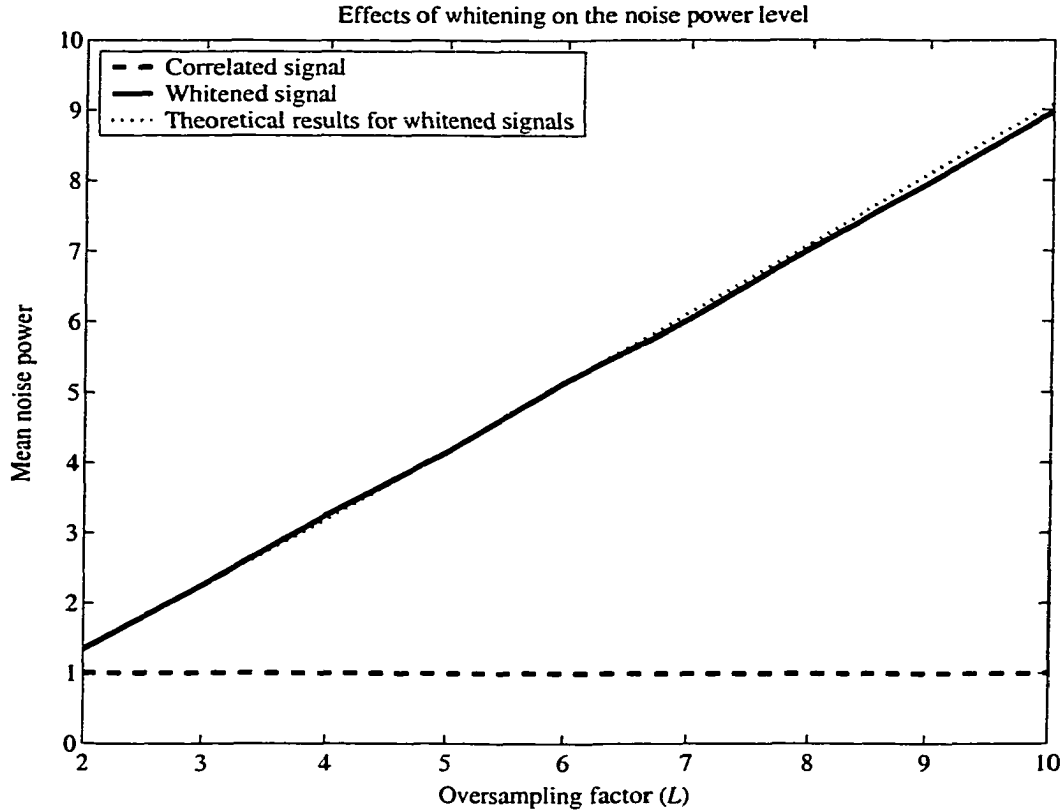


Figure 2.1. Effects of whitening on the noise power level. The noise enhancing effect of the whitening transformation is plotted for oversampling factors from 2 to 10. The result of (2.26) is included to show the agreement between theory and simulations.

The trade-off between noise enhancement and variance reduction makes the whitening transformation useful in cases of relatively large SNR. Although for weather radars the SNR of signals from storms is large, the formulation of the whitening transformation in effect ignores the presence of noise. As a consequence, its use under low SNR conditions will result in significant noise enhancement given by (2.21).

An alternative is to relax the whitening requirements and select a transformation such that the output noise power is also minimized. A transformation that is optimized based on the minimum mean-square error (MMSE) criterion accomplishes the desired goal. The

analysis of this technique is deferred until Chapter 5.

In the following two chapters we will focus on the application of the whitening transformation to the problem of efficient estimation of Doppler spectral moments and polarimetric variables.

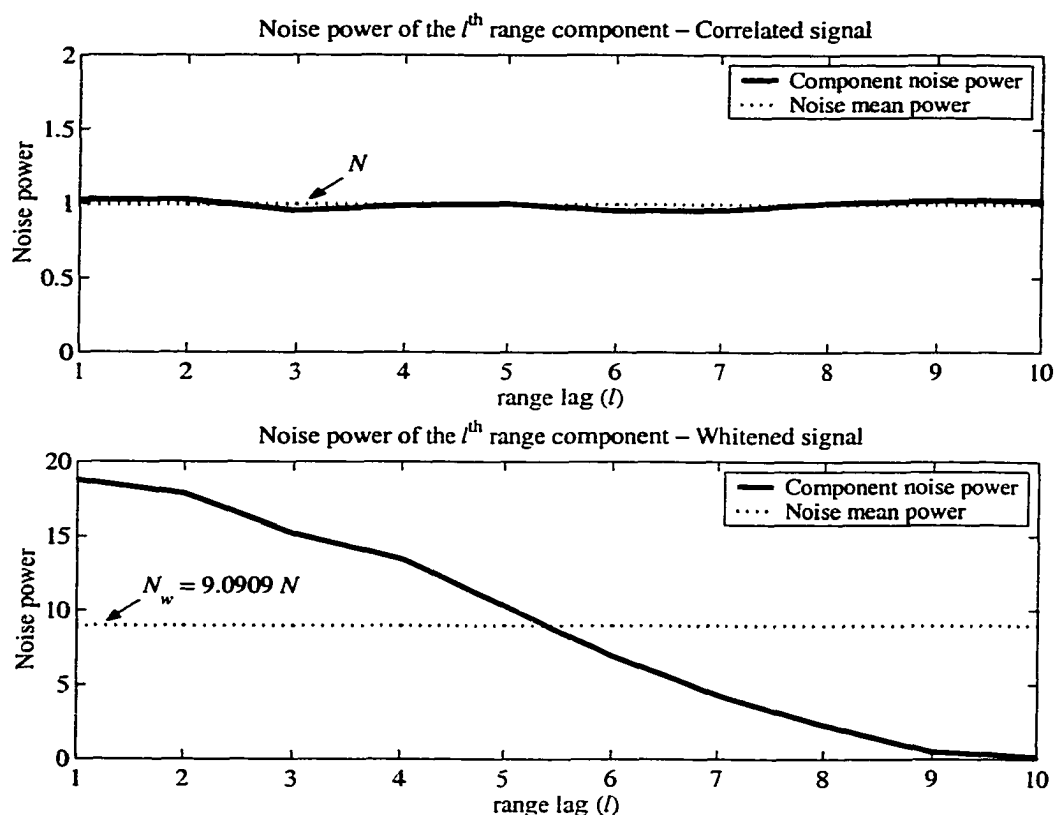


Figure 2.2. Noise power of correlated (top) and whitened (bottom) observations along range time. Dashed lines are at the mean power levels for each case. The predicted enhancement factor of 9.0909 ($L = 10$) is verified through simulations.

3. SPECTRAL MOMENT ESTIMATION

This chapter covers the application of the whitening transformation to the estimation of the Doppler spectrum and its first three moments for weather signals. Whitening-transformation-based (WTB) estimators of weather signal power, Doppler mean velocity, and Doppler spectrum width are discussed in detail. Special importance is given to the statistical performance (bias and variance) of the WTB estimators compared with the case in which the oversampled data are not whitened. Variance reduction factors are derived and theoretical developments are verified through computer simulations.

3.1. Estimation of Signal Power

Weather signal power, or the zeroth moment of the Doppler spectrum, can be related to liquid water content or precipitation rate in the resolution volume (Doviak and Zmic 1993). In this section the usual power estimator (1.23) is extended to handle oversampled signals. The simpler noiseless case is examined first, as the assumption of high SNR leads to compact and meaningful results. Further, weather radar signals from appreciable precipitation are typically much stronger than noise. The noisy case is studied next to make evident the noise-enhancing effect of the whitening transformation discussed in the previous chapter. In both cases, the performance of the power estimator is compared on whitened and correlated (non-whitened) samples.

3.1.1. Noiseless Case

3.1.1.1 *Correlated Samples*

A straightforward extension of the usual power estimator applied to oversampled signals

is given by

$$\hat{S}_{corr} = \frac{1}{LM} \sum_{l=0}^{L-1} \sum_{m=0}^{M-1} |V(l, m)|^2, \quad (3.1)$$

where the subscript “corr” indicates that the power is derived from correlated (non-whitened) samples. In (3.1) $V(l, m)$ is the oversampled (correlated) weather signal, L is the oversampling factor, and M is the number of samples (pulses). This estimator is unbiased because

$$Bias\{\hat{S}_{corr}\} = E[\hat{S}_{corr}] - S = \frac{1}{LM} \sum_{l=0}^{L-1} \sum_{m=0}^{M-1} E[|V(l, m)|^2] - S = 0. \quad (3.2)$$

The variance of the estimator in (3.1) can be computed as

$$\begin{aligned} Var\{\hat{S}_{corr}\} &= E[\hat{S}_{corr}^2] - S^2 \\ &= \frac{1}{L^2 M^2} \sum_{l=0}^{L-1} \sum_{m=0}^{M-1} \sum_{l'=0}^{L-1} \sum_{m'=0}^{M-1} E[V^*(l, m)V(l, m)V^*(l', m')V(l', m')] - S^2, \end{aligned} \quad (3.3)$$

where the expectation operation in this expression can be simplified as

$$\begin{aligned} E[V^*(l, m)V(l, m)V^*(l', m')V(l', m')] &= \\ &= E[V^*(l, m)V(l, m)]E[V^*(l', m')V(l', m')] + E[V^*(l, m)V(l', m')]E[V^*(l', m')V(l, m)] \\ &= R_V(0, 0)R_V(0, 0) + R_V(l'-l, m'-m)R_V(l-l', m-m') \\ &= [R_V(0, 0)]^2 + |R_V(l'-l, m'-m)|^2 \\ &= S^2 + |R_V(l'-l, m'-m)|^2. \end{aligned} \quad (3.4)$$

Introducing (3.4) into (3.3) produces

$$Var\{\hat{S}_{corr}\} = \frac{1}{L^2 M^2} \sum_{l=0}^{L-1} \sum_{m=0}^{M-1} \sum_{l'=0}^{L-1} \sum_{m'=0}^{M-1} |R_V(l'-l, m'-m)|^2. \quad (3.5)$$

The two-dimensional autocorrelation function R_V in (3.5) can be decomposed as the

product of the autocorrelation along range time $R_V^{(R)}$ and the autocorrelation along sample time $R_V^{(T)}$; i.e., $R_V(l, m) = R_V^{(R)}(l)R_V^{(T)}(m)$. In addition, by a change of variables (3.5) reduces to

$$\text{Var}\{\hat{S}_{corr}\} = \frac{S^2}{L^2 M^2} \sum_{l=-L+1}^{L-1} (L-|l|) |\rho_V^{(R)}(l)|^2 \sum_{m=-M+1}^{M-1} (M-|m|) |\rho_V^{(T)}(m)|^2, \quad (3.6)$$

where $\rho_V^{(R)}$ and $\rho_V^{(T)}$ are the correlation coefficients corresponding to $R_V^{(R)}$ and $R_V^{(T)}$, respectively. For a Gaussian sample-time correlation as in (1.1), the magnitude of the sample-time normalized correlation coefficient is

$$|\rho_V^{(T)}(m)| = e^{-8(\pi\sigma_v T_s / \lambda)^2} = e^{-2(\pi\sigma_{vn} m)^2}, \quad (3.7)$$

where $\sigma_{vn} = 2\sigma_v T_s / \lambda$ is the normalized spectrum width. With this assumption and for the usual range of the product $M\sigma_{vn}$, the second summation in (3.6) can be approximated as

$$\sum_{m=-M+1}^{M-1} \frac{M-|m|}{M^2} |\rho_V^{(T)}(m)|^2 \approx \int_{-\infty}^{\infty} \frac{M-|x|}{M^2} e^{-(2\pi\sigma_{vn} x)^2} dx \approx \frac{1}{2M\sigma_{vn}\sqrt{\pi}}. \quad (3.8)$$

The first summation in (3.6) can be rewritten using the identity

$$\sum_{l=-L+1}^{L-1} (L-|l|) R_1(l) R_2^*(l) = \text{tr}\{\mathbf{C}_1 \mathbf{C}_2\}, \quad (3.9)$$

where \mathbf{C}_1 and \mathbf{C}_2 are the correlation matrices corresponding to the correlation functions R_1 and R_2 , respectively. Using (3.8) and (3.9), (3.6) reduces to

$$\text{Var}\{\hat{S}_{corr}\} = \frac{S^2}{2M\sigma_{vn}\sqrt{\pi}} \frac{\text{tr}\{[\mathbf{C}_V^{(R)}]^2\}}{L^2}. \quad (3.10)$$

Recall that the normalized correlation matrix $\mathbf{C}_V^{(R)}$ is defined as the Toeplitz Hermitian

matrix of (2.10), and that $\rho_v^{(R)}$, which depends on the transmitted pulse shape and receiver impulse response, is given in (2.8).

An ideal transmitter/receiver system is defined as having a rectangular transmitter pulse envelope and an infinite-bandwidth receiver filter (consideration of a real system is deferred to Chapter 6). The correlation matrix corresponding to such system can be obtained from the correlation coefficient of (2.9). It is easy to show that

$$\text{tr}\{[\mathbf{C}_v^{(R)}]^2\} = \frac{L^2 + 1}{2}, \text{ hence, from (3.10) the normalized standard error for the ideal}$$

system is

$$\frac{SD\{\hat{S}_{corr}\}}{S} = \left(\frac{L^2 + 1}{4ML^2\sigma_{vn}\sqrt{\pi}} \right)^{1/2}. \quad (3.11)$$

For $L = 1$ (no oversampling), large M , and $\sigma_{vn} \ll 1$, (3.11) becomes equation (6.12) in Doviak and Zrnic (1993).

3.1.1.2 Whitened Samples

As before, the power estimator for oversampled signals is given by

$$\hat{S}_{whitened} = \frac{1}{LM} \sum_{l=0}^{L-1} \sum_{m=0}^{M-1} |X(l, m)|^2; \quad (3.12)$$

however, in this case $X(l, m)$ is the whitened oversampled weather signal obtained as

$$X(l, m) = \sum_{j=0}^{L-1} w_{l,j} V(j, m), \quad (3.13)$$

where $w_{l,j}$ are the entries of the whitening transformation matrix \mathbf{W} . This estimator is unbiased, that is

$$\text{Bias}\{\hat{S}_{\text{whitened}}\} = E[\hat{S}_{\text{whitened}}] - S = \frac{1}{LM} \sum_{l=0}^{L-1} \sum_{m=0}^{M-1} E[|X(l, m)|^2] - S = 0, \quad (3.14)$$

because, as seen in (2.17), the whitening transformation preserves the total power of the original signal.

The variance of the estimator in (3.12) can be computed as in Section 3.1.1.1 to get an expression similar to (3.10); i.e.,

$$\text{Var}\{\hat{S}_{\text{whitened}}\} = \frac{S^2}{2M\sigma_{vn}\sqrt{\pi}} \frac{\text{tr}\{[\mathbf{C}_{\mathbf{x}}^{(R)}]^2\}}{L^2}. \quad (3.15)$$

The normalized correlation matrix in (3.15) can be computed by recalling that due to the whitening transformation $\mathbf{X} = \mathbf{W}\mathbf{V}$, then

$$\mathbf{C}_{\mathbf{x}}^{(R)} = \mathbf{W}\mathbf{C}_{\mathbf{v}}^{(R)}\mathbf{W}^{*T} = (\mathbf{H}^{-1})(\mathbf{H}\mathbf{H}^{*T})(\mathbf{H}^{-1})^{*T} = \mathbf{I}, \quad (3.16)$$

and the data is whitened along range, as expected. Therefore, $\text{tr}\{[\mathbf{C}_{\mathbf{x}}^{(R)}]^2\} = \text{tr}\{\mathbf{I}\} = L$,

$$\text{Var}\{\hat{S}_{\text{whitened}}\} = \frac{S^2}{2ML\sigma_{vn}\sqrt{\pi}}, \quad (3.17)$$

and the normalized standard deviation [compare with (3.11)] is

$$\frac{SD\{\hat{S}_{\text{whitened}}\}}{S} = \left(\frac{1}{2ML\sigma_{vn}\sqrt{\pi}} \right)^{1/2}. \quad (3.18)$$

3.1.1.3 Comparison

Figure 3.1 shows the fractional standard deviation for both correlated and whitened data as a function of the oversampling factor L . The fractional standard error in dB, which can be computed as $10\log_{10}[1 + SD(\hat{S})/S]$, is a quantity often used to assess or specify the

performance of power estimators. It is evident from this figure that the larger the oversampling factor, the better the performance of the WTB estimator. In this regard, the variance reduction factor (*VRF*) for the WTB power estimator can be computed as

$$VRF_{Power} = \frac{Var\{\hat{S}_{corr}\}}{Var\{\hat{S}_{whitened}\}} = \frac{tr\{[C_v^{(R)}]^2\}}{L}, \quad (3.19)$$

which for the ideal case reduces to

$$VRF_{Power} = \frac{L^2 + 1}{2L}. \quad (3.20)$$

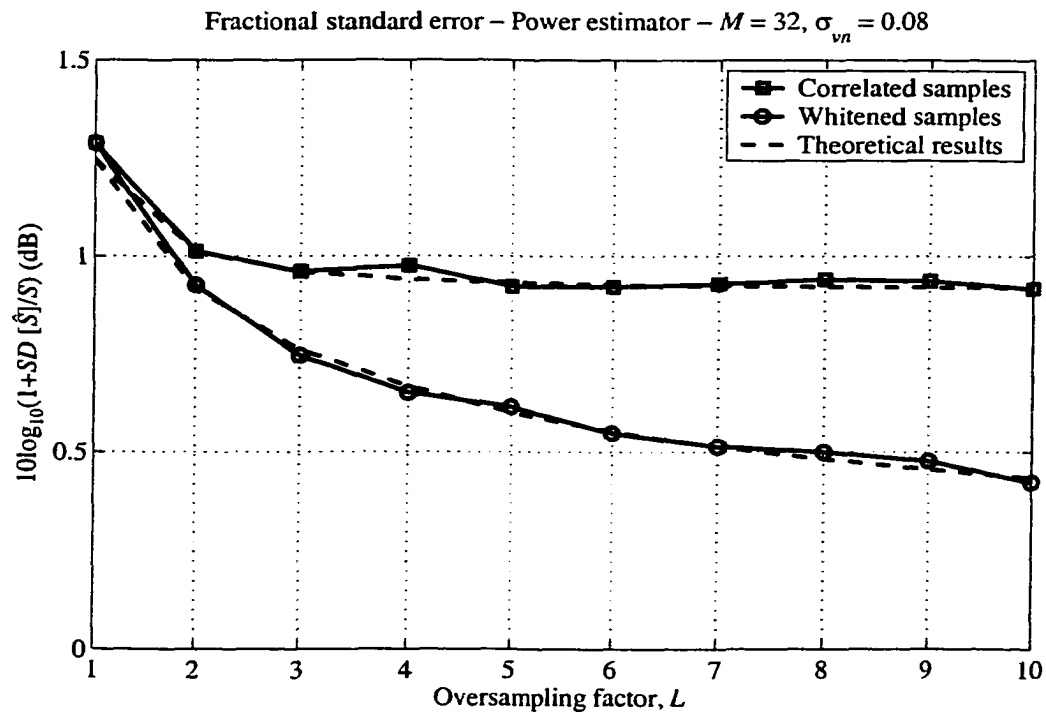


Figure 3.1. Fractional standard deviation for correlated and whitened data as a function of the oversampling factor L for the ideal case. The number of samples M is 32, the normalized spectrum width σ_{vn} is 0.08, and the SNR is very large. Both theoretical results (dashed line) and simulation results (solid line) are plotted.

As expected, the *VER* of the WTB power estimator is an increasing function of the oversampling factor. An interesting question arises: *What is the required number of samples for the power WTB estimator that yields the same errors as the regular power estimator assuming that both use the same oversampling factor and that the regular estimator uses M_{corr} samples?* Equating (3.10) and (3.17) with M_{corr} and $M_{whitened}$ samples, respectively, the following useful relation is obtained for the ideal case

$$M_{whitened} = \frac{LM_{corr}}{tr\{[\mathbf{C}_V^{(R)}]^2\}} = \left(\frac{2L}{L^2 + 1}\right)M_{corr}, \quad (3.21)$$

that is, approximately $L/2$ fewer samples are required by a WTB signal power estimator in order to preserve the performance of the power estimator on correlated data.

3.1.2. Noisy Case

3.1.2.1 Correlated Samples

The signal power estimator for oversampled signals in the presence of additive noise is given by

$$\hat{S}_{corr} = \frac{1}{LM} \sum_{l=0}^{L-1} \sum_{m=0}^{M-1} |V(l, m)|^2 - N, \quad (3.22)$$

where N is the noise power and, as before, $V(l, m)$ is the oversampled weather signal, L is the oversampling factor, and M the number of samples (pulses). This estimator is unbiased because

$$Bias\{\hat{S}_{corr}\} = E[\hat{S}_{corr}] - S = \frac{1}{LM} \sum_{l=0}^{L-1} \sum_{m=0}^{M-1} E[|V(l, m)|^2] - (S + N) = 0. \quad (3.23)$$

The variance of the estimator in (3.22) can be computed as

$$\begin{aligned}
Var\{\hat{S}_{corr}\} &= \frac{1}{L^2 M^2} \sum_{l=0}^{L-1} \sum_{m=0}^{M-1} \sum_{l'=0}^{L-1} \sum_{m'=0}^{M-1} E[V^*(l,m)V(l,m)V^*(l',m')V(l',m')] - \\
&\quad - \frac{2N}{LM} \sum_{l=0}^{L-1} \sum_{m=0}^{M-1} E[|V(l,m)|^2] + N^2 - S^2,
\end{aligned} \tag{3.24}$$

where the expectation operation in this expression can be simplified analogously as in Section 3.1.1 to get

$$\begin{aligned}
E[V^*(l,m)V(l,m)V^*(l',m')V(l',m')] &= \\
&= E[V^*(l,m)V(l,m)]E[V^*(l',m')V(l',m')] + E[V^*(l,m)V(l',m')]E[V^*(l',m')V(l,m)] \\
&= R_V(0,0)R_V(0,0) + R_V(l'-l, m'-m)R_V(l-l', m-m') \\
&= [R_V(0,0)]^2 + |R_V(l'-l, m'-m)|^2 \\
&= (S+N)^2 + |R_V(l'-l, m'-m)|^2.
\end{aligned} \tag{3.25}$$

Hence,

$$Var\{\hat{S}_{corr}\} = \frac{1}{L^2 M^2} \sum_{l=0}^{L-1} \sum_{m=0}^{M-1} \sum_{l'=0}^{L-1} \sum_{m'=0}^{M-1} |R_V(l'-l, m'-m)|^2. \tag{3.26}$$

The autocorrelation of $V(l,m)$, R_V , can be decomposed into a sum of the autocorrelation of the signal R_{V_s} and the autocorrelation of the noise R_{V_N} . In addition, as shown in Section 3.1.1, each two-dimensional autocorrelation function can be written as the product of the corresponding autocorrelation along range time [indicated by the superscript (R)] and autocorrelation along sample time [indicated by the superscript (T)], i.e., $R_V(l,m) = R_{V_s}(l,m) + R_{V_N}(l,m) = R_{V_s}^{(R)}(l)R_{V_s}^{(T)}(m) + R_{V_N}^{(R)}(l)R_{V_N}^{(T)}(m)$. By doing a change of variables in (3.26), the variance of power estimates on correlated samples becomes

$$\begin{aligned}
Var\{\hat{S}_{corr}\} = & \frac{S^2}{L^2 M^2} \sum_{l=-L+1}^{L-1} (L-|l|) |\rho_{V_s}^{(R)}(l)|^2 \sum_{m=-M+1}^{M-1} (M-|m|) |\rho_{V_s}^{(T)}(m)|^2 + \\
& + \frac{2NS}{L^2 M^2} \sum_{l=-L+1}^{L-1} (L-|l|) \rho_{V_s}^{(R)}(l) \rho_{V_N}^{(R)}(l) \sum_{m=-M+1}^{M-1} (M-|m|) \rho_{V_s}^{(T)}(m) \rho_{V_N}^{(T)}(m) + \\
& + \frac{N^2}{L^2 M^2} \sum_{l=-L+1}^{L-1} (L-|l|) |\rho_{V_N}^{(R)}(l)|^2 \sum_{m=-M+1}^{M-1} (M-|m|) |\rho_{V_N}^{(T)}(m)|^2.
\end{aligned} \tag{3.27}$$

For a Gaussian sample-time correlation as in (1.1) and white noise the following applies:

$$|\rho_{V_s}^{(T)}(m)| = e^{-2(\pi\sigma_{vn}m)^2}, \tag{3.28}$$

$$\rho_{V_N}^{(R)}(l) = \delta(l), \tag{3.29}$$

and

$$\rho_{V_N}^{(T)}(m) = \delta(m). \tag{3.30}$$

Hence, by using (3.8) and (3.9), (3.27) reduces to

$$Var\{\hat{S}_{corr}\} = \frac{S^2}{2M\sigma_{vn}\sqrt{\pi}} \frac{tr\{[\mathbf{C}_{V_s}^{(R)}]^2\}}{L^2} + \frac{2SN + N^2}{ML}. \tag{3.31}$$

From the previous expression, the normalized standard deviation is

$$\frac{SD\{\hat{S}_{corr}\}}{S} = \frac{1}{\sqrt{M}} \left[\frac{tr\{[\mathbf{C}_{V_s}^{(R)}]^2\}}{2L^2\sigma_{vn}\sqrt{\pi}} + \frac{2}{L} \left(\frac{N}{S} \right) + \frac{1}{L} \left(\frac{N}{S} \right)^2 \right]^{1/2}; \tag{3.32}$$

further, for the correlation matrix corresponding to the ideal system, $tr\{[\mathbf{C}_{V_s}^{(R)}]^2\} = \frac{L^2 + 1}{2}$

and (3.32) reduces to

$$\frac{SD\{\hat{S}_{corr}\}}{S} = \frac{1}{\sqrt{M}} \left[\frac{L^2 + 1}{4L^2\sigma_{vn}\sqrt{\pi}} + \frac{2}{L} \left(\frac{N}{S} \right) + \frac{1}{L} \left(\frac{N}{S} \right)^2 \right]^{1/2}. \tag{3.33}$$

For $L = 1$ (no oversampling), large M , and $\sigma_{vn} \ll 1$, (3.33) is equivalent to equation (3) in

Sachidananda and Zmic (1985).

Figure 3.2 shows the normalized standard error of power estimates (3.22) versus the normalized spectrum width for several SNRs for the ideal case. It is evident from this plot that results of simulations and theory are in good agreement.

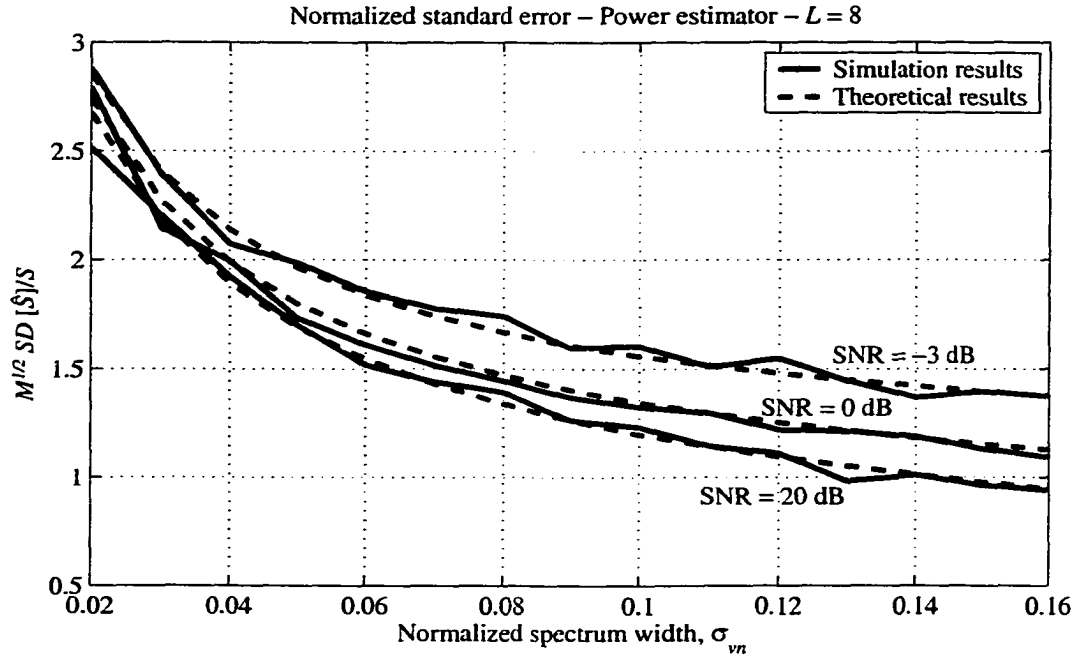


Figure 3.2. Normalized standard error for the power estimates on correlated data versus the normalized spectrum width σ_{vn} with the SNR as a parameter for the ideal case. The oversampling factor L is 8. Both theoretical results (dashed line) and simulation results (solid line) are plotted.

3.1.2.2 Whitened Samples

The power estimator for oversampled whitened signals in noise is given by

$$\hat{S}_{\text{whitened}} = \frac{1}{LM} \sum_{l=0}^{L-1} \sum_{m=0}^{M-1} |X(l, m)|^2 - N(NEF), \quad (3.34)$$

where NEF is the noise-enhancement factor as defined in (2.22), and $X(l, n)$ is the whitened oversampled weather signal as in (3.13).

The estimator in (3.34) is unbiased because

$$\begin{aligned} \text{Bias}\{\hat{S}_{\text{whitened}}\} &= E[\hat{S}_{\text{whitened}}] - S \\ &= \frac{1}{LM} \sum_{l=0}^{L-1} \sum_{m=0}^{M-1} E[|X(l, m)|^2] - [S + N(NEF)] = 0, \end{aligned} \quad (3.35)$$

as the whitening transformation preserves the total signal power and increases the noise power by the noise-enhancement factor.

The variance of the estimator in (3.34) can be computed as in Section 3.1.2.1 to get an expression like (3.27):

$$\begin{aligned} \text{Var}\{\hat{S}_{\text{whitened}}\} &= \frac{S^2}{L^2 M^2} \sum_{l=-L+1}^{L-1} (L-|l|) |\rho_{X_s}^{(R)}(l)|^2 \sum_{m=-M+1}^{M-1} (M-|m|) |\rho_{X_s}^{(T)}(m)|^2 + \\ &+ \frac{2NS}{L^2 M^2} \sum_{l=-L+1}^{L-1} (L-|l|) \rho_{X_s}^{(R)}(l) \rho_{X_N}^{(R)}(l) \sum_{m=-M+1}^{M-1} (M-|m|) \rho_{X_s}^{(T)}(m) \rho_{X_N}^{(T)}(m) + \\ &+ \frac{N^2}{L^2 M^2} \sum_{l=-L+1}^{L-1} (L-|l|) |\rho_{X_N}^{(R)}(l)|^2 \sum_{m=-M+1}^{M-1} (M-|m|) |\rho_{X_N}^{(T)}(m)|^2. \end{aligned} \quad (3.36)$$

For a Gaussian sample-time correlation $|\rho_{X_s}^{(T)}(m)|$ is as in (3.28), and for white noise $\rho_{X_N}^{(T)}(m) = \delta(m)$. In addition, by using (3.8) and (3.9)

$$\text{Var}\{\hat{S}_{\text{whitened}}\} = \frac{S^2}{2M\sigma_{vn}\sqrt{\pi}} \frac{\text{tr}\{[\mathbf{C}_{X_s}^{(R)}]^2\}}{L^2} + \frac{2NS}{M} \frac{\text{tr}\{\mathbf{C}_{X_s}^{(R)}\mathbf{C}_{X_N}^{(R)}\}}{L^2} + \frac{N^2}{M} \frac{\text{tr}\{[\mathbf{C}_{X_N}^{(R)}]^2\}}{L^2}. \quad (3.37)$$

Due to the presence of additive noise, the whitened signal \mathbf{X} can be decomposed into two components corresponding to the signal and noise contributions. That is,

$$\mathbf{X} = \mathbf{X}_S + \mathbf{X}_N = \mathbf{W}\mathbf{V}_S + \mathbf{W}\mathbf{V}_N. \quad (3.38)$$

Therefore, the correlation matrix for the whitened signal along range time is

$$\mathbf{C}_{\mathbf{x}_s}^{(R)} = \mathbf{W}\mathbf{C}_{\mathbf{v}_s}^{(R)}\mathbf{W}^{*T} = (\mathbf{H}^{-1})(\mathbf{H}\mathbf{H}^{*T})(\mathbf{H}^{-1})^{*T} = \mathbf{I}, \quad (3.39)$$

and the data is whitened along range, as expected. On the other hand, for the noise that was originally white

$$\mathbf{C}_{\mathbf{x}_n}^{(R)} = \mathbf{W}\mathbf{C}_{\mathbf{v}_n}^{(R)}\mathbf{W}^{*T} = (\mathbf{H}^{-1})\mathbf{I}(\mathbf{H}^{-1})^{*T} = (\mathbf{H}\mathbf{H}^{*T})^{-1} = [\mathbf{C}_{\mathbf{v}_s}^{(R)}]^{-1}. \quad (3.40)$$

Then,

$$\text{Var}\{\hat{S}_{\text{whitened}}\} = \frac{S^2}{2ML\sigma_{vn}\sqrt{\pi}} + \frac{2NS}{M} \frac{\text{tr}\{[\mathbf{C}_{\mathbf{v}_s}^{(R)}]^{-1}\}}{L^2} + \frac{N^2}{M} \frac{\text{tr}\{[\mathbf{C}_{\mathbf{v}_s}^{(R)}]^{-2}\}}{L^2}, \quad (3.41)$$

and the fractional standard deviation becomes

$$\frac{SD\{\hat{S}_{\text{whitened}}\}}{S} = \frac{1}{\sqrt{M}} \left[\frac{1}{2L\sigma_{vn}\sqrt{\pi}} + 2 \frac{\text{tr}\{[\mathbf{C}_{\mathbf{v}_s}^{(R)}]^{-1}\}}{L^2} \left(\frac{N}{S}\right) + \frac{\text{tr}\{[\mathbf{C}_{\mathbf{v}_s}^{(R)}]^{-2}\}}{L^2} \left(\frac{N}{S}\right)^2 \right]^{1/2}. \quad (3.42)$$

For the correlation matrix corresponding to the ideal system and L greater than one², it is

$$\text{not difficult to show that } \text{tr}\{[\mathbf{C}_{\mathbf{v}_s}^{(R)}]^{-1}\} = \frac{L^3}{L+1} \text{ and } \text{tr}\{[\mathbf{C}_{\mathbf{v}_s}^{(R)}]^{-2}\} = \frac{L^3(3L^2+2L-3)}{2(L+1)^2},$$

therefore (3.42) reduces to

$$\frac{SD\{\hat{S}_{\text{whitened}}\}}{S} = \frac{1}{\sqrt{M}} \left[\frac{1}{2L\sigma_{vn}\sqrt{\pi}} + \frac{2L}{(L+1)} \left(\frac{N}{S}\right) + \frac{L(3L^2+2L-3)}{2(L+1)^2} \left(\frac{N}{S}\right)^2 \right]^{1/2}. \quad (3.43)$$

Figure 3.3 shows the normalized error of power estimates (3.34) versus the normalized

² For the case of $L=1$, the normalized correlation matrix reduces to a scalar, i.e., $\mathbf{C}_{\mathbf{v}_s}=1$ and $\text{tr}\{[\mathbf{C}_{\mathbf{v}_s}]^{-1}\} = \text{tr}\{[\mathbf{C}_{\mathbf{v}_s}]^{-2}\} = 1$. These results do not agree with the general formulas for $\text{tr}\{[\mathbf{C}_{\mathbf{v}_s}]^{-1}\}$ and $\text{tr}\{[\mathbf{C}_{\mathbf{v}_s}]^{-2}\}$ as functions of the oversampling factor L ; however, the case $L=1$ is meaningless as it implies no oversampling. Throughout the remainder of this dissertation $L > 1$ is assumed unless otherwise noted.

spectrum width for several values of SNR for the ideal case. The agreement between theory and simulations is again evident from these plots. By comparing the results in Figure 3.3 to the ones in Figure 3.2 the noise-enhancement effect discussed in Chapter 2 becomes evident. The increase in the standard deviation of power estimates on whitened samples for low values of SNR compared to the results on correlated data is an indication of this phenomenon. Whitened samples exhibit an effective SNR equivalent to the original SNR reduced by the noise-enhancement factor NEF defined in (2.22).

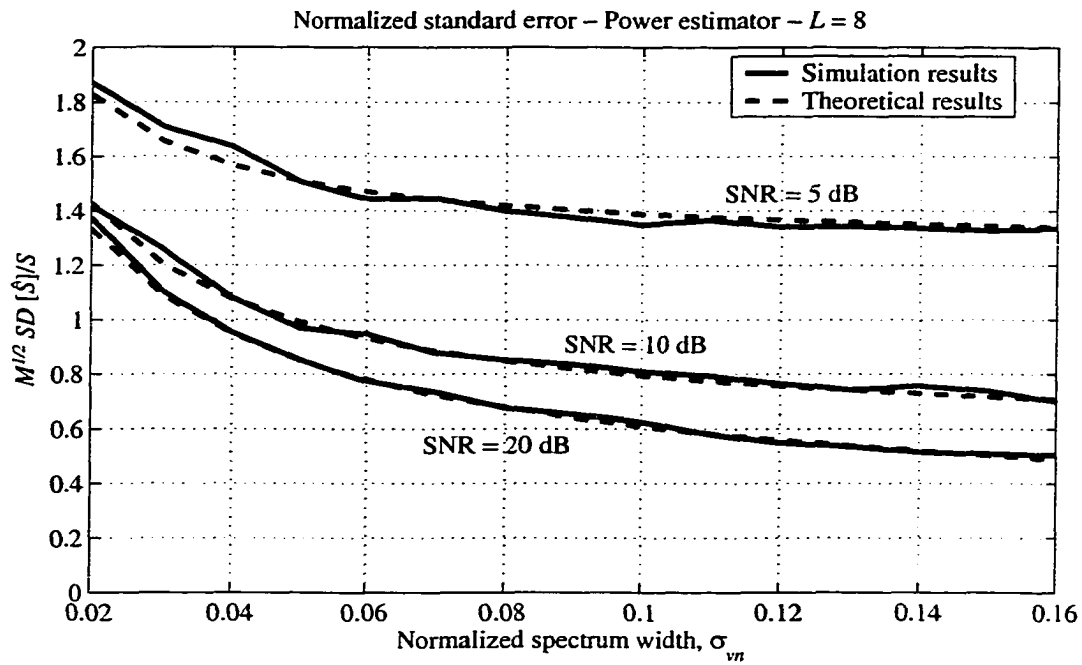


Figure 3.3. Normalized standard error for the power estimates on whitened data versus the normalized spectrum width σ_{vn} with the signal-to-noise ratio (SNR) as a parameter for the ideal case. The oversampling factor L is 8. Both theoretical results (dashed line) and simulation results (solid line) are plotted.

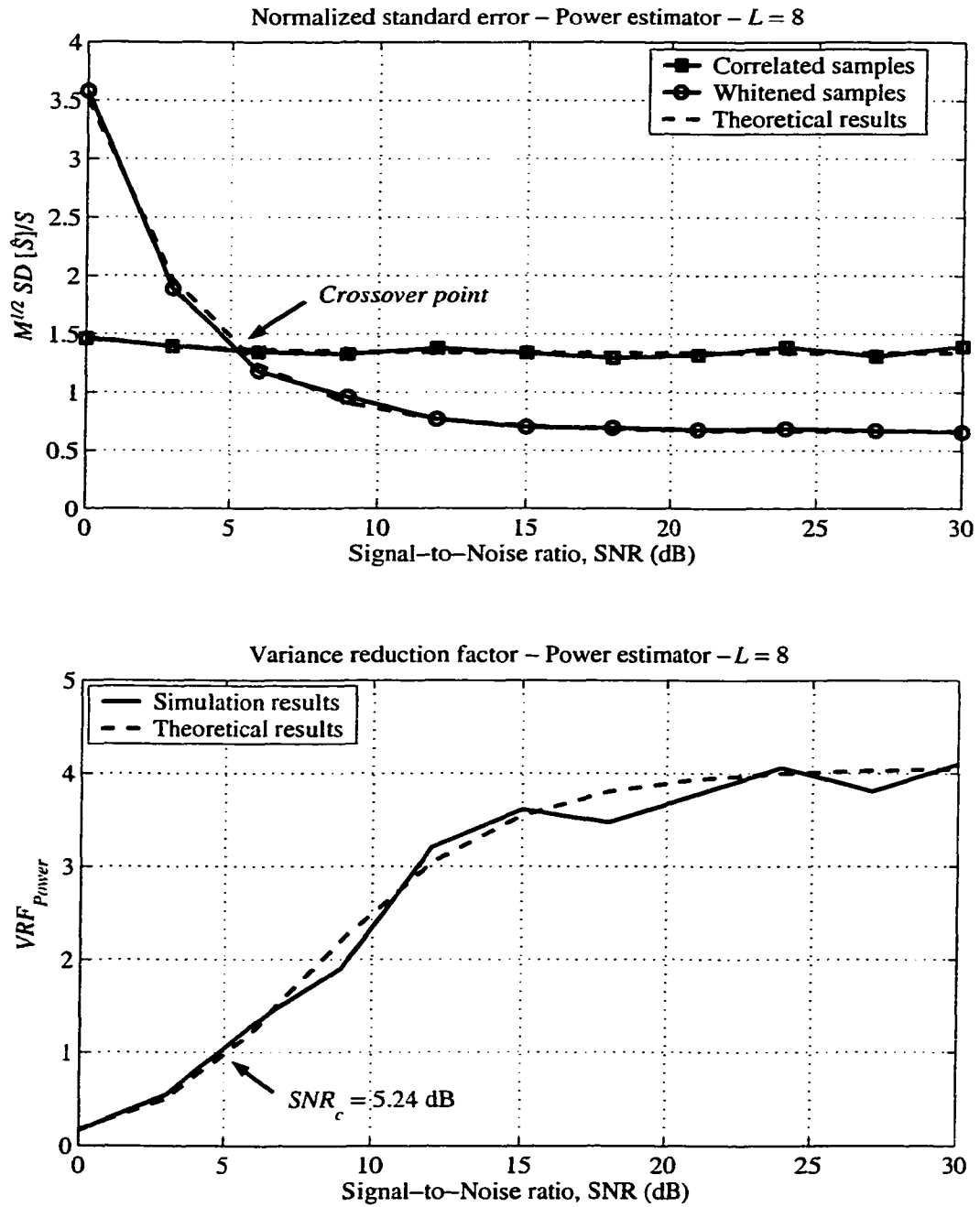


Figure 3.4. (Top) Standard deviation for the power estimator on both correlated and whitened data as a function of the signal-to-noise ratio (SNR) for the ideal case. The oversampling factor L is 8, the normalized spectrum width σ_{v_n} is 0.08. (Bottom) Variance reduction factor for the same parameters. Theoretical results (dashed line) and simulation results (solid line) are plotted in both cases.

3.1.2.3 Comparison

Figure 3.4 (top) shows the normalized standard deviation for both correlated and whitened data as a function of the signal-to-noise ratio where it is evident that the performance of the WTB estimator worsens as the SNR decreases due to the noise-enhancement effect inherent to the whitening transformation. As in Section 3.1.1.3, the variance reduction factor (*VRF*) for the WTB power estimator can be computed as

$$VRF_{Power} = \frac{Var\{\hat{S}_{corr}\}}{Var\{\hat{S}_{whitened}\}}, \quad (3.44)$$

which for the ideal case turns into

$$VRF_{Power} = \frac{\frac{1}{2\sigma_{vn}\sqrt{\pi}} \frac{L^2+1}{2L} + 2\left(\frac{N}{S}\right) + \left(\frac{N}{S}\right)^2}{\frac{1}{2\sigma_{vn}\sqrt{\pi}} + \frac{2L^2}{L+1}\left(\frac{N}{S}\right) + \frac{L^2(3L^2+2L-3)}{2(L+1)^2}\left(\frac{N}{S}\right)^2}. \quad (3.45)$$

Simulation results agree with (3.45) as shown in Figure 3.4 (bottom). It is of practical significance to determine the value of SNR for which the variance of power estimates obtained from whitened samples is equal to the variance of power estimates from correlated samples (see Figure 3.4). This is because WTB estimators should be utilized only for SNRs greater than or equal to SNR_c . By definition, the crossover point SNR_c is found by equating the *VRF* to one:

$$\left[\frac{(L-1)^2}{2L} \frac{1}{2\sigma_{vn}\sqrt{\pi}} \right] (SNR_c)^2 - \left[2 \frac{L^2-L-1}{L+1} \right] (SNR_c) - \left[\frac{3L^4+2L^3-5L^2-4L-2}{2(L+1)^2} \right] = 0. \quad (3.46)$$

For the parameters of Figure 3.4, the solution to (3.46) is $SNR_c = 5.24$ dB, which agrees with the results in that figure.

It is interesting to note that the crossover SNR depends only on the normalized spectrum width for a given oversampling factor and not on the number of samples M . Solving for SNR_c in the quadratic equation (3.46)

$$SNR_c = \alpha\sigma_{vn} + \sqrt{\beta\sigma_{vn}^2 + \gamma\sigma_{vn}}, \quad (3.47)$$

where α , β , and γ are constants that depend only on the oversampling factor L . Therefore, the crossover SNR is directly proportional to the normalized spectrum width, so the larger the spectrum width, the less “useful” the WTB estimator. This is because weather signals look more like white noise as the spectrum width increases, and the noise-enhancing effect becomes more pronounced with noisy signals. In other words, for larger spectrum widths it takes an even larger SNR for the WTB estimator to start performing better than the one operating on correlated samples.

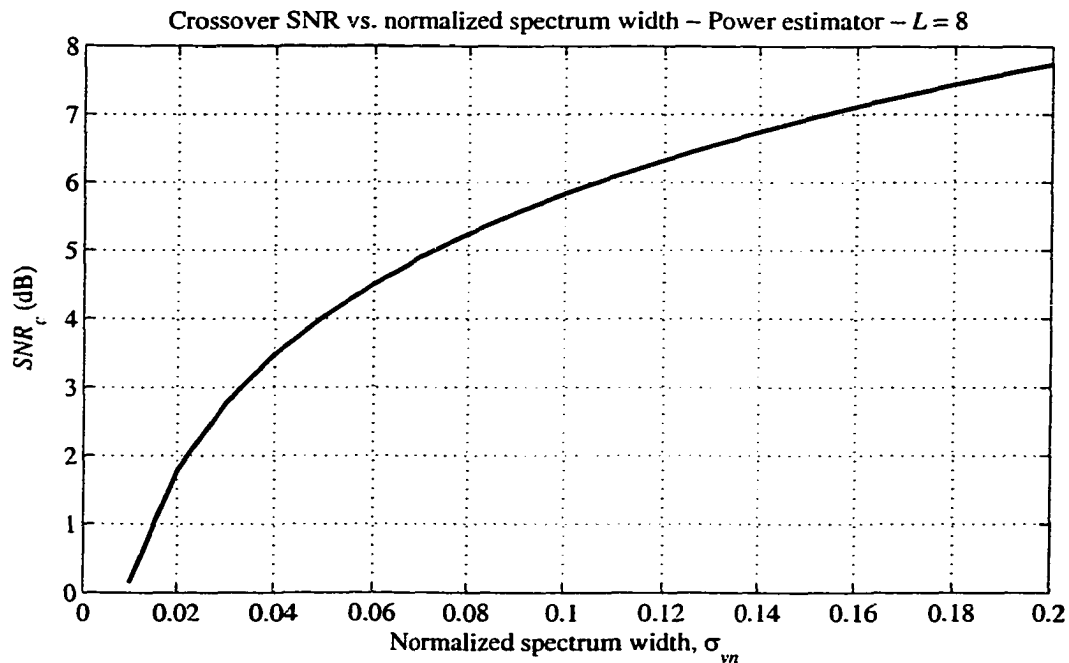


Figure 3.5. Crossover signal-to-noise ratio SNR_c versus the normalized spectrum width for the power estimator in an ideal system. The oversampling factor L is 8.

Figure 3.5 shows the crossover SNR as a function of the normalized spectrum width for the ideal case.

3.2. Estimation of Mean Doppler Velocity

Mean Doppler velocity or the first moment of the Doppler spectrum is essentially the average air motion toward or away from the radar along the direction of the beam. As discussed in Section 1.3, the pulse-pair estimator in (1.30) calculates the Doppler velocity from estimates of the autocorrelation function at lag T_s (i.e., lag one). In what follows that estimator is extended to oversampled data of correlated and whitened samples.

3.2.1. Correlated Samples

The mean Doppler velocity estimator applied to oversampled correlated data is

$$\hat{v}_{corr} = -\frac{\lambda}{4\pi T_s} \arg\{\hat{R}_V^{(T)}(1)\}, \quad (3.48)$$

where lag-one sample-time autocorrelation function for the oversampled correlated signal $V(l, n)$ is estimated as

$$\hat{R}_V^{(T)}(1) = \frac{1}{L} \sum_{l=0}^{L-1} \hat{R}_{V_l}^{(T)}(1) = \frac{1}{L(M-1)} \sum_{l=0}^{L-1} \sum_{m=0}^{M-2} V^*(l, m) V(l, m+1). \quad (3.49)$$

Because (3.49) is an asymptotically unbiased estimator of the autocorrelation for lag one, the Doppler velocity estimator in (3.48) is also asymptotically unbiased. Perturbation analysis is useful to compute the variance of nonlinear estimators such as (3.48). Assumptions for the validity of the perturbation analysis are that the probability densities of the estimates are smooth functions close to the mean and that the perturbations are not

excessive. Under these conditions it can be proved (Zrníc 1977) that

$$\text{Var}\{\hat{v}_{corr}\} = \left(\frac{\lambda}{4\pi T_s}\right)^2 \frac{1}{2} \text{Re} \left\{ E \left[\left| \frac{\hat{R}_V^{(T)}(1)}{R_V^{(T)}(1)} \right|^2 \right] - E \left[\left(\frac{\hat{R}_V^{(T)}(1)}{R_V^{(T)}(1)} \right)^2 \right] \right\}. \quad (3.50)$$

Using a similar analysis as in Section 3.1, the expectation operations inside (3.50) can be computed as

$$\begin{aligned} E \left[\left| \hat{R}_V^{(T)}(1) \right|^2 \right] &= \frac{1}{L^2 (M-1)^2} \sum_{l=0}^{L-1} \sum_{m=0}^{M-2} \sum_{l'=0}^{L-1} \sum_{m'=0}^{M-2} E \left[V^*(l, m) V(l, m+1) V(l', m') V^*(l', m'+1) \right] \\ &= \left| R_V^{(T)}(1) \right|^2 + \frac{1}{L^2 (M-1)^2} \sum_{l=-L+1}^{L-1} \sum_{m=-M+2}^{M-2} (L-|l|)(M-1-|m|) \left| R_V(l, m) \right|^2, \end{aligned} \quad (3.51)$$

and

$$\begin{aligned} E \left[\left(\hat{R}_V^{(T)}(1) \right)^2 \right] &= \frac{1}{L^2 (M-1)^2} \sum_{l=0}^{L-1} \sum_{m=0}^{M-2} \sum_{l'=0}^{L-1} \sum_{m'=0}^{M-2} E \left[V^*(l, m) V(l, m+1) V^*(l', m') V(l', m'+1) \right] \\ &= \left[R_V^{(T)}(1) \right]^2 + \frac{1}{L^2 (M-1)^2} \sum_{l=-L+1}^{L-1} \sum_{m=-M+2}^{M-2} (L-|l|)(M-1-|m|) R_V(l, m+1) R_V^*(l, m-1). \end{aligned} \quad (3.52)$$

As discussed in Section 3.1.2, the autocorrelation of $V(l, n)$ can be decomposed as

$$R_V(l, m) = R_{V_s}(l, m) + R_{V_n}(l, m) = R_{V_s}^{(R)}(l) R_{V_s}^{(T)}(m) + R_{V_n}^{(R)}(l) R_{V_n}^{(T)}(m), \quad (3.53)$$

and with the assumptions of Gaussian sample-time autocorrelation and white noise the following applies:

$$R_{V_s}^{(T)}(m) = S e^{-2(\pi \sigma_m m)^2} e^{-j 2 \pi \nu_n m}, \quad (3.54)$$

$$R_{V_n}^{(R)}(l) = \delta(l), \quad (3.55)$$

and

$$R_{V_N}^{(T)}(m) = N\delta(m) . \quad (3.56)$$

Using (3.8), (3.9) and the previous results (3.50) reduces to

$$\begin{aligned} Var\{\hat{v}_{corr}\} = & \left(\frac{\lambda}{4\pi T_s}\right)^2 \frac{1}{M-1} \left\{ \frac{e^{(2\pi\sigma_m)^2} - 1}{4\sigma_{vn}\sqrt{\pi}} \frac{tr\{[C_{V_s}^{(R)}]^2\}}{L^2} + \right. \\ & \left. + \frac{2\sinh[(2\pi\sigma_{vn})^2]}{L} \left(\frac{N}{S}\right) + \frac{e^{(2\pi\sigma_m)^2}}{2L} \left(\frac{N}{S}\right)^2 \right\} . \end{aligned} \quad (3.57)$$

For $L = 1$, large M , and $\sigma_{vn} \ll 1$, (3.57) is equivalent to equation (6.21) of Doviak and Zrnic (1993) for the case of $T = T_s$. For the ideal case, the normalized standard deviation can be obtained from (3.57) as

$$\begin{aligned} \frac{SD\{\hat{v}_{corr}\}}{2v_a} = & \frac{1}{2\pi\sqrt{M-1}} \left\{ \frac{e^{(2\pi\sigma_m)^2} - 1}{4\sigma_{vn}\sqrt{\pi}} \frac{L^2 + 1}{2L^2} + \right. \\ & \left. + \frac{2\sinh[(2\pi\sigma_{vn})^2]}{L} \left(\frac{N}{S}\right) + \frac{e^{(2\pi\sigma_m)^2}}{2L} \left(\frac{N}{S}\right)^2 \right\}^{1/2} , \end{aligned} \quad (3.58)$$

where $v_a = \lambda/4T_s$ is the maximum unambiguous Doppler velocity.

Figure 3.6 shows the normalized standard deviation of Doppler velocity estimates (3.48) versus the normalized spectrum width for the ideal case and several values of SNR. Theoretical results are verified through simulations as in the previous cases. However, it is important to note that perturbation analysis results are accurate only if

$$2\pi M \sigma_{vn} \gg 1 \quad (3.59)$$

and

$$Me^{-(2\pi\sigma_{vn})^2} \gg \left(\frac{N}{S} + 1\right)^2 , \quad (3.60)$$

which is why theoretical curves do not match the results obtained from simulations very well when the spectrum width is small or the SNR is too low.

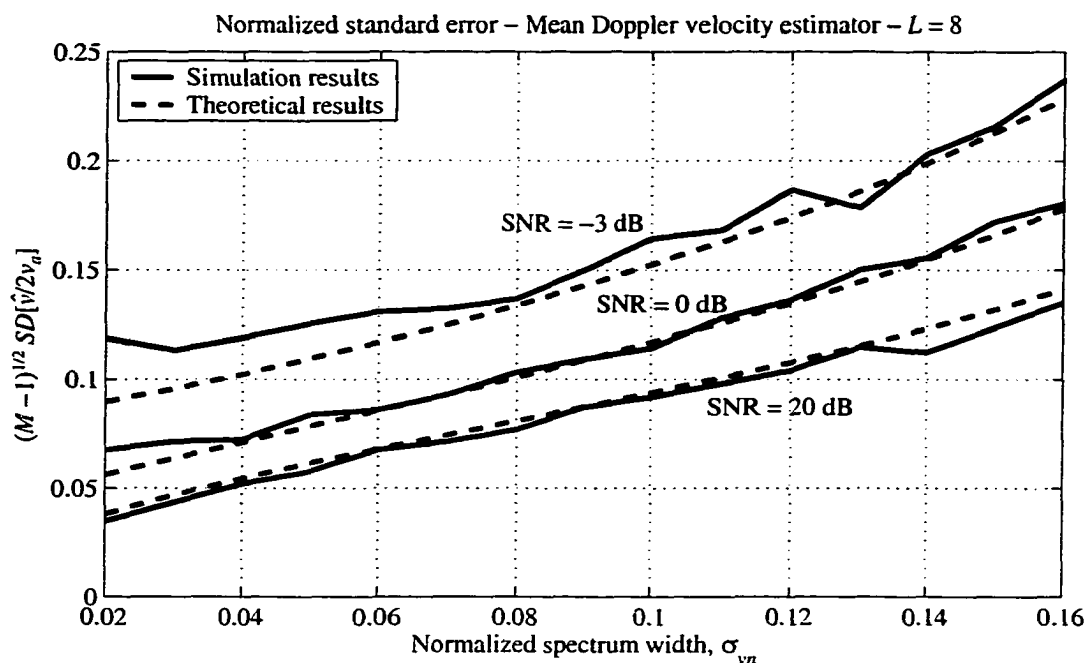


Figure 3.6. Normalized standard deviation of Doppler velocity estimates on correlated data versus the normalized spectrum width with the SNR as a parameter for the ideal case. The oversampling factor L is 8. Both theoretical results (dashed line) and simulation results (solid line) are plotted.

3.2.2. Whitened Samples

The mean Doppler velocity estimator applied to oversampled whitened data is

$$\hat{v}_{whitened} = -\frac{\lambda}{4\pi T_s} \arg\left\{\hat{R}_X^{(T)}(1)\right\}, \quad (3.61)$$

where the lag-one sample-time autocorrelation function for the oversampled whitened signal $X(l, n)$ is estimated as

$$\hat{R}_X^{(T)}(1) = \frac{1}{L} \sum_{l=0}^{L-1} \hat{R}_{X_l}^{(T)}(1) = \frac{1}{L(M-1)} \sum_{l=0}^{L-1} \sum_{m=0}^{M-2} X^*(l, m) X(l, m+1). \quad (3.62)$$

For the same reasons as before, the Doppler velocity estimator in (3.61) is asymptotically unbiased, and its variance is given by

$$\text{Var}\{\hat{v}_{\text{whitened}}\} = \left(\frac{\lambda}{4\pi T_s}\right)^2 \frac{1}{2} \text{Re} \left\{ E \left[\left| \frac{\hat{R}_X^{(T)}(1)}{\hat{R}_V^{(T)}(1)} \right|^2 \right] - E \left[\left(\frac{\hat{R}_X^{(T)}(1)}{\hat{R}_V^{(T)}(1)} \right)^2 \right] \right\}. \quad (3.63)$$

Using a similar analysis as in Section 3.2.1 it is possible to obtain the variance of Doppler velocity estimates as

$$\begin{aligned} \text{Var}\{\hat{v}_{\text{whitened}}\} = & \left(\frac{\lambda}{4\pi T_s}\right)^2 \frac{1}{M-1} \left\{ \frac{e^{(2\pi\sigma_{vn})^2} - 1}{4L\sigma_{vn}\sqrt{\pi}} + 2 \sinh[(2\pi\sigma_{vn})^2] \frac{\text{tr}\{[\mathbf{C}_{V_s}^{(R)}]^{-1}\}}{L^2} \left(\frac{N}{S}\right) + \right. \\ & \left. + \frac{e^{(2\pi\sigma_{vn})^2}}{2} \frac{\text{tr}\{[\mathbf{C}_{V_s}^{(R)}]^{-2}\}}{L^2} \left(\frac{N}{S}\right)^2 \right\}. \end{aligned} \quad (3.64)$$

For the ideal case, the normalized standard deviation can be obtained using the identities of Section 3.1.2.2 from (3.64) as

$$\begin{aligned} \frac{SD\{\hat{v}_{\text{whitened}}\}}{2v_a} = & \frac{1}{2\pi\sqrt{M-1}} \left\{ \frac{e^{(2\pi\sigma_{vn})^2} - 1}{4\sigma_{vn}\sqrt{\pi}} \frac{1}{L} + 2 \sinh[(2\pi\sigma_{vn})^2] \frac{L}{L+1} \left(\frac{N}{S}\right) + \right. \\ & \left. + e^{(2\pi\sigma_{vn})^2} \frac{L(3L^2 + 2L - 3)}{4(L+1)^2} \left(\frac{N}{S}\right)^2 \right\}^{1/2}. \end{aligned} \quad (3.65)$$

Figure 3.7 shows the normalized standard deviation of Doppler velocity estimates (3.61) versus the normalized spectrum width for the ideal case and several values of SNR. Theoretical results are verified through simulations with the exceptions as noted in Section 3.2.1 pertaining to the conditions for the validity of the perturbation analysis.

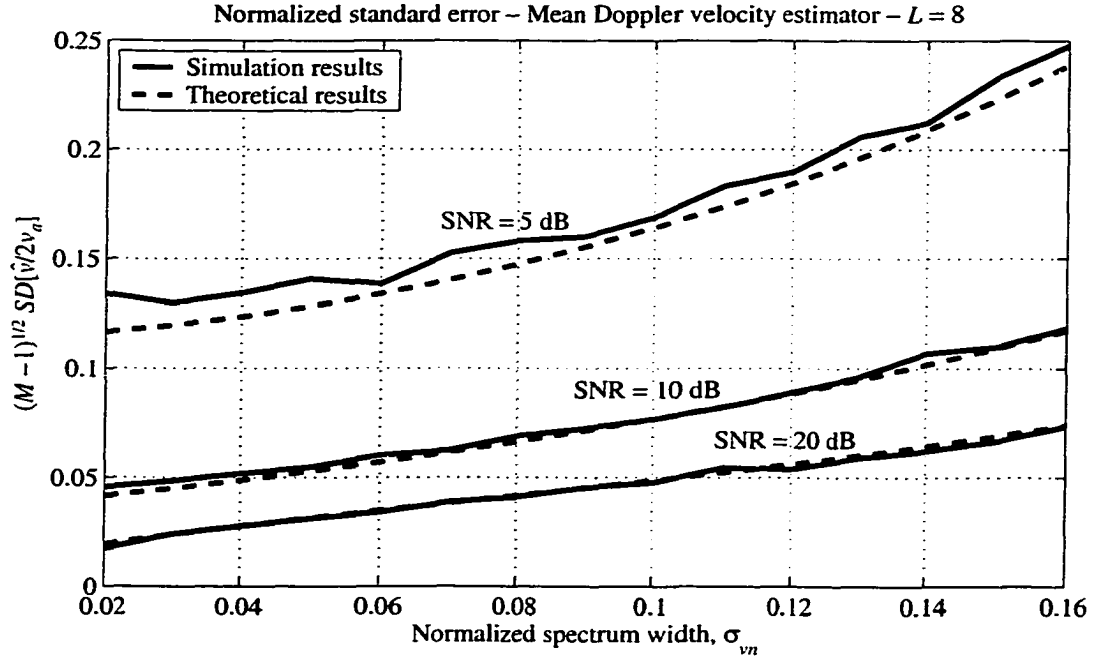


Figure 3.7. Normalized standard deviation of Doppler velocity estimates on whitened data versus the normalized spectrum width with the SNR as a parameter for the ideal case. The oversampling factor L is 8. Both theoretical results (dashed line) and simulation results (solid line) are plotted.

3.2.3. Comparison

Comparison between the results in Figure 3.6 and Figure 3.7 reveals significant improvement (reduction) of standard deviation for the WTB Doppler velocity estimator at large SNR (20 dB). However, for lower SNR, processing of correlated samples produces better estimates, as expected. Note that the SNR of -3 dB for correlated samples give similar errors as an SNR of 5 dB for whitened samples.

As in the case of the signal power estimator, the WTB Doppler velocity estimator worsens as the SNR decreases due to the noise-enhancement effect. The variance reduction factor (VRF) for the WTB velocity estimator can be computed as

$$VRF_{\text{Velocity}} = \frac{\text{Var}\{\hat{v}_{\text{corr}}\}}{\text{Var}\{\hat{v}_{\text{whitened}}\}}, \quad (3.66)$$

which for the ideal case reduces to

$$VRF_{Velocity} = \frac{\frac{[e^{(2\pi\sigma_m)^2} - 1](L^2 + 1)}{8L^2\sigma_{vn}\sqrt{\pi}} + \frac{2\sinh[(2\pi\sigma_{vn})^2]}{L} \left(\frac{N}{S}\right) + \frac{e^{(2\pi\sigma_m)^2}}{2L} \left(\frac{N}{S}\right)^2}{\frac{e^{(2\pi\sigma_m)^2} - 1}{4L\sigma_{vn}\sqrt{\pi}} + \frac{2L\sinh[(2\pi\sigma_{vn})^2]}{L+1} \left(\frac{N}{S}\right) + \frac{e^{(2\pi\sigma_m)^2} L(3L^2 + 2L - 3)}{4(L+1)^2} \left(\frac{N}{S}\right)^2}. \quad (3.67)$$

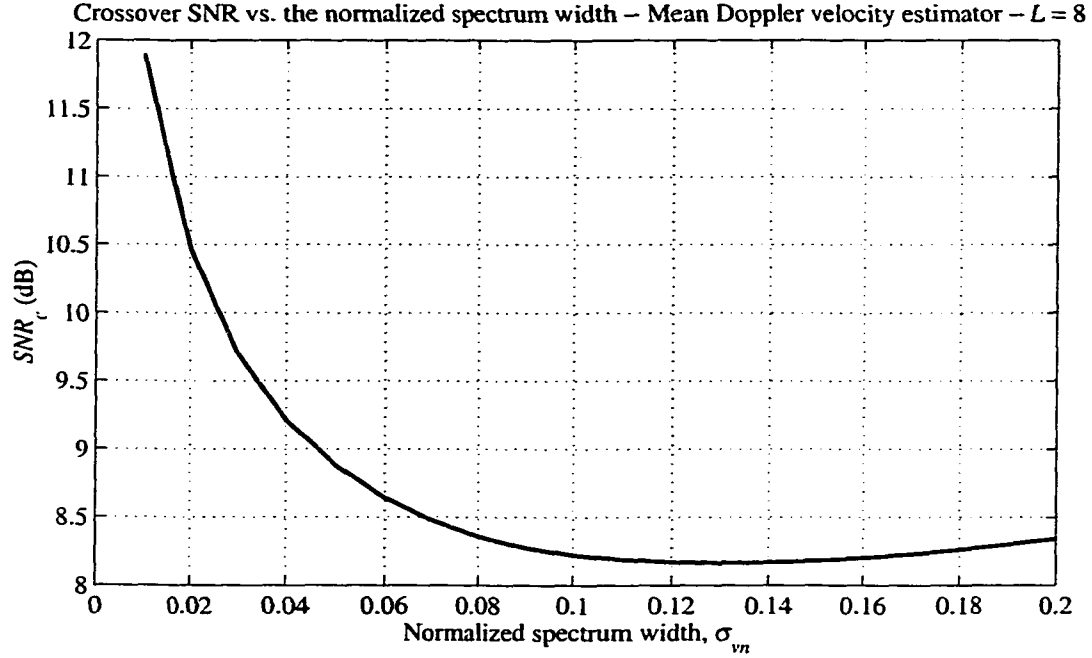


Figure 3.8. Crossover signal-to-noise ratio SNR_c versus the normalized spectrum width for the mean Doppler velocity estimator and an ideal system. The oversampling factor L is 8.

Equation (3.67) is useful to determine the crossover point SNR_c for a given oversampling factor and normalized spectrum width. Figure 3.8 shows the crossover SNR as a function of the normalized spectrum width for the ideal case, where it is interesting to note that the relation between SNR_c and σ_{vn} is not the same as the one in Figure 3.5 due to the different nature of the Doppler velocity estimator. Therefore, for some moderate SNR (approximately less than 12 dB) whitening may be effective for power estimation but not for velocity estimation.

3.3. Estimation of Doppler Spectrum Width

Doppler spectrum width or the square root of the second central moment of the spectrum is a measure of the velocity dispersion, that is, shear or turbulence within the resolution volume. As discussed in Section 1.3, the pulse-pair estimator calculates the Doppler spectrum width from estimates of the signal power and the autocorrelation function at lag T_s (lag one) as in (1.31). In what follows that estimator is extended to deal with oversampled data from correlated and whitened samples.

3.3.1. Correlated Samples

The Doppler spectrum width estimator applied to oversampled correlated samples is

$$\hat{\sigma}_{v_{corr}} = \frac{\lambda}{2\pi T_s \sqrt{2}} \left| \ln \left(\frac{\hat{S}_{corr}}{|\hat{R}_v^{(T)}(1)|} \right) \right|^{1/2} \text{sgn} \left[\ln \left(\frac{\hat{S}_{corr}}{|\hat{R}_v^{(T)}(1)|} \right) \right], \quad (3.68)$$

where \hat{S}_{corr} and $\hat{R}_v^{(T)}(1)$ are given in equations (3.22) and (3.49), respectively.

Due to the statistical performance of the estimators (3.22) and (3.49), the Doppler spectrum width estimator in (3.68) is asymptotically unbiased. As with the mean Doppler velocity, perturbation analysis is useful to compute the variance of spectrum width estimates. It can be proved (Zrnic 1977) that

$$\begin{aligned} \text{Var}\{\hat{\sigma}_{v_{corr}}\} = & \left(\frac{\lambda^2}{8\pi^2 T_s^2} \frac{|R_v^{(T)}(1)|}{2\sigma_v S} \right)^2 \left[\text{Var} \left(\frac{\hat{S}_{corr}}{S} \right) + \right. \\ & \left. + \frac{1}{2} \text{Re} \left\{ E \left[\left| \frac{\hat{R}_v^{(T)}(1)}{R_v^{(T)}(1)} - 1 \right|^2 \right] + E \left[\left(\frac{\hat{R}_v^{(T)}(1)}{R_v^{(T)}(1)} - 1 \right)^2 \right] \right\} - 2 \text{Re} \left\{ \text{Cov} \left(\frac{\hat{S}_{corr}}{S}, \frac{\hat{R}_v^{(T)}(1)}{R_v^{(T)}(1)} \right) \right\} \right]. \quad (3.69) \end{aligned}$$

Using a similar analysis as in Section 3.2, the expectation operations inside (3.69) can be

computed as

$$\begin{aligned}
E\left[\left|\hat{R}_V^{(T)}(1) - R_V^{(T)}(1)\right|^2\right] &= \\
&= \frac{1}{L^2(M-1)^2} \sum_{l=0}^{L-1} \sum_{m=0}^{M-2} \sum_{l'=0}^{L-1} \sum_{m'=0}^{M-2} E\left[V^*(l, m)V(l, m+1)V(l', m')V^*(l', m'+1)\right] - \left|R_V^{(T)}(1)\right|^2 \\
&= \frac{1}{L^2(M-1)^2} \sum_{l=-L+1}^{L-1} \sum_{m=-M+2}^{M-2} (L-|l|)(M-1-|m|) |R_V(l, m)|^2, \tag{3.70}
\end{aligned}$$

$$\begin{aligned}
E\left[\left(\hat{R}_V^{(T)}(1) - R_V^{(T)}(1)\right)^2\right] &= \\
&= \frac{1}{L^2(M-1)^2} \sum_{l=0}^{L-1} \sum_{m=0}^{M-2} \sum_{l'=0}^{L-1} \sum_{m'=0}^{M-2} E\left[V^*(l, m)V(l, m+1)V^*(l', m')V(l', m'+1)\right] - \left[R_V^{(T)}(1)\right]^2 \\
&= \frac{1}{L^2(M-1)^2} \sum_{l=-L+1}^{L-1} \sum_{m=-M+2}^{M-2} (L-|l|)(M-1-|m|) R_V(l, m+1) R_V^*(l, m-1), \tag{3.71}
\end{aligned}$$

and

$$\begin{aligned}
Cov(\hat{S}_{corr}, \hat{R}_V^{(T)}(1)) &= \\
&= \frac{1}{L^2(M-1)^2} \sum_{l=0}^{L-1} \sum_{m=0}^{M-2} \sum_{l'=0}^{L-1} \sum_{m'=0}^{M-2} E\left[V^*(l, m)V(l, m)V^*(l', m')V(l', m'+1)\right] - R_V^{(T)}(0)R_V^{(T)}(1) \\
&= \frac{1}{L^2(M-1)^2} \sum_{l=-L+1}^{L-1} \sum_{m=-M+2}^{M-2} (L-|l|)(M-1-|m|) R_V(l, m+1) R_V^*(l, m). \tag{3.72}
\end{aligned}$$

As previously discussed, the autocorrelation of $V(l, n)$ can be decomposed into signal and noise parts as

$$R_V(l, m) = R_{V_S}(l, m) + R_{V_N}(l, m) = R_{V_S}^{(R)}(l)R_{V_S}^{(T)}(m) + R_{V_N}^{(R)}(l)R_{V_N}^{(T)}(m), \tag{3.73}$$

and with the assumptions of Gaussian sample-time autocorrelation and white noise we have that

$$R_{V_S}^{(T)}(m) = S e^{-2(\pi\sigma_m m)^2} e^{-j2\pi\nu_n m}, \tag{3.74}$$

$$R_{V_N}^{(R)}(l) = \delta(l), \quad (3.75)$$

and

$$R_{V_N}^{(T)}(m) = N\delta(m), \quad (3.76)$$

where the normalized velocity v_n is defined as $v_n = v/2v_a$. Using (3.8) and (3.9), equation (3.69) becomes

$$\begin{aligned} \text{Var}\{\hat{\sigma}_{v_{corr}}\} = & \left(\frac{\lambda}{8\pi^2 T_s \sigma_{vn}} \right)^2 \frac{1}{M-1} \left\{ \frac{e^{(2\pi\sigma_{vn})^2} - 4e^{(\pi\sigma_{vn})^2} + 3 \text{tr}\{[\mathbf{C}_{V_s}^{(R)}]^2\}}{4\sigma_{vn}\sqrt{\pi}} \frac{1}{L^2} + \right. \\ & \left. + \frac{2\{\cosh[(2\pi\sigma_{vn})^2] - 1\}}{L} \left(\frac{N}{S} \right) + \frac{e^{(2\pi\sigma_{vn})^2} + 2\left(\frac{N}{S}\right)^2}{2L} \right\}. \end{aligned} \quad (3.77)$$

For $L = 1$, large M , and $\sigma_{vn} \ll 1$, (3.77) is equivalent to equation (6.30a) of Doviak and Zmric (1993) for the case of $T = T_s$.

For the ideal case, the normalized standard deviation can be obtained from (3.77) as

$$\begin{aligned} \frac{SD\{\hat{\sigma}_{v_{corr}}\}}{2v_a} = & \left(\frac{1}{4\pi^2 \sigma_{vn}} \right) \frac{1}{\sqrt{M-1}} \left\{ \frac{e^{(2\pi\sigma_{vn})^2} - 4e^{(\pi\sigma_{vn})^2} + 3 \frac{L^2 + 1}{2L^2}}{4\sigma_{vn}\sqrt{\pi}} + \right. \\ & \left. + \frac{2\{\cosh[(2\pi\sigma_{vn})^2] - 1\}}{L} \left(\frac{N}{S} \right) + \frac{e^{(2\pi\sigma_{vn})^2} + 2\left(\frac{N}{S}\right)^2}{2L} \right\}^{1/2}. \end{aligned} \quad (3.78)$$

Figure 3.9 shows the normalized standard deviation of Doppler spectrum width estimates (3.68) versus the normalized spectrum width for the ideal case and several values of SNR. Theoretical results are verified through simulations with the exceptions noted in Section 3.2 regarding the limitation of perturbation analysis.

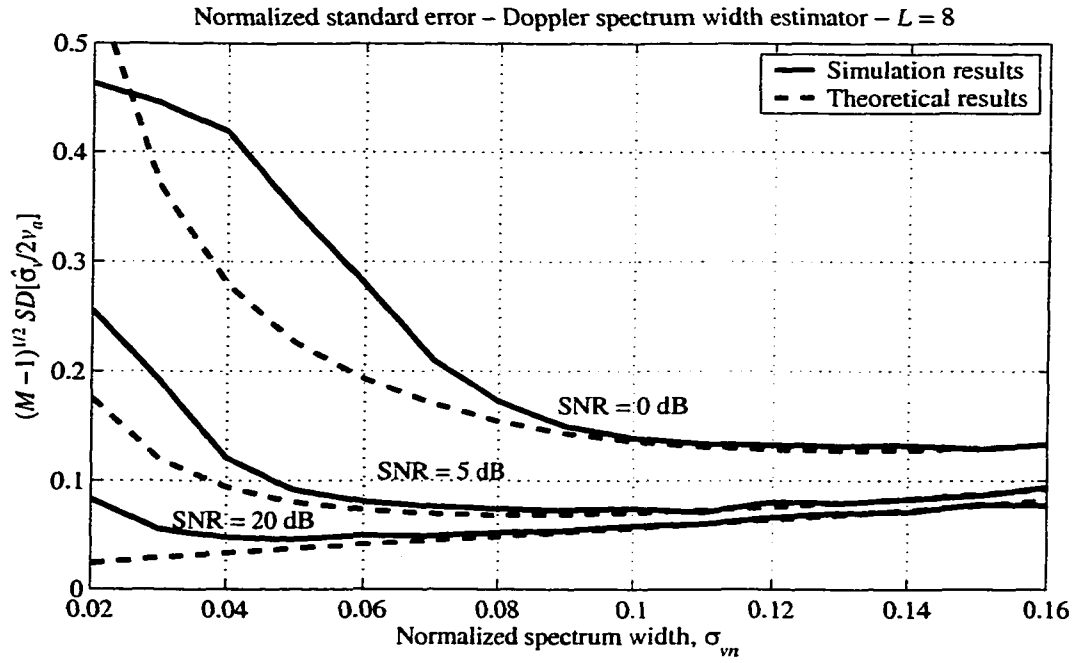


Figure 3.9. Normalized standard deviation of Doppler spectrum width estimates on correlated data versus the normalized spectrum width with the SNR as a parameter for the ideal case. The oversampling factor L is 8. Both theoretical results (dashed line) and simulation results (solid line) are plotted.

3.3.2. Whitened Samples

The Doppler spectrum width estimator applied to oversampled whitened data is

$$\hat{\sigma}_{v_{\text{whitened}}} = \frac{\lambda}{2\pi T_s \sqrt{2}} \left| \ln \left(\frac{\hat{S}_{\text{whitened}}}{|\hat{R}_X^{(T)}(1)|} \right) \right|^{1/2} \text{sgn} \left[\ln \left(\frac{\hat{S}_{\text{whitened}}}{|\hat{R}_X^{(T)}(1)|} \right) \right], \quad (3.79)$$

where $\hat{S}_{\text{whitened}}$ and $\hat{R}_X^{(T)}(1)$ are given in equations (3.34) and (3.62), respectively.

Due to the statistical performance of the estimators (3.34) and (3.62), the Doppler spectrum width estimator in (3.79) is asymptotically unbiased. As in Section 3.3.1, it can be proved that

$$\begin{aligned} \text{Var}\{\hat{\sigma}_{v, \text{whitened}}\} = & \left(\frac{\lambda^2}{8\pi^2 T_s^2} \frac{|R_v^{(T)}(1)|^2}{2\sigma_v S} \right)^2 \left[\text{Var}\left(\frac{\hat{S}_{\text{whitened}}}{S} \right) + \right. \\ & \left. + \frac{1}{2} \text{Re} \left\{ E \left[\left| \frac{\hat{R}_x^{(T)}(1)}{R_v^{(T)}(1)} - 1 \right|^2 \right] + E \left[\left(\frac{\hat{R}_x^{(T)}(1)}{R_v^{(T)}(1)} - 1 \right)^2 \right] \right\} - 2 \text{Re} \left\{ \text{Cov} \left(\frac{\hat{S}_{\text{whitened}}}{S}, \frac{\hat{R}_x^{(T)}(1)}{R_v^{(T)}(1)} \right) \right\} \right], \quad (3.80) \end{aligned}$$

which can be simplified using the same procedure as in the previous section to

$$\begin{aligned} \text{Var}\{\hat{\sigma}_{v, \text{whitened}}\} = & \left(\frac{\lambda}{8\pi^2 T_s \sigma_{vn}} \right)^2 \frac{1}{M-1} \left\{ \frac{e^{(2\pi\sigma_m)^2} - 4e^{(\pi\sigma_m)^2} + 3}{4L\sigma_{vn}\sqrt{\pi}} + \right. \\ & \left. + 2 \left\{ \cosh[(2\pi\sigma_{vn})^2] - 1 \right\} \frac{\text{tr}\{[\mathbf{C}_{v_s}^{(R)}]^{-1}\}}{L^2} \left(\frac{N}{S} \right) + \frac{e^{(2\pi\sigma_m)^2} + 2}{2} \frac{\text{tr}\{[\mathbf{C}_{v_s}^{(R)}]^{-2}\}}{L^2} \left(\frac{N}{S} \right)^2 \right\}. \quad (3.81) \end{aligned}$$

For the ideal case, the normalized standard deviation can be obtained from (3.81) using the identities in Section 3.1.2.2 as

$$\begin{aligned} \frac{SD\{\hat{\sigma}_{v, \text{whitened}}\}}{2v_a} = & \left(\frac{1}{4\pi^2 \sigma_{vn}} \right) \frac{1}{\sqrt{M-1}} \left\{ \frac{e^{(2\pi\sigma_{vn})^2} - 4e^{(\pi\sigma_{vn})^2} + 3}{4L\sigma_{vn}\sqrt{\pi}} + \right. \\ & \left. + \left\{ \cosh[(2\pi\sigma_{vn})^2] - 1 \right\} \frac{4L}{L+1} \left(\frac{N}{S} \right) + \left[e^{(2\pi\sigma_m)^2} + 2 \right] \frac{L(3L^2 + 2L - 3)}{4(L+1)^2} \left(\frac{N}{S} \right)^2 \right\}^{1/2}. \quad (3.82) \end{aligned}$$

Figure 3.10 shows the normalized standard deviation of Doppler spectrum width estimates (3.79) versus the normalized spectrum width for the ideal case and several values of SNR. Theoretical results are verified through simulations with the exceptions as discussed in Section 3.2.1.

3.3.3. Comparison

Comparison between the results in Figure 3.9 and Figure 3.10 reveals significant improvement (reduction) of standard deviation for the WTB spectrum width estimator at

large SNR (20 dB). However, for lower SNR, processing of correlated samples produces better estimates, as expected. Note that a SNR of 0 dB for correlated samples give similar errors as an SNR of 10 dB for whitened samples.

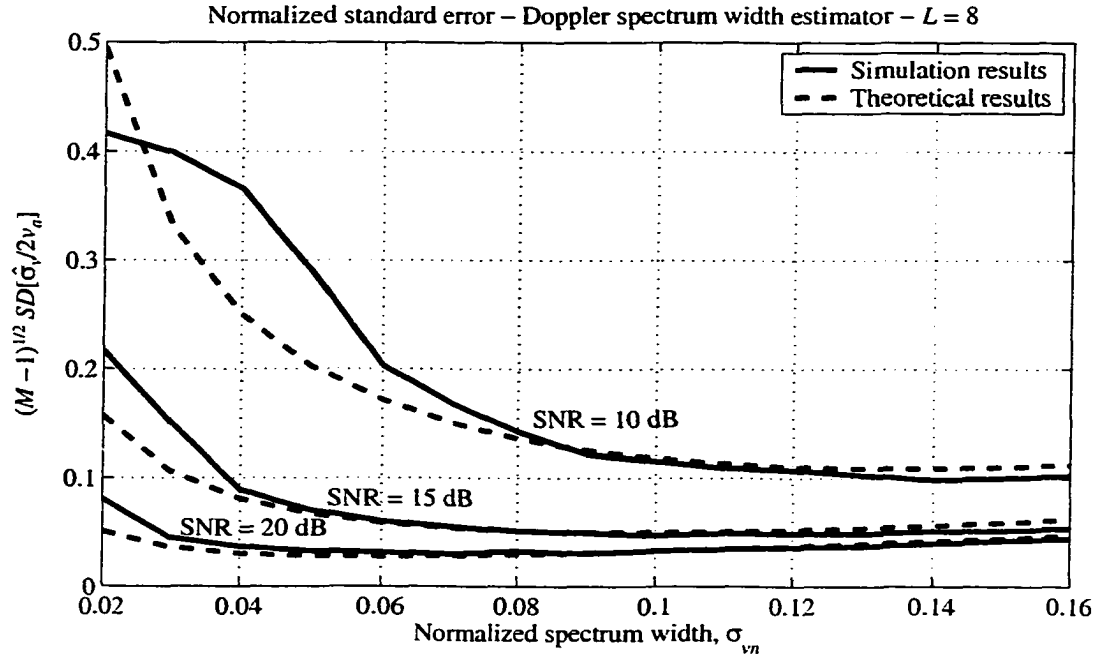


Figure 3.10. Normalized standard deviation Doppler spectrum width estimates on whitened data versus the normalized spectrum width with the SNR as a parameter for the ideal case. The oversampling factor L is 8. Both theoretical results (dashed line) and simulation results (solid line) are plotted.

It is expected once again that the performance of the WTB Doppler spectrum width estimator worsens as the SNR decreases due to the noise-enhancement effect. As in the previous sections, the variance reduction factor (VRF) for the WTB spectrum width estimator can be computed as

$$VRF_{width} = \frac{Var\{\hat{\sigma}_{v_{corr}}\}}{Var\{\hat{\sigma}_{v_{whitened}}\}}, \quad (3.83)$$

which for the ideal case reduces to

$$\begin{aligned}
VRF_{Width} = & \left[\frac{(e^{(2\pi\sigma_m)^2} - 4e^{(\pi\sigma_m)^2} + 3)(L^2 + 1)}{8L^2\sigma_{vn}\sqrt{\pi}} + \frac{2[\cosh(2\pi\sigma_{vn})^2 - 1]\left(\frac{N}{S}\right)}{L} + \right. \\
& + \frac{e^{(2\pi\sigma_m)^2} + 2\left(\frac{N}{S}\right)^2}{2L} \left. \right] \times \left[\frac{e^{(2\pi\sigma_m)^2} - 4e^{(\pi\sigma_m)^2} + 3}{4L\sigma_{vn}\sqrt{\pi}} + \frac{4L[\cosh(2\pi\sigma_{vn})^2 - 1]\left(\frac{N}{S}\right)}{L+1} + \right. \\
& \left. \left. + \frac{L(e^{(2\pi\sigma_m)^2} + 2)(3L^2 + 2L - 3)\left(\frac{N}{S}\right)^2}{4(L+1)^2} \right]^{-1} \quad (3.84)
\end{aligned}$$

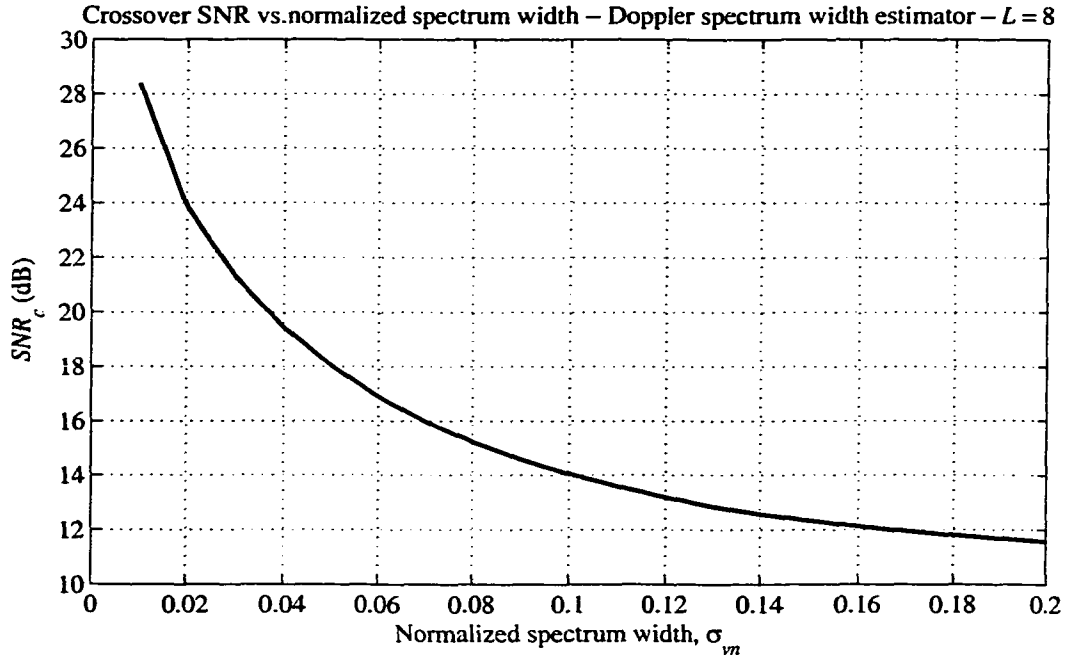


Figure 3.11. Crossover signal-to-noise ratio SNR_c versus the normalized spectrum width for the Doppler spectrum width estimator and an ideal system. The oversampling factor L is 8.

The previous equation is useful to determine the crossover point for a given oversampling factor and normalized spectrum width. Figure 3.11 shows the crossover SNR as a function of the normalized spectrum width for the ideal case, where the relation between SNR_c and σ_{vn} is inverse for the usual range of spectrum widths. This means that the range

of SNR where the WTB spectrum width estimator is preferred becomes larger for broader spectrum widths.

3.4. Estimation of Doppler Spectrum

The power spectrum of weather signals, often referred to as the Doppler spectrum (Doviak and Zrnic 1993), is a power-weighted distribution of the radial velocities of the scatterers in the resolution volume. The three first spectral moments can be estimated using either a few lags of the weather signal autocorrelation function, as with the pulse-pair algorithm, or using the Doppler spectrum by applying so-called *spectral processing methods*. The primary difference between these two approaches is that the information concerning the lower spectral moments is distributed over several frequencies of the power spectrum, while it is concentrated in the small lags of the sample-time autocorrelation function. The advantage of measuring the full Doppler spectrum is that factors that tend to produce spectral artifacts, such as point scatterers, ground clutter, bi-modal spectra, and others, can be recognized and dealt with appropriately by using intuitive algorithms.

The Doppler power spectrum may be estimated from the Discrete Fourier Transform (DFT) of the complex weather signal V as

$$\hat{S}(k) = \frac{T_s}{M} \left| \sum_{m=0}^{M-1} V(m) e^{-j(2\pi/M)mk} \right|^2, \quad 0 \leq k \leq M-1. \quad (3.85)$$

A straightforward extension of this estimator to accommodate oversampled signals is (Urkowitz and Katz 1996)

$$\hat{S}_{corr}(k) = \frac{T_s}{L^2 M} \left| \sum_{l=0}^{L-1} \sum_{m=0}^{M-1} V(l, m) e^{-j(2\pi l M)mk} \right|^2, \quad 0 \leq k \leq M-1, \quad (3.86)$$

for correlated samples and

$$\hat{S}_{whitened}(k) = \frac{T_s}{L^2 M} \left| \sum_{l=0}^{L-1} \sum_{m=0}^{M-1} X(l, m) e^{-j(2\pi l M)mk} \right|^2, \quad 0 \leq k \leq M-1, \quad (3.87)$$

for whitened samples.

Equations (3.86) and (3.87) can be rewritten as

$$\hat{S}_{corr}(k) = \frac{T_s}{M} \left| \frac{1}{L} \sum_{l=0}^{L-1} Z_{corr}(l, k) \right|^2, \quad 0 \leq k \leq M-1, \quad (3.88)$$

and

$$\hat{S}_{whitened}(k) = \frac{T_s}{M} \left| \frac{1}{L} \sum_{l=0}^{L-1} Z_{whitened}(l, k) \right|^2, \quad 0 \leq k \leq M-1, \quad (3.89)$$

respectively. In (3.88) and (3.89), $Z(l, k)$ is the DFT along the sample-time axis of the correlated or whitened l -th oversampled component of the weather signal. That is,

$$Z_{corr}(l, k) = \sum_{m=0}^{M-1} V(l, m) e^{-j(2\pi l M)mk}, \quad (3.90)$$

and

$$Z_{whitened}(l, k) = \sum_{m=0}^{M-1} X(l, m) e^{-j(2\pi l M)mk} = \sum_{m=0}^{M-1} \left[\sum_{i=0}^{L-1} w_{i,l} V(i, m) \right] e^{-j(2\pi l M)mk}, \quad (3.91)$$

where $w_{i,j}$ are the entries of the whitening transformation matrix. In other words, the Doppler spectrum is found by averaging spectral coefficients obtained from either correlated or whitened samples. Since the DFT is a linear operation, it follows that estimates originating from whitened samples will achieve lower errors compared to the

estimates from correlated (non-whitened) data.

Another equivalent approach to estimating the Doppler spectrum using a WTB estimator consists of moving the whitening stage one step further into the processing chain. The whitening transformation is then applied to the complex Fourier coefficients instead of the oversampled weather signal. That is,

$$\hat{S}_{whitened}(k) = \frac{T_s}{M} \left| \frac{1}{L} \sum_{l=0}^{L-1} \left[\sum_{i=0}^{L-1} w_{i,l} Z_{corr}(i, k) \right] \right|^2, \quad 0 \leq k \leq M-1, \quad (3.92)$$

where w_{ij} are the entries of a whitening transformation for the complex Fourier coefficients and Z_{corr} is defined in (3.90). This method will be discussed with more detail in Chapter 5.

A similar analysis as in the previous sections can be carried out for these estimators; however, such deeper analysis of the WTB Doppler spectrum estimator is beyond the scope of this dissertation.

3.5. Results

Sections 3.1 through 3.4 discussed the application of the whitening transformation to the estimation of the Doppler spectrum and its moments. Estimators operating on whitened signals were termed whitening-transformation-based (WTB) estimators, and they exhibit reduced standard errors if the signal-to-noise ratio is relatively large.

A performance comparison of all WTB estimators with estimators on correlated data for the ideal case showed that for all the variables the variance reduction factor for large SNR is

$$VRF = \frac{L^2 + 1}{2L}, \quad (3.93)$$

where L is the oversampling factor. That is, approximately $L/2$ fewer samples are needed for WTB estimators to keep the same errors as the ones obtained without the aid of the whitening transformation.

For low SNR the performance of all WTB estimators deteriorates as the noise-enhancing effect discussed in Section 2.5 becomes important. In such cases, the estimates on non-whitened data result in better performance; the rule for selecting the best estimate is given by

$$\hat{\theta} = \begin{cases} \hat{\theta}_{corr} & \text{if } SNR < SNR_c \\ \hat{\theta}_{whitened} & \text{if } SNR \geq SNR_c. \end{cases} \quad (3.94)$$

In equation (3.94), θ is any of the variables discussed in this chapter, namely S , v , or σ_v , and SNR_c is the crossover SNR defined as the SNR that conduces to a variance reduction factor of one. Theoretical expressions for the variance of estimates as derived in the previous sections become useful if one needs to compute the value of SNR_c for a given variable under specific conditions without the need of simulations (see Figures 3.5, 3.8, and 3.11). Under appropriate limiting conditions, these expressions agree with the ones available in the literature. Finally, it is interesting to observe that the SNR_c as functions of σ_{v_n} for velocity and spectrum width estimates have similar behaviors (Figures 3.8 and 3.11), but differ from the one for power estimates (Figure 3.5) due to the dissimilar nature of the estimators.

4. POLARIMETRIC VARIABLE ESTIMATION

One of the evolutionary enhancements planned for the national network of weather radars (NEXRAD) is the addition of a polarimetric capability to improve rainfall estimation and to identify precipitation types; e.g., to distinguish rain from hail, snow, etc. (Doviak et al., 2000). This chapter covers the application of the whitening transformation to the estimation of polarimetric variables, namely the differential reflectivity, the total differential phase shift, and the magnitude of the cross-correlation coefficient at lag zero. Special emphasis is given to the statistical performance of WTB estimators compared with estimators that do not employ a whitening transformation. Variance reduction factors are derived, and theoretical developments are verified through computer simulations. The analysis in this chapter is for simultaneous transmission and reception of horizontally and vertically polarized signals [see for example Scott et al. (2001)]. Nonetheless, the same principle is applicable to alternate (switched) transmissions and receptions (Doviak et al., 2000). Because the antenna scan rate is a function of the rate at which samples can be acquired and the number of samples required for a given accuracy, it is demonstrated that WTB estimators allow for faster antenna rotation rates compared to regular estimators for the same accuracy in the meteorological fields. This is of special significance for the polarimetric variables.

4.1. Estimation of Differential Reflectivity

As discussed in Section 1.3, the differential reflectivity Z_{DR} is the ratio of reflected horizontal and vertical power returns. Capability of dual polarized radars to estimate

rainfall rate with better accuracy via differential reflectivity measurement has been well established (Aydin et al. 1990). In addition, Z_{DR} makes identification of hail possible (Zrnice and Ryzhkov 1999). However, one of the problems with Z_{DR} measurement has been its relatively long acquisition time because accurate rainfall rate estimation requires Z_{DR} fractional errors less than 0.1 dB; hence, more samples and thus a slower antenna rotation rate is necessary. It is shown in this section that WTB estimators of Z_{DR} achieve the required small errors with fewer samples than the usual estimator; therefore, faster scan rates are possible without degradation in the accuracy of Z_{DR} estimates.

4.1.1. Correlated Samples

The differential reflectivity estimator applied to oversampled correlated samples is

$$\hat{Z}_{DR_{corr}} = \frac{\hat{S}_{H_{corr}}}{\hat{S}_{V_{corr}}}, \quad (4.1)$$

where

$$\hat{S}_{H_{corr}} = \frac{1}{LM} \sum_{l=0}^{L-1} \sum_{m=0}^{M-1} |V_H(l, m)|^2 - N_H, \quad (4.2)$$

$$\hat{S}_{V_{corr}} = \frac{1}{LM} \sum_{l=0}^{L-1} \sum_{m=0}^{M-1} |V_V(l, m)|^2 - N_V. \quad (4.3)$$

In (4.2) and (4.3) V_H , V_V , N_H , and N_V are the oversampled correlated signals and noise corresponding to the horizontal (H) and vertical (V) channel, respectively. For most practical situations it can be assumed that noise powers in the horizontal and vertical channels are equal; hence $N_H = N_V = N$ will be assumed throughout the remainder of this chapter.

Perturbation analysis to compute the variance of differential reflectivity estimates (Sachidananda and Zmic 1985) results in

$$Var(\hat{Z}_{DR_{corr}}) = Z_{DR}^2 \left[Var\left(\frac{\hat{S}_{H_{corr}}}{S_H}\right) + Var\left(\frac{\hat{S}_{V_{corr}}}{S_V}\right) + 2Cov\left(\frac{\hat{S}_{H_{corr}}}{S_H}, \frac{\hat{S}_{V_{corr}}}{S_V}\right) \right]. \quad (4.4)$$

The first two terms inside (4.4) can be computed from (3.27) by substituting S_H or S_V for S , respectively. The covariance term in (4.4) is computed as

$$Cov\left(\frac{\hat{S}_{H_{corr}}}{S_H}, \frac{\hat{S}_{V_{corr}}}{S_V}\right) = \frac{E[\hat{S}_{H_{corr}} \hat{S}_{V_{corr}}]}{S_H S_V} - 1, \quad (4.5)$$

where

$$\begin{aligned} E[\hat{S}_{H_{corr}} \hat{S}_{V_{corr}}] &= \frac{1}{L^2 M^2} \sum_{l=0}^{L-1} \sum_{m=0}^{M-1} \sum_{l'=0}^{L-1} \sum_{m'=0}^{M-1} E[V_H^*(l, m) V_H(l, m) V_V^*(l', m') V_V(l', m')] \\ &= S_H S_V + \sum_{l=-L+1}^{L-1} \sum_{m=-M+1}^{M-1} (L - |l|)(M - |m|) |R_{V_H V_V}(l, m)|^2. \end{aligned} \quad (4.6)$$

Throughout this analysis it is assumed that the cross-coupling between horizontal and vertical channels is negligible, which is true for any well-designed system. Therefore, the cross-correlation between the noise in the horizontal and vertical channels is zero. Further, using the same reasoning as Sachidananda and Zmic (1985), the two-dimensional autocorrelation function $R_{V_H V_V}$ can be decomposed as

$$R_{V_H V_V}(l, m) = \sqrt{S_H S_V} \rho_{V_H V_V}(l, m) = \sqrt{S_H S_V} \rho_{HV}(0) \rho_{V_S}^{(R)}(l) \rho_{V_S}^{(T)}(m). \quad (4.7)$$

With the assumptions of Gaussian sample-time autocorrelation and white noise as in Chapter 3, (4.4) reduces to

$$\text{Var}\{\hat{Z}_{DR_{corr}}\} = \frac{Z_{DR}^2}{M} \left[\frac{1 - |\rho_{HV}(0)|^2}{\sigma_{vn} \sqrt{\pi}} \frac{\text{tr}\{[\mathbf{C}_{vs}^{(R)}]^2\}}{L^2} + 2 \frac{1 + Z_{DR}}{L} \left(\frac{N}{S_H} \right) + \frac{1 + Z_{DR}^2}{L} \left(\frac{N}{S_H} \right)^2 \right]. \quad (4.8)$$

The previous equation is equivalent to equation (7) of Sachidananda and Zmic (1985) if $L = 1$, $N_H = N_V$, $N_c = 0$, M is large, and $\sigma_{vn} \ll 1$. For the ideal case, the normalized standard deviation can be obtained from (4.8) as

$$\frac{SD\{\hat{Z}_{DR_{corr}}\}}{Z_{DR}} = \frac{1}{\sqrt{M}} \left[\frac{1 - |\rho_{HV}(0)|^2}{\sigma_{vn} \sqrt{\pi}} \frac{L^2 + 1}{2L^2} + 2 \frac{1 + Z_{DR}}{L} \left(\frac{N}{S_H} \right) + \frac{1 + Z_{DR}^2}{L} \left(\frac{N}{S_H} \right)^2 \right]^{1/2}. \quad (4.9)$$

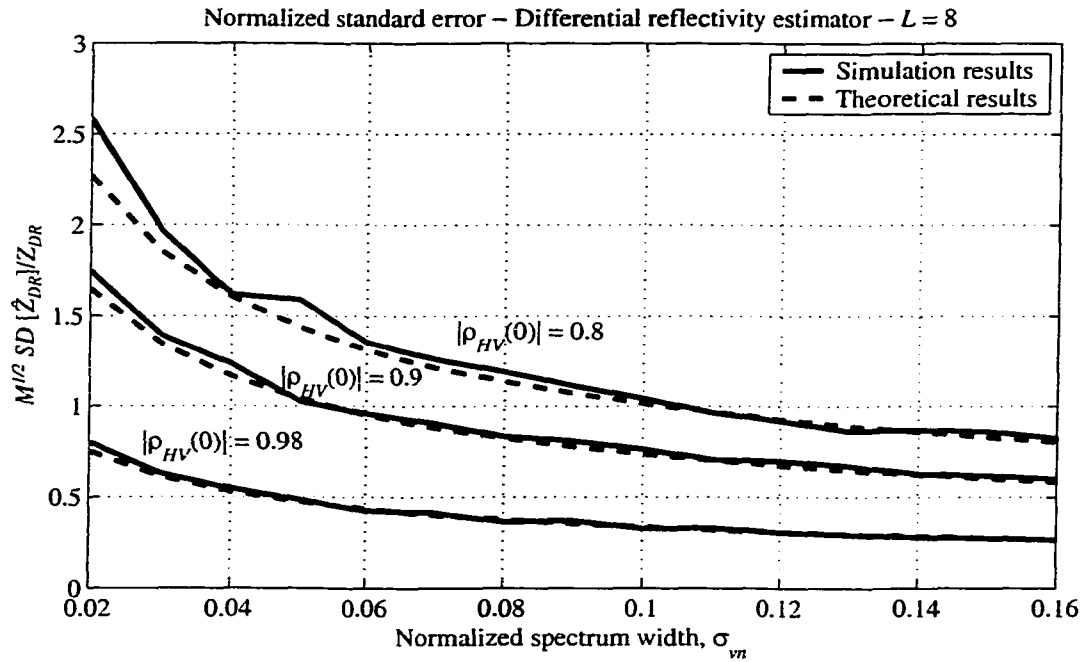


Figure 4.1. Normalized standard deviation of differential reflectivity estimates on correlated data versus the normalized spectrum width with the correlation coefficient $|\rho_{HV}(0)|$ as a parameter for the ideal case. The oversampling factor L is 8 and the SNR is very large. Both theoretical results (dashed line) and simulation results (solid line) are plotted.

Figure 4.1 shows the normalized standard deviation of differential reflectivity estimates (4.1) versus the normalized spectrum width for the ideal case. Curves are plotted for several values of $|\rho_{HV}(0)|$, where a correlation coefficient of 0.98 is representative of pure

rain, and $|\rho_{HV}(0)| = 0.9$ is typical of hail (Straka et al., 2000). It is evident from this plot that theoretical results are in good agreement with simulations.

4.1.2. Whitenes Samples

The differential reflectivity estimator applied to oversampled whitenes samples is

$$\hat{Z}_{DR_{whitened}} = \frac{\hat{S}_{H_{whitened}}}{\hat{S}_{V_{whitened}}}, \quad (4.10)$$

where

$$\hat{S}_{H_{whitened}} = \frac{1}{LM} \sum_{l=0}^{L-1} \sum_{m=0}^{M-1} |X_H(l, m)|^2 - N(NEF), \quad (4.11)$$

$$\hat{S}_{V_{whitened}} = \frac{1}{LM} \sum_{l=0}^{L-1} \sum_{m=0}^{M-1} |X_V(l, m)|^2 - N(NEF). \quad (4.12)$$

In (4.11) and (4.12) X_H and X_V are the oversampled whitenes signals corresponding to the horizontal and vertical polarizations, respectively; NEF is the noise enhancement factor as defined in (2.22).

Analogously as in the previous section, the variance of the estimator in (4.10) is

$$Var(\hat{Z}_{DR_{whitened}}) = Z_{DR}^2 \left[Var\left(\frac{\hat{S}_{H_{whitened}}}{S_H}\right) + Var\left(\frac{\hat{S}_{V_{whitened}}}{S_V}\right) + 2Cov\left(\frac{\hat{S}_{H_{whitened}}}{S_H}, \frac{\hat{S}_{V_{whitened}}}{S_V}\right) \right]. \quad (4.13)$$

The first two terms inside (4.13) can be computed from (3.36) by substituting S_H or S_V for S , respectively. The covariance term in (4.13) is computed as in (4.5). With the result of (3.40) and the usual assumptions, (4.13) reduces to

$$\begin{aligned} \text{Var}\{\hat{Z}_{DR_{\text{whitened}}}\} = \frac{Z_{DR}^2}{M} & \left[\frac{1 - |\rho_{HV}(0)|^2}{\sigma_{vn} \sqrt{\pi}} \frac{1}{L} + 2(1 + Z_{DR}) \frac{\text{tr}\{[\mathbf{C}_{V_s}^{(R)}]^{-1}\}}{L^2} \left(\frac{N}{S_H}\right) + \right. \\ & \left. + (1 + Z_{DR}^2) \frac{\text{tr}\{[\mathbf{C}_{V_s}^{(R)}]^{-2}\}}{L^2} \left(\frac{N}{S_H}\right)^2 \right]. \end{aligned} \quad (4.14)$$

For the ideal case, the normalized standard deviation can be obtained from (4.14) as

$$\begin{aligned} \frac{SD\{\hat{Z}_{DR_{\text{whitened}}}\}}{Z_{DR}} = \frac{1}{\sqrt{M}} & \left[\frac{1 - |\rho_{HV}(0)|^2}{\sigma_{vn} \sqrt{\pi}} \frac{1}{L} + (1 + Z_{DR}) \frac{2L}{L+1} \left(\frac{N}{S_H}\right) + \right. \\ & \left. + (1 + Z_{DR}^2) \frac{L(3L^2 + 2L - 3)}{2(L+1)^2} \left(\frac{N}{S_H}\right)^2 \right]^{1/2}. \end{aligned} \quad (4.15)$$

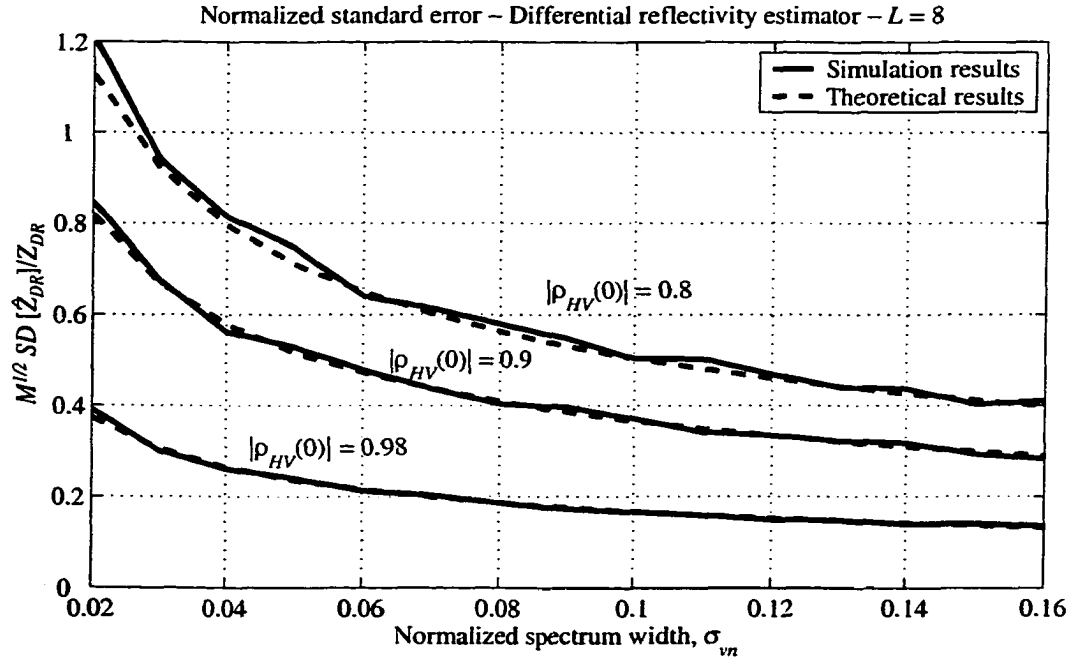


Figure 4.2. Normalized standard deviation of differential reflectivity estimates on whitened data versus the normalized spectrum width with the correlation coefficient $|\rho_{HV}(0)|$ as a parameter for the ideal case. The oversampling factor L is 8 and the SNR is very large. Both theoretical results (dashed line) and simulation results (solid line) are plotted.

Figure 4.2 shows the normalized standard deviation of differential reflectivity estimates versus the normalized spectrum width for the ideal case and several values of $|\rho_{HV}(0)|$. It is evident from this plot that theoretical results are in good agreement with simulations once again.

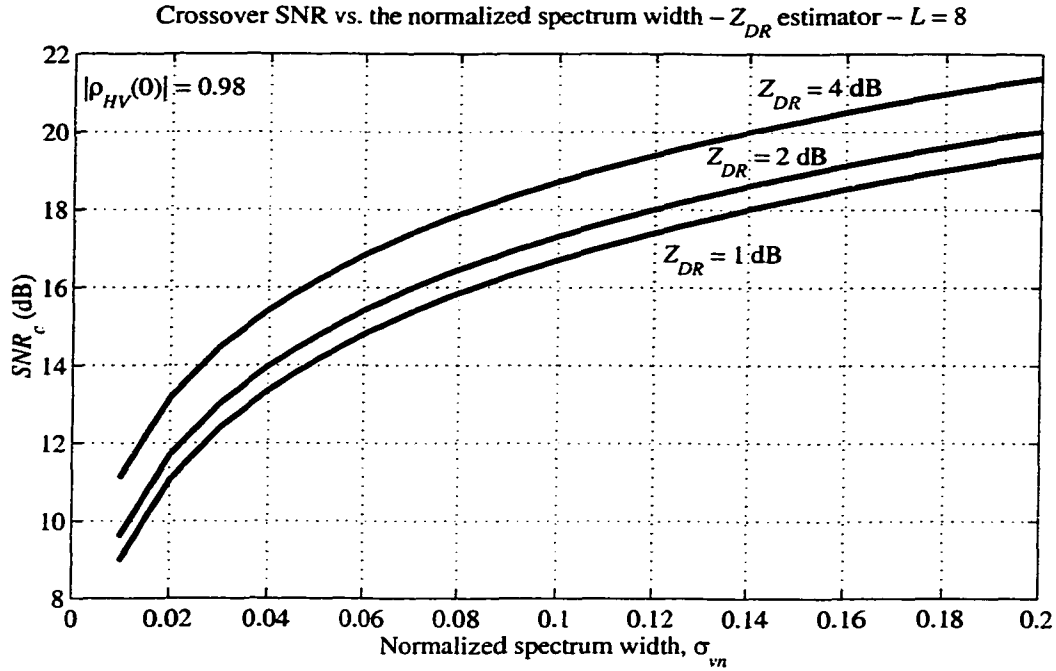


Figure 4.3. Crossover signal-to-noise ratio SNR_c versus the normalized spectrum width for the differential reflectivity estimator and an ideal system using the actual differential reflectivity (Z_{DR}) as a parameter. The oversampling factor L is 8 and the magnitude of the cross-correlation coefficient $|\rho_{HV}(0)|$ is 0.98.

4.1.3. Comparison

Comparison between the results in Figure 4.1 and Figure 4.2 reveals significant improvement (reduction) of standard deviation for the WTB differential reflectivity estimator at large SNR. However, for lower SNRs we expect the noise-enhancement effect to begin dominating and consequently deteriorating the performance of the WTB estimator. The crossover SNR (SNR_c) is a good indicator of this effect and is plotted in

Figure 4.3 as a function of the normalized spectrum width for several values of Z_{DR} . Differential reflectivity values between 1 dB and 4 dB are typical in rain (Straka et al., 2000).

4.2. Estimation of Differential Phase

The differential phase is a comparison of the returned phase difference between the horizontal and vertical pulses where both backscattering and propagation effects are included. Mathematically, $\arg\{\rho_{HV}(0)\} = \phi_{DP}(1-2\sigma_\psi^2) - \delta_i$, where ϕ_{DP} is the differential phase due to propagation, σ_ψ^2 is the variance of the canting angle (i.e., the angle between the incident electric field and the projection of the axis of symmetry on the plane of polarization) of particles along the propagation path, and δ_i is the intrinsic differential phase. However, in most cases of interest (e.g., uniform rain) $\phi_{DP} \gg \delta_i$ and σ_ψ is very small, so $\arg\{\rho_{HV}(0)\} \approx \phi_{DP}$ represents propagation effects only. Although Z_{DR} measurements result in better rainfall rate estimates, Seliga and Bringi (1978) suggested that the differential propagation phase shift ϕ_{DP} as another polarimetric variable that could be used in a similar manner as Z_{DR} to estimate rainfall rates. Their theoretical analysis showed that the use of ϕ_{DP} results in more accurate rainfall rate estimates when the estimates errors are kept below one degree. Differential phase may also prove to be very useful in hydrometeor type identification (Zrnica and Ryzhkov 1999). It is shown in this section that WTB estimators of ϕ_{DP} achieve the required errors with fewer samples than the regular ϕ_{DP} estimator, therefore resulting in the same advantages as discussed for the differential reflectivity.

4.2.1. Correlated Samples

The differential phase estimator applied to oversampled correlated samples is

$$\hat{\phi}_{DP_{corr}} = \arg\left\{\hat{R}_{V_H V_V}^{(T)}(0)\right\}, \quad (4.16)$$

where

$$\hat{R}_{V_H V_V}^{(T)}(0) = \frac{1}{LM} \sum_{l=0}^{L-1} \sum_{m=0}^{M-1} V_H(l, m) V_V^*(l, m). \quad (4.17)$$

In (4.17) V_H and V_V are the oversampled correlated signals corresponding to the horizontal and vertical channels, respectively.

Perturbation analysis can be used to compute the variance of differential phase estimates as (Ryzhkov and Zrnic 1998)

$$\text{Var}\left\{\hat{\phi}_{DP_{corr}}\right\} = \frac{1}{2} \text{Re} \left\{ E \left[\left| \frac{\hat{R}_{V_H V_V}^{(T)}(0)}{R_{V_H V_V}^{(T)}(0)} \right|^2 \right] - E \left[\left(\frac{\hat{R}_{V_H V_V}^{(T)}(0)}{R_{V_H V_V}^{(T)}(0)} \right)^2 \right] \right\}. \quad (4.18)$$

Using a similar technique as in previous derivations, the expectation operations inside (4.18) can be computed as

$$\begin{aligned} E \left[\left| \hat{R}_{V_H V_V}^{(T)}(0) \right|^2 \right] &= \frac{1}{L^2 M^2} \sum_{l=0}^{L-1} \sum_{m=0}^{M-1} \sum_{l'=0}^{L-1} \sum_{m'=0}^{M-1} E \left[V_H(l, m) V_V^*(l, m) V_H^*(l', m') V_V(l', m') \right] \\ &= \left| R_{V_H V_V}^{(T)}(0) \right|^2 + \frac{1}{L^2 M^2} \sum_{l=-L+1}^{L-1} \sum_{m=-M+1}^{M-1} (L-|l|)(M-|m|) R_{V_H}^*(l, m) R_{V_V}(l, m), \end{aligned} \quad (4.19)$$

and

$$E \left[\left(\hat{R}_{V_H V_V}^{(T)}(0) \right)^2 \right] = \frac{1}{L^2 M^2} \sum_{l=0}^{L-1} \sum_{m=0}^{M-1} \sum_{l'=0}^{L-1} \sum_{m'=0}^{M-1} E \left[V_H(l, m) V_V^*(l, m) V_H(l', m') V_V^*(l', m') \right]$$

$$= \left(R_{V_H V_V}^{(T)}(0) \right)^2 + \frac{1}{L^2 M^2} \sum_{l=-L+1}^{L-1} \sum_{m=-M+1}^{M-1} (L-|l|)(M-|m|) R_{V_H V_V}(l, m) R_{V_H V_V}(-l, -m). \quad (4.20)$$

Autocorrelation functions inside the summations in (4.19) can be decomposed as in (3.53), and cross-correlation functions inside the summations in (4.20) as in (4.7). With the typical assumptions of Gaussian sample-time autocorrelation and white noise, (4.18) reduces to

$$\begin{aligned} \text{Var}\{\hat{\phi}_{DP_{corr}}\} = \frac{1}{2M} & \left[\frac{|\rho_{HV}(0)|^{-2} - 1}{2\sigma_{vn}\sqrt{\pi}} \frac{\text{tr}\{[\mathbf{C}_{V_s}^{(R)}]^2\}}{L^2} + \frac{1+Z_{DR}}{L|\rho_{HV}(0)|^2} \left(\frac{N}{S_H} \right) + \right. \\ & \left. + \frac{Z_{DR}}{L|\rho_{HV}(0)|^2} \left(\frac{N}{S_H} \right)^2 \right]. \end{aligned} \quad (4.21)$$

For the ideal case the standard deviation expressed in degrees can be obtained from (4.21)

as

$$\begin{aligned} SD\{\hat{\phi}_{DP_{corr}}\} = \frac{90}{\pi\sqrt{M}} & \left[\frac{|\rho_{HV}(0)|^{-2} - 1}{2\sigma_{vn}\sqrt{\pi}} \frac{L^2 + 1}{2L^2} + \frac{1+Z_{DR}}{L|\rho_{HV}(0)|^2} \left(\frac{N}{S_H} \right) + \right. \\ & \left. + \frac{Z_{DR}}{L|\rho_{HV}(0)|^2} \left(\frac{N}{S_H} \right)^2 \right]^{1/2}. \end{aligned} \quad (4.22)$$

Equation (4.22) is equivalent to (A18) of Ryzhkov and Zmic (1988) if $L = 1$, the SNR is very large, M is large, and $\sigma_{vn} \ll 1$.

Figure 4.4 shows the normalized standard deviation of differential phase estimates (4.16) versus the normalized spectrum width for the ideal case and several values of $|\rho_{HV}(0)|$.

Once again, theoretical results are in good agreement with simulations.

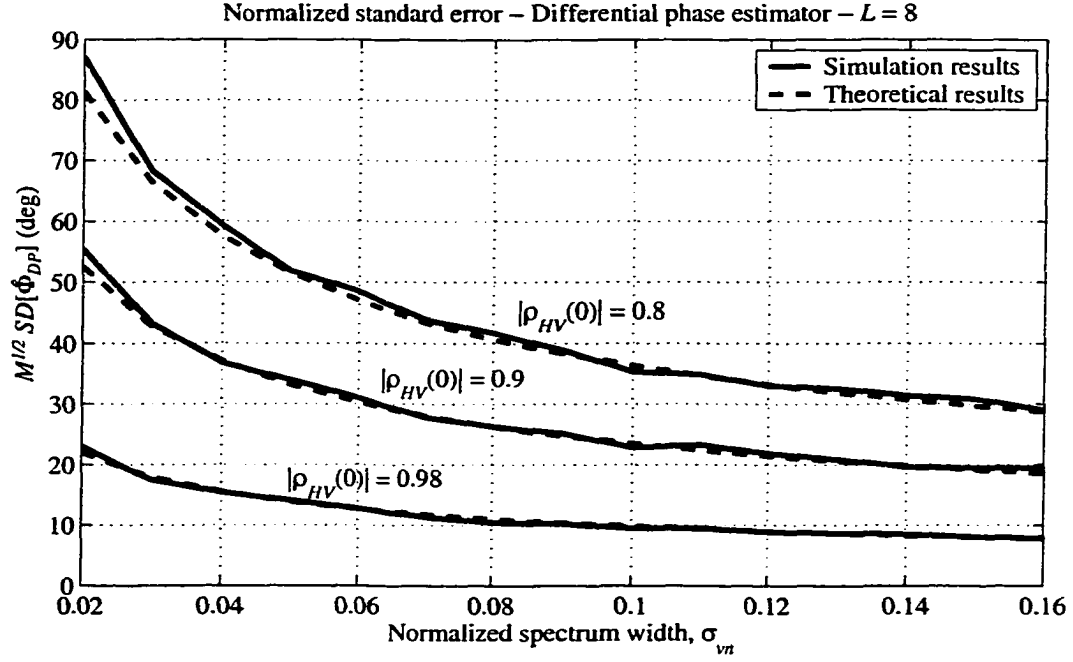


Figure 4.4. Normalized standard deviation of differential phase estimates on correlated data versus the normalized spectrum width with the correlation coefficient $|\rho_{HV}(0)|$ as a parameter for the ideal case. The oversampling factor L is 8 and the SNR is very large. Both theoretical results (dashed line) and simulation results (solid line) are plotted.

4.2.2. Whitened Samples

The differential phase estimator applied to oversampled whitened samples is

$$\hat{\phi}_{DP_{\text{whitened}}} = \arg\{\hat{R}_{X_H X_V}^{(T)}(0)\}, \quad (4.23)$$

where

$$\hat{R}_{X_H X_V}^{(T)}(0) = \frac{1}{LM} \sum_{l=0}^{L-1} \sum_{m=0}^{M-1} X_H(l, m) X_V^*(l, m). \quad (4.24)$$

In (4.24) X_H and X_V are the oversampled whitened signals corresponding to the horizontal and vertical channels, respectively.

Analogously as in the previous section, the variance of the estimator in (4.23) is

$$Var\{\hat{\phi}_{DP_{whitened}}\} = \frac{1}{2} \text{Re} \left\{ E \left[\left| \frac{\hat{R}_{X_H X_V}^{(T)}(0)}{R_{V_H V_V}^{(T)}(0)} \right|^2 \right] - E \left[\left(\frac{\hat{R}_{X_H X_V}^{(T)}(0)}{R_{V_H V_V}^{(T)}(0)} \right)^2 \right] \right\}. \quad (4.25)$$

The expectation operations inside (4.25) can be computed as in the previous section, where X_H and X_V are used instead of V_H and V_V , respectively. Then, with the typical assumptions (4.25) reduces to

$$Var\{\hat{\phi}_{DP_{whitened}}\} = \frac{1}{2M} \left[\frac{|\rho_{HV}(0)|^{-2} - 1}{2\sigma_{vn}\sqrt{\pi}} \frac{1}{L} + \frac{1 + Z_{DR}}{L|\rho_{HV}(0)|^2} \frac{\text{tr}\{[\mathbf{C}_{V_s}^{(R)}]^{-1}\}}{L^2} \left(\frac{N}{S_H} \right) + \frac{Z_{DR}}{L|\rho_{HV}(0)|^2} \frac{\text{tr}\{[\mathbf{C}_{V_s}^{(R)}]^{-2}\}}{L^2} \left(\frac{N}{S_H} \right)^2 \right]. \quad (4.26)$$

For the ideal case the standard deviation in degrees can be obtained from (4.26) as

$$SD\{\hat{\phi}_{DP_{whitened}}\} = \frac{90}{\pi\sqrt{M}} \left[\frac{|\rho_{HV}(0)|^{-2} - 1}{2\sigma_{vn}\sqrt{\pi}} \frac{1}{L} + \frac{1 + Z_{DR}}{|\rho_{HV}(0)|^2} \frac{L}{L+1} \left(\frac{N}{S_H} \right) + \frac{Z_{DR}}{|\rho_{HV}(0)|^2} \frac{L(3L^2 + 2L - 3)}{2(L+1)^2} \left(\frac{N}{S_H} \right)^2 \right]^{1/2}. \quad (4.27)$$

Figure 4.5 shows the normalized standard deviation of differential phase estimates (4.23) versus the normalized spectrum width for the ideal case and several values of $|\rho_{HV}(0)|$. As observed before, theoretical results are in good agreement with simulations.

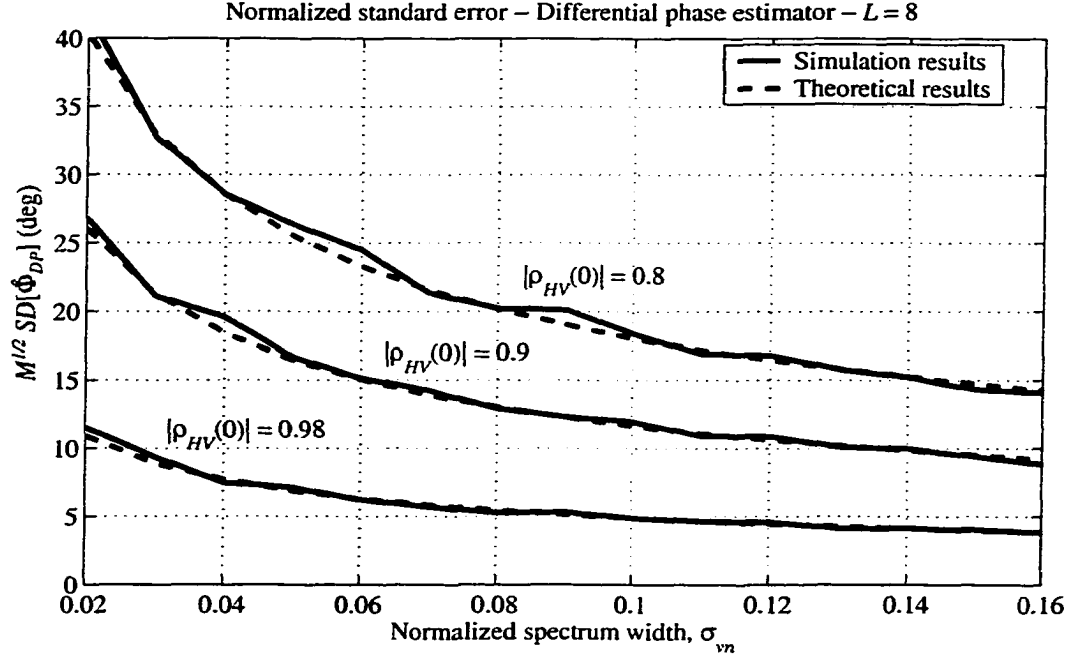


Figure 4.5. Normalized standard deviation of differential phase estimates on whitened data versus the normalized spectrum width with the correlation coefficient $|\rho_{HV}(0)|$ as a parameter for the ideal case. The oversampling factor L is 8 and the SNR is very large. Both theoretical results (dashed line) and simulation results (solid line) are plotted.

4.2.3. Comparison

Comparison between the results in Figure 4.4 and Figure 4.5 reveals significant reduction of errors for the WTB differential phase estimator at large SNR. However, for lower SNRs the noise-enhancement effect begins to dominate and consequently deteriorates the performance of the WTB estimator. As discussed in the previous section, the crossover SNR (SNR_c) is a good indicator of this effect and is plotted in Figure 4.6 as a function of the normalized spectrum width for several values of Z_{DR} . It is interesting to observe that SNR_c for ϕ_{DP} is almost the same as SNR_c for Z_{DR} at $Z_{DR} = 1$ dB and only slightly lower at $Z_{DR} = 4$ dB (compare Figures 4.3 and 4.6).

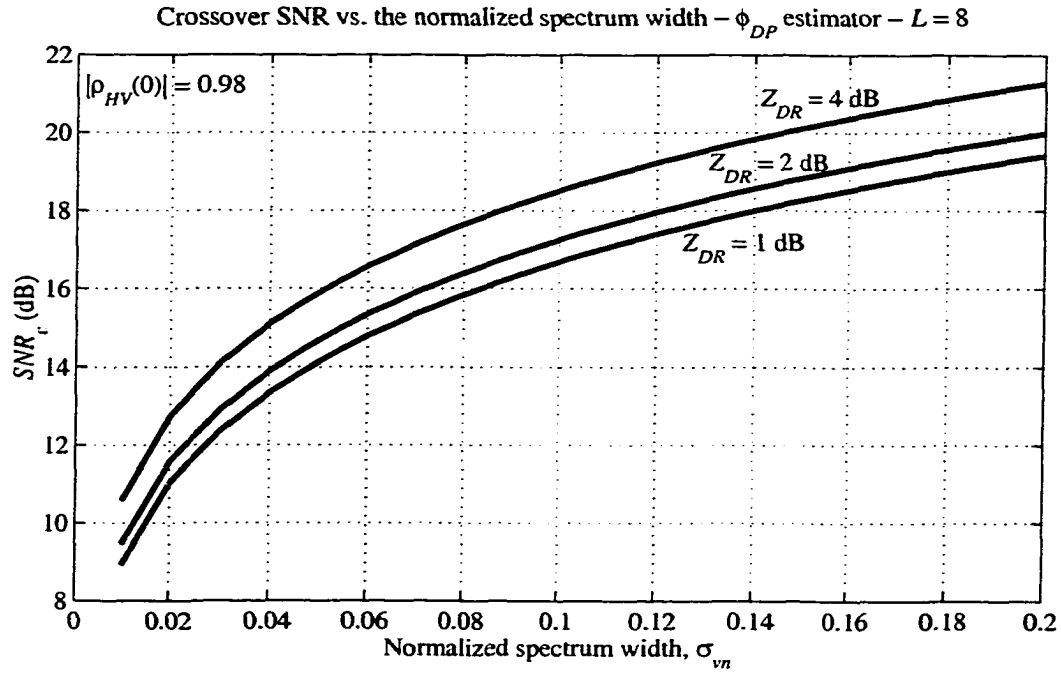


Figure 4.6. Crossover signal-to-noise ratio SNR_c versus the normalized spectrum width for the differential phase estimator and an ideal system using the differential reflectivity (Z_{DR}) as a parameter. The oversampling factor L is 8 and the magnitude of the cross-correlation coefficient $|\rho_{HV}(0)|$ is 0.98.

4.3. Estimation of the Magnitude of the Cross-Correlation Coefficient

The cross-correlation coefficient ρ_{HV} is the normalized correlation between the reflected horizontal and vertical voltage returns. At lag zero, the magnitude of ρ_{HV} is a good indicator of regions where there is a mixture of precipitation types, such as rain and snow. The magnitude of the cross-correlation coefficient for lag zero, loosely referred to in the literature as simply the “cross-correlation coefficient”, depends on the shape, oscillation, wobbling, and canting angle distribution of hydrometeors (Sachidananda and Zmic 1985). This polarimetric variable has been recently investigated for application to hail sizing,

improving polarization estimates of rainfall, and detection of melting level in both convective and stratiform precipitation (Liu et al. 1994). It is shown next that WTB estimators of $|\rho_{HV}(0)|$ achieve small errors with fewer samples than classical estimators, resulting in the same advantages as discussed for the previous variables.

4.3.1. Correlated Samples

The cross-correlation coefficient estimator applied to oversampled correlated samples is

$$|\hat{\rho}_{HV}(0)|_{corr} = \frac{|\hat{R}_{V_H V_V}^{(T)}(0)|}{\sqrt{\hat{S}_{H_{corr}} \hat{S}_{V_{corr}}}}, \quad (4.28)$$

where

$$\hat{R}_{V_H V_V}^{(T)}(0) = \frac{1}{LM} \sum_{l=0}^{L-1} \sum_{m=0}^{M-1} V_H(l, m) V_V^*(l, m), \quad (4.29)$$

$$\hat{S}_{H_{corr}} = \frac{1}{LM} \sum_{l=0}^{L-1} \sum_{m=0}^{M-1} |V_H(l, m)|^2 - N, \quad (4.30)$$

$$\hat{S}_{V_{corr}} = \frac{1}{LM} \sum_{l=0}^{L-1} \sum_{m=0}^{M-1} |V_V(l, m)|^2 - N, \quad (4.31)$$

In (4.29), (4.30), and (4.31) V_H and V_V are the oversampled correlated signals corresponding to the horizontal and vertical channels, respectively. As before, N is the noise power in horizontal and vertical channels.

Perturbation analysis can be used to compute the variance of cross-correlation coefficient estimates (Liu et al. 1994) as

$$\begin{aligned}
\text{Var}\{\hat{\rho}_{HV}(0)|_{corr}\} &= |\rho_{HV}(0)|^2 \left[\frac{1}{2} \text{Re} \left\{ E \left[\left(\frac{\hat{R}_{V_H V_V}^{(T)}(0) - R_{V_H V_V}^{(T)}(0)}{R_{V_H V_V}^{(T)}(0)} \right)^2 \right] \right\} + \right. \\
&+ E \left[\left| \frac{\hat{R}_{V_H V_V}^{(T)}(0) - R_{V_H V_V}^{(T)}(0)}{R_{V_H V_V}^{(T)}(0)} \right|^2 \right] \left. - \text{Re} \left\{ \text{Cov} \left[\frac{\hat{S}_{H_{corr}}}{S_H}, \frac{\hat{R}_{V_H V_V}^{(T)}(0)}{R_{V_H V_V}^{(T)}(0)} \right] \right\} - \right. \\
&- \text{Re} \left\{ \text{Cov} \left[\frac{\hat{S}_{V_{corr}}}{S_V}, \frac{\hat{R}_{V_H V_V}^{(T)}(0)}{R_{V_H V_V}^{(T)}(0)} \right] \right\} + \frac{1}{4} \text{Var} \left(\frac{\hat{S}_{H_{corr}}}{S_H} \right) + \\
&+ \frac{1}{2} \text{Cov} \left(\frac{\hat{S}_{H_{corr}}}{S_H}, \frac{\hat{S}_{V_{corr}}}{S_V} \right) + \frac{1}{4} \text{Var} \left(\frac{\hat{S}_{V_{corr}}}{S_V} \right) \left. \right]. \quad (4.32)
\end{aligned}$$

The expectation operations in (4.32) are computed below:

$$E \left[\left(\hat{R}_{V_H V_V}^{(T)}(0) - R_{V_H V_V}^{(T)}(0) \right)^2 \right] = E \left[\left(\hat{R}_{V_H V_V}^{(T)}(0) \right)^2 \right] - \left(R_{V_H V_V}^{(T)}(0) \right)^2, \quad (4.33)$$

where the first term on the right-hand side of (4.33) is given in (4.20).

$$E \left[\left| \hat{R}_{V_H V_V}^{(T)}(0) - R_{V_H V_V}^{(T)}(0) \right|^2 \right] = E \left[\left| \hat{R}_{V_H V_V}^{(T)}(0) \right|^2 \right] - \left| R_{V_H V_V}^{(T)}(0) \right|^2, \quad (4.34)$$

where the first term on the right-hand side of (4.34) is given in (4.19).

$$\text{Cov} \left[\frac{\hat{S}_{H_{corr}}}{S_H}, \frac{\hat{R}_{V_H V_V}^{(T)}(0)}{R_{V_H V_V}^{(T)}(0)} \right] = E \left[\frac{\hat{S}_{H_{corr}} \hat{R}_{V_H V_V}^{(T)}(0)}{S_H R_{V_H V_V}^{(T)}(0)} \right] - 1, \quad (4.35)$$

where

$$\begin{aligned}
E \left[\hat{S}_{H_{corr}} \hat{R}_{V_H V_V}^{(T)}(0) \right] &= \frac{1}{L^2 M^2} \sum_{l=0}^{L-1} \sum_{m=0}^{M-1} \sum_{l'=0}^{L-1} \sum_{m'=0}^{M-1} E \left[V_H(l, m) V_H^*(l, m) V_H(l', m') V_V^*(l', m') \right] - \\
&- \frac{N}{LM} \sum_{l'=0}^{L-1} \sum_{m'=0}^{M-1} E \left[V_H(l', m') V_V^*(l', m') \right] \\
&= \frac{1}{L^2 M^2} \sum_{l=-L+1}^{L-1} \sum_{m=-M+1}^{M-1} (L-|l|)(M-|m|) R_{V_V V_H}^*(l, m) R_{V_H V_H}(l, m) + S_H R_{V_H V_V}^{(T)}(0). \quad (4.36)
\end{aligned}$$

$$\text{Cov}\left[\frac{\hat{S}_{V_{corr}}}{S_V}, \frac{\hat{R}_{V_H V_V}^{(T)}(0)}{R_{V_H V_V}^{(T)}(0)}\right] = E\left[\frac{\hat{S}_{V_{corr}} \hat{R}_{V_H V_V}^{(T)}(0)}{S_V R_{V_H V_V}^{(T)}(0)}\right] - 1, \quad (4.37)$$

where

$$\begin{aligned} E\left[\hat{S}_{V_{corr}} \hat{R}_{V_H V_V}^{(T)}(0)\right] &= \frac{1}{L^2 M^2} \sum_{l=0}^{L-1} \sum_{m=0}^{M-1} \sum_{l'=0}^{L-1} \sum_{m'=0}^{M-1} E[V_V(l, m) V_V^*(l, m) V_H(l', m') V_V^*(l', m')] - \\ &\quad - \frac{N}{LM} \sum_{l'=0}^{L-1} \sum_{m'=0}^{M-1} E[V_H(l', m') V_V^*(l', m')] \\ &= \frac{1}{L^2 M^2} \sum_{l=-L+1}^{L-1} \sum_{m=-M+1}^{M-1} (L-|l|)(M-|m|) R_{V_H V_V}(l, m) R_{V_V}^*(l, m) + S_V R_{V_H V_V}^{(T)}(0). \end{aligned} \quad (4.38)$$

In addition, $\text{Var}\left(\frac{\hat{S}_{H_{corr}}}{S_H}\right)$ and $\text{Var}\left(\frac{\hat{S}_{V_{corr}}}{S_V}\right)$ can be computed from (3.27) by substituting S_H

or S_V for S , respectively. Finally, $\text{Cov}\left(\frac{\hat{S}_{H_{corr}}}{S_H}, \frac{\hat{S}_{V_{corr}}}{S_V}\right)$ was computed in Section 4.1.1 in

equations (4.5) and (4.6). With the usual assumptions (4.32) reduces to

$$\begin{aligned} \text{Var}\left\{|\hat{\rho}_{HV}(0)|_{corr}\right\} &= \frac{1}{M} \left[\frac{1 - 2|\rho_{HV}(0)|^2 + |\rho_{HV}(0)|^4}{4\sigma_{vn}\sqrt{\pi}} \frac{\text{tr}\{[\mathbf{C}_{V_S}^{(R)}]^2\}}{L^2} + \right. \\ &\quad \left. + \frac{(1 - |\rho_{HV}(0)|^2)(1 + Z_{DR})}{2L} \left(\frac{N}{S_H}\right) + \frac{|\rho_{HV}(0)|^2 + 2Z_{DR} + |\rho_{HV}(0)|^2 Z_{DR}^2}{4L} \left(\frac{N}{S_H}\right)^2 \right]. \end{aligned} \quad (4.39)$$

An analytic expression for the variance of $|\rho_{HV}(0)|$ for simultaneous transmission has not been found in the literature; though Liu et al. (1994) provide similar results for the case of alternate transmission of horizontally and vertically polarized signals. For the ideal case, the standard deviation can be obtained from (4.39) as

$$SD\{\hat{\rho}_{HV}(0)_{corr}\} = \frac{1}{\sqrt{M}} \left[\frac{1 - 2|\rho_{HV}(0)|^2 + |\rho_{HV}(0)|^4}{4\sigma_{vn}\sqrt{\pi}} \frac{L^2 + 1}{2L^2} + \frac{(1 - |\rho_{HV}(0)|^2)(1 + Z_{DR})}{2L} \left(\frac{N}{S_H} \right) + \frac{|\rho_{HV}(0)|^2 + 2Z_{DR} + |\rho_{HV}(0)|^2 Z_{DR}^2}{4L} \left(\frac{N}{S_H} \right)^2 \right]^{1/2}. \quad (4.40)$$

Figure 4.7 shows the normalized standard deviation of cross-correlation coefficient estimates versus the normalized spectrum width for the ideal case and several values of $|\rho_{HV}(0)|$. It is evident from this plot that theoretical results are in good agreement with simulations.

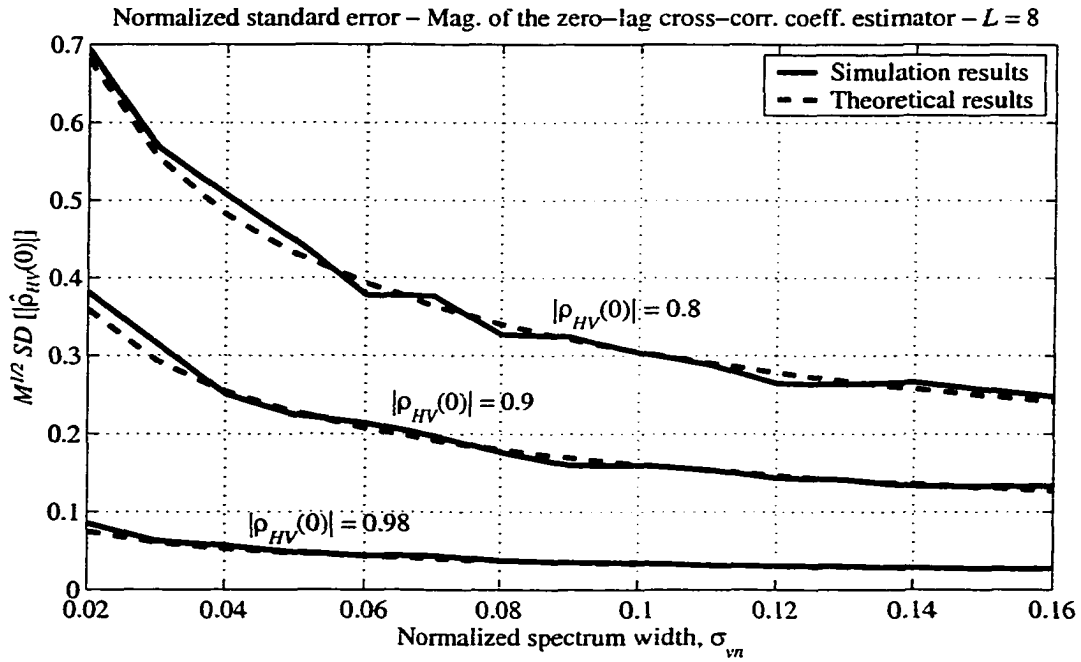


Figure 4.7. Normalized standard deviation of cross-correlation coefficient estimates on correlated data versus the normalized spectrum width with the actual correlation coefficient $|\rho_{HV}(0)|$ as a parameter for the ideal case. The oversampling factor L is 8 and the SNR is very large. Both theoretical results (dashed line) and simulation results (solid line) are plotted.

4.3.2. Whitened Samples

The cross-correlation coefficient estimator applied to oversampled whitened samples is

$$|\hat{\rho}_{HV}(0)|_{\text{whitened}} = \frac{|\hat{R}_{X_H X_V}^{(T)}(0)|}{\sqrt{\hat{S}_{H \text{ whitened}} \hat{S}_{V \text{ whitened}}}}, \quad (4.41)$$

where

$$\hat{R}_{X_H X_V}^{(T)}(0) = \frac{1}{LM} \sum_{l=0}^{L-1} \sum_{m=0}^{M-1} X_H(l, m) X_V^*(l, m), \quad (4.42)$$

$$\hat{S}_{H \text{ whitened}} = \frac{1}{LM} \sum_{l=0}^{L-1} \sum_{m=0}^{M-1} |X_H(l, m)|^2 - N(NEF), \quad (4.43)$$

$$\hat{S}_{V \text{ whitened}} = \frac{1}{LM} \sum_{l=0}^{L-1} \sum_{m=0}^{M-1} |X_V(l, m)|^2 - N(NEF). \quad (4.44)$$

In (4.42), (4.43), and (4.44) X_H and X_V are the oversampled whitened signals corresponding to the horizontal and vertical channels, respectively. As before, N is the noise power in the horizontal and vertical channels, and NEF is the noise-enhancement factor.

Analogously as in the previous section, the variance of the estimator in (4.41) is

$$\begin{aligned} \text{Var}\{|\hat{\rho}_{HV}(0)|_{\text{whitened}}\} &= |\rho_{HV}(0)|^2 \left[\frac{1}{2} \text{Re} \left\{ E \left[\left(\frac{\hat{R}_{X_H X_V}^{(T)}(0) - R_{V_H V_V}^{(T)}(0)}{R_{V_H V_V}^{(T)}(0)} \right)^2 \right] \right. \right. \\ &+ E \left[\left| \frac{\hat{R}_{X_H X_V}^{(T)}(0) - R_{V_H V_V}^{(T)}(0)}{R_{V_H V_V}^{(T)}(0)} \right|^2 \right] \left. \right\} - \text{Re} \left\{ \text{Cov} \left[\frac{\hat{S}_{H \text{ whitened}}}{S_H}, \frac{\hat{R}_{X_H X_V}^{(T)}(0)}{R_{V_H V_V}^{(T)}(0)} \right] \right\} - \\ &- \text{Re} \left\{ \text{Cov} \left[\frac{\hat{S}_{V \text{ whitened}}}{S_V}, \frac{\hat{R}_{X_H X_V}^{(T)}(0)}{R_{V_H V_V}^{(T)}(0)} \right] \right\} + \frac{1}{4} \text{Var} \left(\frac{\hat{S}_{H \text{ whitened}}}{S_H} \right) + \\ &+ \frac{1}{2} \text{Cov} \left(\frac{\hat{S}_{H \text{ whitened}}}{S_H}, \frac{\hat{S}_{V \text{ whitened}}}{S_V} \right) + \frac{1}{4} \text{Var} \left(\frac{\hat{S}_{V \text{ whitened}}}{S_V} \right) \left. \right]. \quad (4.45) \end{aligned}$$

The expectation operations inside (4.45) can be computed as in the previous section, where X_H and X_V are used instead of V_H and V_V . Then, with the typical assumptions (4.45) reduces to

$$\begin{aligned} \text{Var}\{|\hat{\rho}_{HV}(0)|_{\text{whitened}}\} = & \frac{1}{M} \left[\frac{1 - 2|\rho_{HV}(0)|^2 + |\rho_{HV}(0)|^4}{4\sigma_{vn}\sqrt{\pi}} \frac{1}{L} + \right. \\ & + \frac{(1 - |\rho_{HV}(0)|^2)(1 + Z_{DR})}{2} \frac{\text{tr}\{[\mathbf{C}_{\mathbf{v}_s}^{(R)}]^{-1}\}}{L^2} \left(\frac{N}{S_H} \right) + \\ & \left. + \frac{|\rho_{HV}(0)|^2 + 2Z_{DR} + |\rho_{HV}(0)|^2 Z_{DR}^2}{4} \frac{\text{tr}\{[\mathbf{C}_{\mathbf{v}_s}^{(R)}]^{-2}\}}{L^2} \left(\frac{N}{S_H} \right)^2 \right]. \end{aligned} \quad (4.46)$$

For the ideal case, the standard deviation can be obtained from (4.46) as

$$\begin{aligned} \text{SD}\{|\hat{\rho}_{HV}(0)|_{\text{whitened}}\} = & \frac{1}{\sqrt{M}} \left[\frac{1 - 2|\rho_{HV}(0)|^2 + |\rho_{HV}(0)|^4}{4\sigma_{vn}\sqrt{\pi}} \frac{1}{L} + \right. \\ & + \frac{L(1 - |\rho_{HV}(0)|^2)(1 + Z_{DR})}{2(L+1)} \left(\frac{N}{S_H} \right) + \\ & \left. + \frac{L(3L^2 + 2L - 3)}{8(L+1)^2} \left(|\rho_{HV}(0)|^2 + 2Z_{DR} + |\rho_{HV}(0)|^2 Z_{DR}^2 \right) \left(\frac{N}{S_H} \right)^2 \right]^{1/2}. \end{aligned} \quad (4.47)$$

Figure 4.8 shows the normalized standard deviation of cross-correlation coefficient estimates versus the normalized spectrum width for the ideal case and several values of $|\rho_{HV}(0)|$. Once again, theoretical results are in good agreement with simulations.

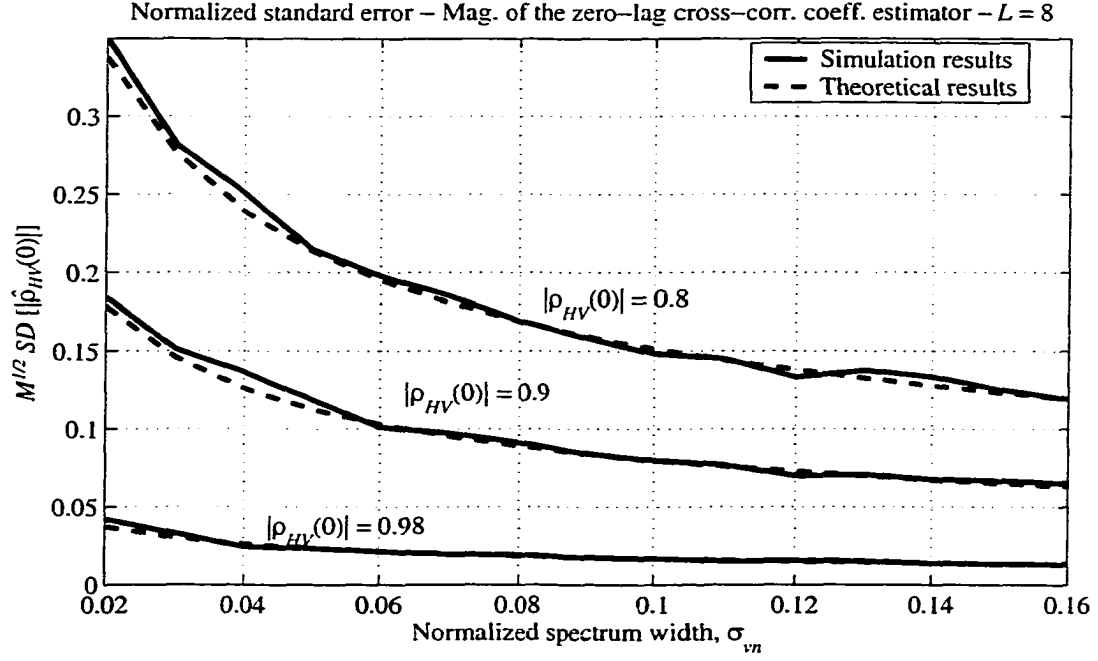


Figure 4.8. Normalized standard deviation of cross-correlation coefficient estimates on whitened data versus the normalized spectrum width with the actual correlation coefficient $|\rho_{HV}(0)|$ as a parameter for the ideal case. The oversampling factor L is 8 and the SNR is very large. Both theoretical results (dashed line) and simulation results (solid line) are plotted.

4.3.3. Comparison

Comparison between the results in Figure 4.7 and Figure 4.8 reveals significant reduction of errors for the WTB cross-correlation coefficient estimator at large SNR. Once more, for lower SNRs the noise-enhancement effect begins to dominate and consequently deteriorates the performance of the WTB estimator. The crossover SNR (SNR_c), which is a good indicator of this effect, is plotted in Figure 4.9 as a function of the normalized spectrum width for several values of Z_{DR} . It is interesting to observe that SNR_c for $|\rho_{HV}(0)|$ is always higher than SNR_c for both ϕ_{DP} and Z_{DR} (compare Figures 4.3, 4.6, and 4.9).

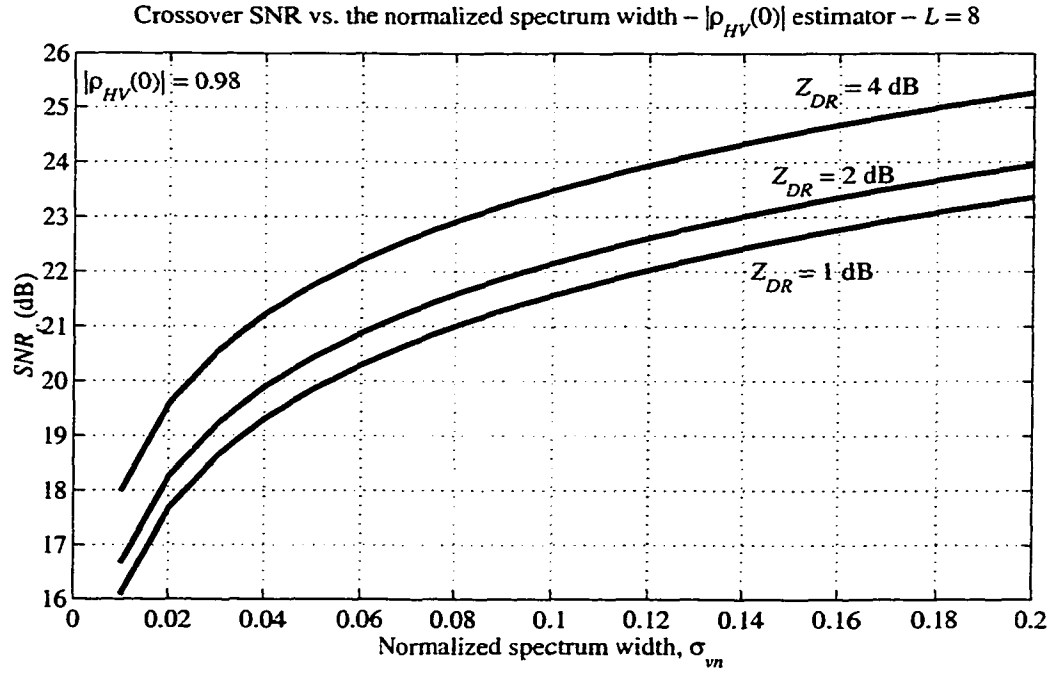


Figure 4.9. Crossover signal-to-noise ratio SNR_c versus the normalized spectrum width for the cross-correlation coefficient estimator and an ideal system using the differential reflectivity (Z_{DR}) as a parameter. The oversampling factor L is 8 and the magnitude of the cross-correlation coefficient $|\rho_{HV}(0)|$ is 0.98.

4.4. Results

Sections 4.1 through 4.3 discussed the application of the whitening transformation to the estimation of polarimetric variables. Estimators operating on whitened signals were termed whitening-transformation-based (WTB) estimators, and they exhibit reduced standard errors if the signal-to-noise ratio is relatively large.

A performance comparison of all WTB estimators with estimators on correlated data for the ideal case showed that for all the variables the variance reduction for large SNR is

$$VRF = \frac{L^2 + 1}{2L}, \quad (4.48)$$

where L is the oversampling factor. That is, as with the spectral moments, approximately

$L/2$ fewer samples are needed for WTB estimators of polarimetric variables to keep the same errors as the ones obtained without the aid of the whitening transformation.

For low SNR, the performance of all WTB estimators deteriorates as the noise-enhancing effect discussed in Section 2.5 becomes important. In such case, the estimates on non-whitened data result in better performance, and the rule for selecting the best estimate is as in Chapter 3:

$$\hat{\theta} = \begin{cases} \hat{\theta}_{corr} & \text{if } SNR < SNR_c \\ \hat{\theta}_{whitened} & \text{if } SNR \geq SNR_c. \end{cases} \quad (4.49)$$

In equation (4.49) θ is any of the variables discussed in this chapter, namely Z_{DR} , Φ_{DP} , or $|\rho_{HV}(0)|$, and SNR_c is the crossover SNR defined as the SNR that conduces to a variance reduction factor of one. Theoretical expressions for the variance of estimates as derived in the previous sections become useful if one needs to compute the value of SNR_c for a given variable under specific conditions without the need of simulations (see Figures 4.3, 4.6, and 4.9). Under appropriate limiting conditions, these expressions match the ones found in the literature, if available. It is interesting to observe that the SNR_c as functions of σ_{vn} for estimates of the three polarimetric variables discussed in this chapter are at different levels but exhibit the same behavior (Figures 4.3, 4.6, and 4.9).

The variance reduction obtained with WTB estimators is of considerable importance for the polarimetric variables. Unlike errors in the spectral moments, errors in polarimetric variables at the current antenna rotation rates do not always meet the required accuracy. Consequently, the use of WTB estimators for the polarimetric variables can reduce errors to acceptable levels without sacrificing (slowing down) the antenna rotational speed.

5. THE WHITENING TRANSFORMATION IN PERSPECTIVE

Since the origin of radar meteorology in the early 1940s, around the time when the term *radar* became the official acronym of equipment built for radio detecting and ranging of objects, engineers and meteorologists have been working on ways to survey the atmosphere with increased resolution, at faster speeds, and producing more accurate estimates of the variables of interest. The whitening transformation described in this dissertation is a novel technique in a class of several others that use range samples to reduce the errors of estimates on weather radars. The first part of this chapter presents a comparative study of such techniques. The second part is devoted to the analysis of several variations of the whitening transformation that attempt to overcome the problems discussed in previous chapters.

5.1. Alternatives to the Whitening Transformation

Soon after Doppler radars became a reality, researchers recognized that the variance of estimators could be reduced with little degradation of the spatial resolution by further averaging of range samples (Zrnic 1979). That is, in order to obtain more accurate estimates in Doppler weather radars, range-time averaging can be performed in addition to the conventional sample-time averaging.

The method of averaging oversampled data along range time, which is identified here as “regular pulse with averaging in range”, was one of the first techniques that used range samples to reduce the variance of estimates. Despite its simplicity, the variance reduction

attained with this procedure depends not only on the number of averaged samples but also on their correlation. Doviak and Zrnic (1979) computed the correlation of samples along range time, and later Walker et al. (1980) applied this result to the computation of the equivalent number of independent samples (M_I) for different types of receivers.

Because highly correlated samples result in a small equivalent number of independent samples, it is desirable to reduce the correlation of samples along range time by either shortening the pulse length or increasing the receiver's bandwidth. The method involving "short pulse with averaging in range" addresses this variation by reducing the pulse length to match the oversampling period. Unfortunately, a reduced pulse length requires a larger transmission bandwidth and, more importantly, it decreases the average transmitted power, which can hinder the radar's normal modes of operation.

Pulse compression techniques achieve the average transmitted power of a relatively long pulse while obtaining the range resolution of a short pulse. Averaging the fine-scale (uncorrelated) range measurements obtained by means of pulse compression techniques in fact results in an optimum utilization of range samples in terms of estimate variance reduction (Mudukutore et al. 1998). Nonetheless, pulse compression does not come without a rather expensive price. The need for a larger transmission bandwidth and the presence of range sidelobes that tend to smear the returns in range are two major drawbacks of this technique.

As discussed in previous chapters, the whitening transformation produces independent range samples that lead to a maximum reduction in the variances of estimates. Because the transmitter pulse remains unchanged, this technique does not require a large

transmission bandwidth, a very expensive commodity in the modern world of telecommunications. Computationally equivalent to pulse compression, the whitening transformation presents the best compromise: independent oversampled range samples and little sacrifice in range resolution.

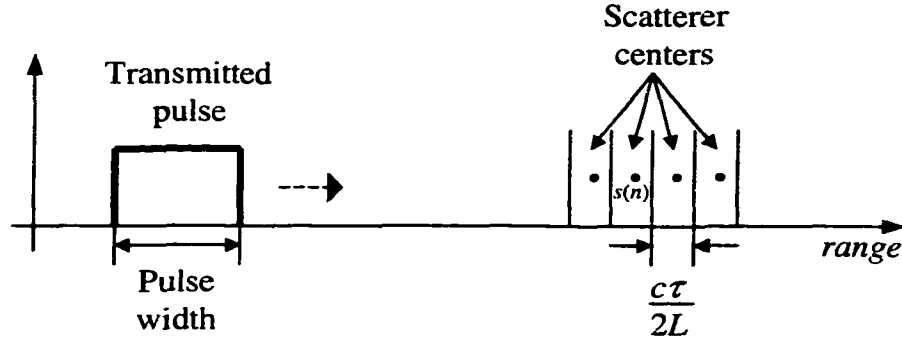


Figure 5.1. Hydrometeors in each resolution volume are represented by their equivalent scatterer center, spaced by $c\tau/2L$ along range. Returns at the receiver front end are weighted by the transmitted pulse envelope.

In the comparative analysis that follows a sampling rate of L/τ is assumed, thus for simplification, equivalent scatterer centers $s(n)$ are spaced by $c\tau/2L$ (see Figure 5.1). Also, it is assumed that the power backscattered by the scatterer centers is uniform; i.e., $E[|s(l)|^2] = \sigma_s^2$ for every l . The receiver bandwidth is larger than L/τ and constant, resulting in an effective noise power N ; the transmitted peak power P_t is also constant; and SNR computations are referred to the composite sample as follows: (i) for the short and long pulses with regular averaging it is the V sample as defined in (2.5), (ii) for the regular pulse with whitened range samples it is the whitened X sample as defined in (2.15), and (iii) for pulse compression it is the sample of the compressed pulse. Only reflectivity estimates for one pulse ($M = 1$) are considered in this comparison since the processing along sample time is the same in all the cases. In addition to depending on the

signal power S , reflectivity estimates at a fixed range location r depend on the transmitted pulse length (τ_{pulse}) and several radar parameters collected into K_{radar} that remain constant throughout this analysis; that is

$$\hat{Z}_e = \frac{K_{radar} r^2 \hat{S}}{\tau_{pulse}}. \quad (5.1)$$

Figure 5.2 depicts the simplified block diagram of a digital-receiver-based system used for the analyses in the following sections.

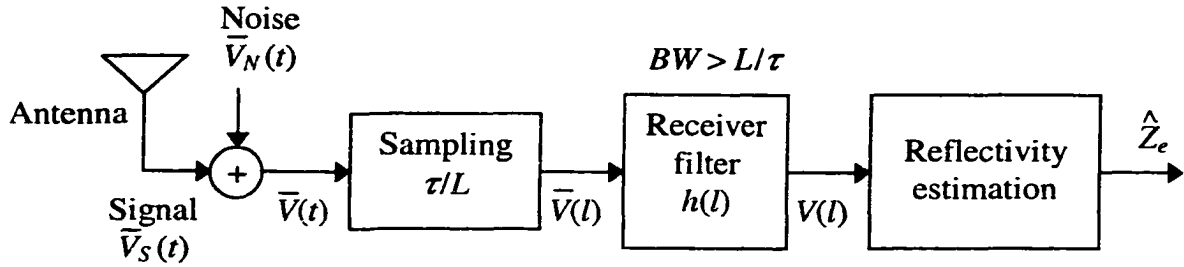


Figure 5.2. Simplified block diagram of a digital-receiver-based weather radar for the estimation of reflectivity.

5.1.1. Regular Pulse with Averaging in Range

In this method, a rectangular pulse of τ seconds is transmitted so there are L samples in the pulse. Processing of samples consists of (1) taking the magnitude squared of complex return samples, (2) computing the average of these quantities in blocks of L samples, and (3) scaling the power estimate to the proper range location and radar parameters (see Figure 5.3). Hence, there is one reflectivity estimate every τ seconds.

The weather signal power estimator at range $r_k = ck\tau/2$ ($k = 0, 1, 2, \dots$) is

$$\hat{S}(k) = \frac{1}{L} \sum_{l=k}^{k+L-1} |V(l)|^2 - N, \quad (5.2)$$

where $V(l)$ can be computed using (2.5) as

$$V(l) = \left[\sum_{n=l}^{l+L-1} s(n) p(L-1-n+l) \right] * h(l) \approx \sum_{n=l}^{l+L-1} s(n). \quad (5.3)$$

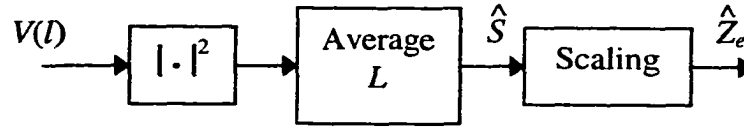


Figure 5.3. Processing for the estimation of reflectivity in the case of regular pulse with averaging in range.

The approximation in (5.3) is possible because the envelope of the transmitted pulse is rectangular and the receiver bandwidth is much larger than the reciprocal of the pulse length. Therefore, if the SNR is very large, the expected value of power estimates is given by

$$E[\hat{S}(k)] = \frac{1}{L} \sum_{l=k}^{k+L-1} E[|V(l)|^2] = \frac{1}{L} \sum_{l=k}^{k+L-1} \sum_{n=l}^{l+L-1} \sum_{n'=l}^{l+L-1} E[s(n)s^*(n')]. \quad (5.4)$$

Because the signals backscattered by non-overlapping slabs are uncorrelated

$$E[\hat{S}(k)] = \frac{1}{L} \sum_{l=k}^{k+L-1} \sum_{n=l}^{l+L-1} \sum_{n'=l}^{l+L-1} \sigma_s^2 \delta(n-n') = \frac{1}{L} \sum_{l=k}^{k+L-1} \sum_{n=l}^{l+L-1} \sigma_s^2 = L\sigma_s^2 = S. \quad (5.5)$$

Hence, the SNR of each complex sample is

$$SNR = \frac{S}{N} = \frac{L\sigma_s^2}{N}. \quad (5.6)$$

Under practical conditions, the SNR for regular pulse with averaging in range would be about L times higher than the value in (5.6) thanks to the matched filter that can be

included in the receiver for this particular case (see Chapter 6).

The variance of power estimates is

$$\begin{aligned}
 \text{Var}[\hat{S}(k)] &= \frac{1}{L^2} \sum_{l=k}^{k+L-1} \sum_{l'=k}^{k+L-1} \text{Cov}[|V(l)|^2, |V(l')|^2] \\
 &= \frac{1}{L^2} \sum_{l=k}^{k+L-1} \sum_{l'=k}^{k+L-1} E[V(l)V^*(l)V(l')V^*(l')] - S^2 \\
 &= \frac{1}{L^2} \sum_{l=k}^{k+L-1} \sum_{l'=k}^{k+L-1} (E[V(l)V^*(l)]^2 + E[V(l)V^*(l')]E[V(l')V^*(l)] - S^2) \\
 &= \frac{1}{L^2} \sum_{l=k}^{k+L-1} \sum_{l'=k}^{k+L-1} S^2 + |R_V^{(R)}(l-l')|^2 - S^2 \\
 &= \frac{S^2}{L^2} \sum_{l=-L+1}^{L-1} (L-|l|) |\rho_V^{(R)}(l)|^2 = \frac{L^2+1}{2L^2} S^2, \tag{5.7}
 \end{aligned}$$

where the normalized autocorrelation for range samples $\rho_V^{(R)}(l)$ in an ideal system is given in (2.9).

5.1.2. Short Pulse with Averaging in Range

In this method, a short rectangular pulse of τ/L seconds is transmitted so there is only one sample in the pulse. Processing of samples consists of (1) taking the magnitude squared of complex return samples, (2) computing the average of these quantities in blocks of L samples, and (3) scaling the power estimate to the proper range location and radar parameters (Figure 5.4). Hence, there is one reflectivity estimate every τ seconds.

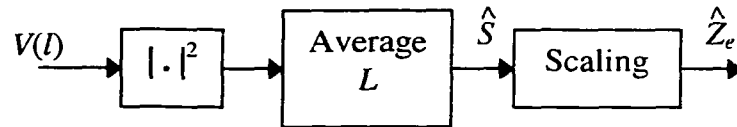


Figure 5.4. Processing and estimation for the case of short pulse with averaging in range.

The signal power estimator at range $r_k = ck\tau/2$ ($k = 0, 1, 2, \dots$) is

$$\hat{S}(k) = \frac{1}{L} \sum_{l=k}^{k+L-1} |V(l)|^2 - N, \quad (5.8)$$

where in this case

$$V(l) = s(l). \quad (5.9)$$

Therefore, if the SNR is very large, the expected value of power estimates is given by

$$E[\hat{S}(k)] = \frac{1}{L} \sum_{l=k}^{k+L-1} E[|V(l)|^2] = \frac{1}{L} \sum_{l=k}^{k+L-1} E[|s(l)|^2] = \frac{1}{L} \sum_{l=k}^{k+L-1} \sigma_s^2 = \sigma_s^2 = S. \quad (5.10)$$

Hence, the SNR of each complex sample is

$$SNR = \frac{\sigma_s^2}{N}. \quad (5.11)$$

The variance of power estimates is

$$\begin{aligned} Var[\hat{S}(k)] &= \frac{1}{L^2} \sum_{l=k}^{k+L-1} \sum_{l'=k}^{k+L-1} Cov[|V(l)|^2, |V(l')|^2] = \\ &= \frac{1}{L^2} \sum_{l=k}^{k+L-1} \sum_{l'=k}^{k+L-1} E[s(l)s^*(l)s(l')s^*(l')] - S^2 \\ &= \frac{1}{L^2} \sum_{l=k}^{k+L-1} \sum_{l'=k}^{k+L-1} (E[s(l)s^*(l)])^2 + E[s(l)s^*(l')]E[s(l')s^*(l)] - S^2 \\ &= \frac{1}{L^2} \sum_{l=k}^{k+L-1} \sum_{l'=k}^{k+L-1} S^2 + S^2 \delta(l-l') - S^2 \\ &= \frac{1}{L^2} \sum_{l=k}^{k+L-1} S^2 = \frac{S^2}{L}. \end{aligned} \quad (5.12)$$

Although the SNR using a regular pulse with average in range is L times larger, the fractional variance in this case is approximately $L/2$ times smaller.

5.1.3. Pulse Compression

In this method, a pulse of τ seconds is modulated by a suitable phase code $c(l)$ of length L , so there are L samples in the pulse corresponding to the number of sub-pulses in the phase-modulated transmitted pulse. Pulse modulation in this context refers to a change of phase of the RF sinusoidal carrier every τ/L seconds. A special case of phase codes are binary codes (e.g., Barker codes) for which the carrier of each sub-pulse is shifted either 0° or 180° . Processing of samples consists of (1) correlating or “compressing” the received signal with a sample of the transmitted pulse, (2) taking the magnitude squared of complex return samples, (3) computing the average of these quantities in blocks of L samples, and (4) scaling the power estimate to the proper range location and radar parameters (Figure 5.5). Hence, there is one reflectivity estimate every τ seconds.

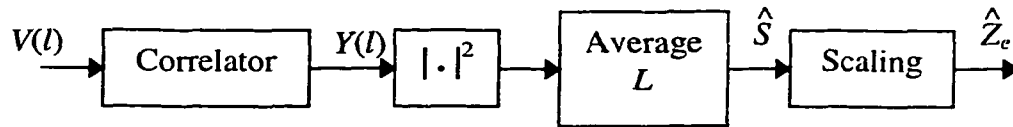


Figure 5.5. Processing and estimation for the case of pulse compression.

The weather signal power estimator at range $r_k = ck\tau/2$ ($k = 0, 1, 2, \dots$) is

$$\hat{S}(k) = \frac{1}{L} \sum_{l=k}^{k+L-1} |Y(l)|^2 - LN, \quad (5.13)$$

where the noise is enhanced by a factor of L due to the correlator or pulse compressor.

Pulse compressed samples $Y(l)$ in (5.13) are obtained as

$$Y(l) = \sum_{n=0}^{L-1} V(l-n)c(n), \quad (5.14)$$

where

$$V(l) = \left[\sum_{n=0}^{L-1} s(l+n)p(L-1-n)c(n) \right] * h(l) \approx \sum_{n=0}^{L-1} s(l+n)c(n), \quad (5.15)$$

because the pulse is rectangular and the receiver bandwidth is very large compared to the reciprocal of the pulse length. Substituting (5.15) into (5.14)

$$\begin{aligned} Y(l) &= \sum_{n'=0}^{L-1} c(n') \sum_{n=0}^{L-1} s(l-n'+n)c(n) \\ &= \sum_{n'=0}^{L-1} c(n') \sum_{n=-L+1}^{L-1} s(l+n)c(n'+n) \\ &= \sum_{n=-L+1}^{L-1} s(l+n) \left[\sum_{n'=0}^{L-1} c(n')c(n'+n) \right] \\ &= \sum_{n=-L+1}^{L-1} s(l+n)\phi(n), \end{aligned} \quad (5.16)$$

where for Barker codes (Nathanson 1969)

$$\phi(l) = \sum_{n=0}^{L-1} c(n)c(n+l) = \begin{cases} L & \text{if } l = 0 \\ 0, \pm 1 & \text{if } l \neq 0. \end{cases} \quad (5.17)$$

Therefore, if the SNR is very large, the expected value of power estimates is given by

$$\begin{aligned} E[\hat{S}(k)] &= \frac{1}{L} \sum_{l=k}^{k+L-1} E[|Y(l)|^2] \\ &= \frac{1}{L} \sum_{l=k}^{k+L-1} \sum_{n=-L+1}^{L-1} \sum_{n'=-L+1}^{L-1} E[s(l+n)s^*(l+n')]\phi(n)\phi(n') \\ &= \frac{1}{L} \sum_{l=k}^{k+L-1} \sum_{n=-L+1}^{L-1} \sum_{n'=-L+1}^{L-1} \sigma_s^2 \phi(n)\phi(n')\delta(n-n') \end{aligned}$$

$$\begin{aligned}
&= \frac{1}{L} \sum_{l=k}^{k+L-1} \sum_{n=-L+1}^{L-1} \sigma_s^2 \phi^2(n) \\
&= \sigma_s^2 \sum_{n=-L+1}^{L-1} \phi^2(n) ,
\end{aligned} \tag{5.18}$$

which reduces to

$$E[\hat{S}(k)] = L^2 \sigma_s^2 = S \tag{5.19}$$

for the ideal case where there are no sidelobes. The range-sidelobe effect of pulse compression techniques is evident in the non-uniform case by observing that if $E[|s(l)|^2] = \sigma_s^2(l)$ (5.18) turns into

$$E[\hat{S}(k)] = \frac{1}{L} \sum_{l=k}^{k+L-1} \sum_{n=-L+1}^{L-1} \sigma_s^2(l+n) \phi^2(n) = \frac{1}{L} \sum_{l=k}^{k+L-1} S(l) , \tag{5.20}$$

and backscattered powers $S(l)$ corresponding to a range $r_l = cl\tau/2L$ include contributions from ranges up to $(L-1)c\tau/2L$ meters around r_l .

From (5.19), the SNR of each complex sample (considering power from the sidelobes as another source of noise) is

$$SNR = \frac{L^2 \sigma_s^2}{LN + \sigma_s^2 \sum_{n \neq 0} \phi^2(n)} , \tag{5.21}$$

which reduces to

$$SNR = \frac{L \sigma_s^2}{N} \tag{5.22}$$

neglecting range sidelobes.

The variance of power estimates is

$$\begin{aligned}
Var[\hat{S}(k)] &= \frac{1}{L^2} \sum_{l=k}^{k+L-1} \sum_{l'=k}^{k+L-1} Cov[|Y(l)|^2, |Y(l')|^2] \\
&= \frac{1}{L^2} \sum_{l=k}^{k+L-1} \sum_{l'=k}^{k+L-1} E[Y(l)Y^*(l)Y(l')Y^*(l')] - S^2 \\
&= \frac{1}{L^2} \sum_{l=-L+1}^{L-1} (L-|l|) |R_Y^{(R)}(l)|^2.
\end{aligned} \tag{5.23}$$

In (5.23), the autocorrelation for range samples after the correlator in an ideal system is

$$\begin{aligned}
R_Y(l) &= E[Y^*(l')Y(l'+l)] \\
&= \sum_{n=-L+1}^{L-1} \sum_{n'=-L+1}^{L-1} E[s^*(l'+n)s(l'+l+n')] \phi(n)\phi^*(n') \\
&= \sigma_s^2 \sum_{n=-L+1}^{L-1} \phi(n)\phi^*(n-l) = \sigma_s^2 \varphi(l),
\end{aligned} \tag{5.24}$$

where $\varphi(l) = \phi(l) * \phi^*(-l)$. Introducing (5.24) into (5.23), the variance of power estimates simplifies to

$$Var[\hat{S}(k)] = \frac{S^2}{L^2} \sum_{l=-L+1}^{L-1} (L-|l|) |\varphi(l)|^2, \tag{5.25}$$

which in the ideal case where there are no sidelobes reduces to

$$Var[\hat{S}(k)] = \frac{S^2}{L}. \tag{5.26}$$

5.1.4. Regular Pulse with Whitening in Range

In this case, a rectangular pulse of τ seconds is transmitted so there are L samples in the pulse. Processing of samples consists of (1) whitening a block of L samples, (2) taking the magnitude squared of the whitened complex return samples, (3) computing the average of these quantities in blocks of L samples, and (4) scaling the power estimate to

the proper range location and radar parameters (Figure 5.6). Hence, there is one reflectivity estimate every τ seconds.

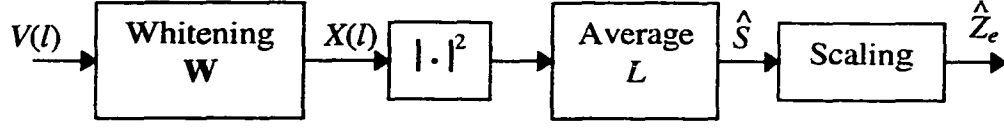


Figure 5.6. Processing and estimation for the case of regular pulse with whitening in range.

The signal power estimator at range $r_k = ck\tau/2$ ($k = 0, 1, 2, \dots$) is

$$\hat{S}(k) = \frac{1}{L} \sum_{l=k}^{k+L-1} |X(l)|^2 - N(NEF), \quad (5.27)$$

where the noise is affected by the noise-enhancement factor (NEF) given in (2.22).

Whitened samples are obtained as

$$X(l) = \sum_{n=0}^{L-1} w_{l,n} V(n), \quad (5.28)$$

where $w_{l,n}$ are the entries of the whitening transformation matrix and $V(l)$ is given by

$$V(l) = \left[\sum_{n=l}^{l+L-1} s(n) p(L-1-n+l) \right] * h(l) \approx \sum_{n=l}^{l+L-1} s(n). \quad (5.29)$$

As proved in previous chapters, the expected value of power estimates is given by

$$E[\hat{S}(k)] = \frac{1}{L} \sum_{l=k}^{k+L-1} E[|X(l)|^2] = L\sigma_s^2 = S. \quad (5.30)$$

Hence, the SNR of each complex sample is

$$SNR = \frac{L\sigma_s^2}{N(NEF)}, \quad (5.31)$$

which reduces to

$$SNR = \frac{(L+1)\sigma_s^2}{LN} \quad (5.32)$$

for the ideal case [see (2.26)]. The variance of power estimates is

$$Var[\hat{S}(k)] = \frac{S^2}{L}. \quad (5.33)$$

5.1.5. Comparison

The results of sections 5.1.1 through 5.1.4 are summarized in Table 5.1. Whereas regular pulse with averaging in range is (a) the simplest method, (b) does not require a larger transmission bandwidth, and (c) exhibits an excellent SNR (even better with a matched filter); the statistical performance of the power estimator for this setting is the poorest. Short pulse with averaging in range achieves the desired statistical performance by genuinely obtaining independent samples in range. Nonetheless, as the average transmitted power is decreased, the SNR is L times smaller, and more importantly, it requires a larger transmission bandwidth. Pulse compression restores the SNR to the value that the regular pulse would have while still achieving almost independent samples, but transmission bandwidth requirements are still prohibitive for its practical implementation. Regular pulse with whitening in range inherently deteriorates the SNR due to the noise enhancement effect. Still, independent range samples are obtained

without the need for a larger transmission bandwidth. The extent of the range weighting function is the same as with the regular pulse and averaging in range, but almost twice as large as with the other two schemes.

The advantages and disadvantages of each technique that can be derived from Table 5.1 offer different trade-offs. Thus, the decision about which method is best depends on engineering conditions such as the freedom to increase transmission/reception bandwidths, the capability to increase processing power, or the peak power limitation of transmitters.

	Regular pulse with averaging in range	Short pulse with averaging in range	Pulse compression	Regular pulse with whitening in range
Pulse length	τ	τ/L	τ (τ/L after compression)	τ
Received signal power	$L\sigma_s^2$	σ_s^2	$L^2\sigma_s^2$	$L\sigma_s^2$
Normalized variance of signal power	$(L^2+1)/2L^2$	$1/L$	$1/L$	$1/L$
SNR of composite samples	$L\sigma_s^2/N$	σ_s^2/N	$L\sigma_s^2/N$	$(L+1)\sigma_s^2/LN$
Extent of the range weighting function	$(2L-1)c\tau/2L$	$c\tau/2$	$c\tau/2$	$(2L-1)c\tau/2L$
Independent samples	No	Yes	Yes	Yes
Processing complexity	Low	Low	High	Medium
Transmission bandwidth	Normal	Large	Large	Normal
Other disadvantages	Variance reduction due to averaging is not maximum	Lower transmitted average power	Range sidelobes	Noise enhancement effect

Table 5.1. Comparison of methods that use range samples to reduce the variance of estimates.

5.2. Modifications of the Whitening Transformation

Two drawbacks of the whitening transformation are the noise-enhancement effect and its increased computational complexity. Noise enhancement can be minimized if the noise statistical properties are taken into account when designing the transformation for range samples. The best trade-off between sample independence and noise power boost is obtained by a minimum mean-square error (MMSE) approach, as with MMSE equalizers (Proakis and Salehi, 2000). However, this method requires precise knowledge of the SNR for every range gate, making it impractical for weather signals with typical dynamic ranges of 80 dB. A pseudo-whitening transformation, on the other hand, trades “whitening” for noise reduction in a more controlled fashion without the need for detailed information about the SNR.

In principle, computational complexity for the whitening transformation could be cut down by reducing the dimension of the transformation matrix. Because the estimation of spectral moments requires only the first few autocorrelation estimates, discussed next is the feasibility of whitening autocorrelation estimates, instead of range samples. As this approach fails, the whitening of Fourier coefficients is revisited (see Section 3.4) as a means of reducing the amount of data to be whitened.

The previous list of variations to the whitening transformation is not by any means exhaustive. As with any uncharted field, more modifications of the same problem are expected to surface with the anticipated increased excitement and continued research efforts on this topic.

5.2.1. Minimum Mean-Square Error Equalization

Chapter 2 discussed the trade-off between noise enhancement and variance reduction that makes the whitening transformation useful only in cases of relatively large SNR. Although for weather radars the SNR of signals from storms is large, the formulation of the whitening transformation in effect ignores the presence of noise. The whitening transformation is designed to produce equalization of the signal power spectrum. Accordingly, for spectral regions where the signal is weak, this transformation exhibits large gains enhancing the corresponding noise component in an uncontrolled manner. An alternative is to relax the whitening requirements and select a transformation such that the output noise power is also minimized. A transformation that is optimized based on the minimum mean-square error (MMSE) criterion accomplishes the desired goal. In Section 2.4 the contributions to the sampled complex weather signal at a fixed range location were decomposed into L contributions from contiguous elemental shells in the resolution volume. Equation (2.5) shows this decomposition, and is repeated below for an ideal receiver filter:

$$V(l, n) = \sum_{i=0}^{L-1} s(l+i, n) p(L-1-i). \quad (5.34)$$

A good transformation can be viewed as one that “recovers” the elemental shells’ contributions $s(l, n)$ from the available samples $\mathbf{V}_n = [V(0, n), V(1, n), \dots, V(L-1, n)]^T$. Analogous to the zero-forcing equalization problem, given the vector of observations \mathbf{V}_n and the relation $\mathbf{V}_n = \mathbf{P} \mathbf{s}_n$, we would like to estimate the vector of uncorrelated weather signal samples $\mathbf{s}_n = [s(0, n), s(1, n), \dots, s(2L-2, n)]^T$ through a linear transformation on \mathbf{V}_n ; i.e., $\hat{\mathbf{s}}_n = \mathbf{T} \mathbf{V}_n$. From (5.34) \mathbf{P} is readily recognized as

$$\mathbf{P} = \begin{bmatrix} p(L-1) & p(L-2) & \cdots & p(0) & 0 & 0 & \cdots & 0 \\ 0 & p(L-1) & \cdots & p(1) & p(0) & 0 & \cdots & 0 \\ \vdots & \vdots & \ddots & \vdots & \vdots & & & \vdots \\ 0 & 0 & \cdots & p(L-1) & p(L-2) & \cdots & \cdots & p(0) \end{bmatrix}, \quad (5.35)$$

and \mathbf{T} is the sought-after transformation matrix.

Considering now the presence of additive noise, (5.34) can be modified as

$$V(l, n) = \sum_{i=0}^{L-1} s(l+i, n) p(L-1-i) + \eta(l, n), \quad (5.36)$$

and the problem in vector notation becomes the recovery of \mathbf{s}_n from the set of observations \mathbf{V}_n , where

$$\mathbf{V}_n = \mathbf{P} \mathbf{s}_n + \boldsymbol{\eta}_n, \quad (5.37)$$

and

$$\hat{\mathbf{s}}_n = \mathbf{T} \mathbf{V}_n. \quad (5.38)$$

In the previous equations $\boldsymbol{\eta}_n = [\eta(0, n), \eta(1, n), \dots, \eta(L-1, n)]^T$ is the additive noise vector, and the principle of MMSE can be applied to find the transformation matrix \mathbf{T} . The MMSE solution for the linear model in (5.37) is well known (see for example Section 10.6 of Kay 1993) and only the results are presented here. The transformation \mathbf{T} that minimizes the mean square error $E\{\|\hat{\mathbf{s}}_n - \mathbf{s}_n\|^2\}$ is

$$\mathbf{T} = \mathbf{C}_s \mathbf{P}^{*T} (\mathbf{P} \mathbf{C}_s \mathbf{P}^{*T} + \mathbf{C}_\eta)^{-1}, \quad (5.39)$$

where \mathbf{C}_s and \mathbf{C}_η are the covariance matrices for \mathbf{s}_n and $\boldsymbol{\eta}_n$, respectively. In our problem, these covariance matrices are multiples of the identity matrix as both \mathbf{s}_n and $\boldsymbol{\eta}_n$ are white

and stationary. Let $\mathbf{C}_s = S\mathbf{I}$ and $\mathbf{C}_\eta = N\mathbf{I}$, where S and N are signal and noise powers, respectively; then,

$$\mathbf{T} = \mathbf{P}^{*T} \left[\mathbf{P}\mathbf{P}^{*T} + \left(\frac{N}{S}\right)\mathbf{I} \right]^{-1}. \quad (5.40)$$

Although this transformation outperforms the whitening transformation in terms of the noise enhancement effect, its implementation requires knowledge of the signal-to-noise ratio for every range sample, rendering it impractical. Further study beyond the scope of this dissertation is required to assess the performance of this transformation if the SNR is not known and has to be estimated. Since the SNR of weather signals may vary greatly from one resolution volume to another, its on-line estimation would require the continuous re-computation of \mathbf{T} , which would considerably increase the computational complexity of this method [compare (5.40) with (2.12)]. Indeed, these issues should be addressed in the future to gauge the trade-off between the “simple-yet-noisy” whitening transformation and its more robust MMSE counterpart.

5.2.2. Pseudo Whitening Transformation

The main disadvantage of the MMSE transformation is that its design requires detailed knowledge of the SNR for each sample to be processed (Ebbini et al. 1993). In this sense, there exist several more realistic implementations termed as partial or pseudo-whitening that present a compromise between computational complexity and good SNR. Two of them will be discussed here.

One approach consists of approximating \mathbf{H}^{-1} [see (2.12)] by a “sharpening filter” of bounded magnitude (Herrmann and Kelley 1989). The pseudo-whitening transformation based on the sharpening filter is given by

$$\mathbf{W} = \frac{1}{\sqrt{SEF}} \left[p\mathbf{H} + \frac{(\mathbf{H}^{*T})^{-1}}{p} \right]^{-1}, \quad (5.41)$$

where SEF is the signal enhancement factor needed to preserve the total signal power after the transformation and is given by

$$SEF = \text{tr} \left\{ (\mathbf{H}^{*T} \mathbf{H}) \left[p^2 (\mathbf{H}^{*T} \mathbf{H}) + 2\mathbf{I} + \frac{(\mathbf{H}^{*T} \mathbf{H})^{-1}}{p^2} \right]^{-1} \right\} / L. \quad (5.42)$$

The parameter p in (5.41) is called a “sharpening parameter” and may assume values between 0 and ∞ . For $p = 0$, \mathbf{W} reduces to \mathbf{H}^{*T} , which represents the matched filter offering the best SNR. At the other extreme, for $p \rightarrow \infty$, \mathbf{W} equals \mathbf{H}^{-1} , i.e., the whitening transformation. Hence, the degree of “sharpening” or whitening is dictated by p .

Another approach to limit the gain of the whitening transformation to reduce the noise enhancement effect arises from the relation between the eigenvalues of a correlation matrix and the corresponding power spectral density. That is, the range spanned by the power spectral density matches closely the range of eigenvalues (Johnson and Dudgeon 1993). Accordingly, by limiting the span of eigenvalues, it is possible to place a bound on the gain of the transformation. The correlation matrix of white noise passing through the whitening transformation is given by \mathbf{C}_v^{-1} and its eigenvalues are λ_i^{-1} ($i = 1, 2, \dots, L$), where λ_i are the eigenvalues of \mathbf{C}_v . Hence, by placing a lower bound on the eigenvalues it is possible to limit the gain of the whitening transformation. This is easily realized by looking at the whitening transformation obtained by the eigenvalue decomposition of \mathbf{C}_v as in (2.14). Then, the pseudo-whitening transformation based on eigenvalue “clipping” is given by

$$\mathbf{W} = \tilde{\mathbf{D}}\mathbf{U}^{*T}. \quad (5.43)$$

In (5.43) \mathbf{U} is the matrix with the eigenvectors of \mathbf{C}_v , and $\tilde{\mathbf{D}}$ is a diagonal matrix with elements

$$\tilde{d}_i = \begin{cases} \lambda_i^{-1/2} & \text{if } \lambda_i > \beta \\ \beta^{-1/2} & \text{otherwise} \end{cases}, \quad 1 \leq i \leq L, \quad (5.44)$$

where β is a threshold that can take values between $\min\{\lambda_i\}_{i=1}^L$ and $\max\{\lambda_i\}_{i=1}^L$. The parameter β controls the trade-off between whitening and noise enhancement due to large gains in a similar fashion as the parameter p does it in the sharpening filter.

As predicted by the previous analysis, the performance of Doppler spectral moment and polarimetric variable estimators on pseudo-whitened samples will lie somewhere between the results obtained with whitened samples ($p \rightarrow \infty$, $\beta = \min\{\lambda_i\}_{i=1}^L$) and the ones obtained with correlated (non-whitened) samples ($p = 0$, $\beta = \max\{\lambda_i\}_{i=1}^L$), depending on the selected value for the corresponding adjustable parameter. Figure 5.7 shows the performance of the sharpening filter with parameter $p = 3$ as a function of the SNR. Although samples at the output of the sharpening filter are not completely whitened (observe that the variance reduction is not as large as the one obtained with whitened samples), the noise characteristics are improved given that the crossover point has shifted to the left. A more detailed study on optimum choices for p or β is beyond the scope of this dissertation and remains pending for future work.

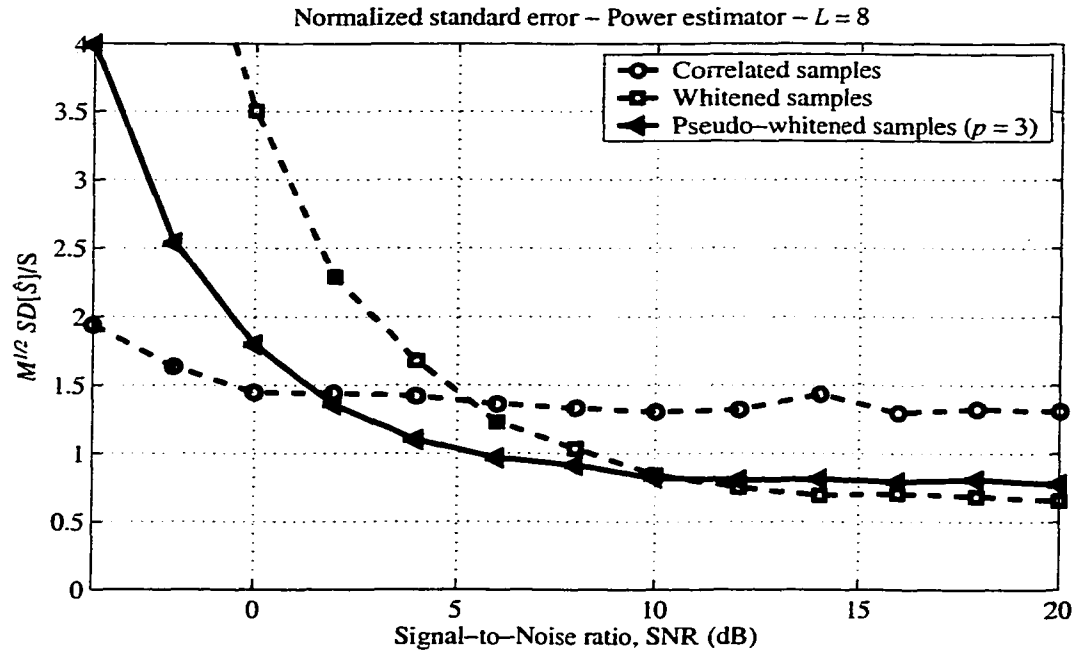


Figure 5.7. Normalized standard deviation for power estimates from correlated, whitened, and pseudo-whitened data as a function of the signal-to-noise ratio (SNR) for the ideal case. The oversampling factor L is 8, the normalized spectrum width σ_{vn} is 0.08. The pseudo-whitening transformation is based on a sharpening filter with parameter $p = 3$.

5.2.3. Whitening of Correlation Estimates

A way to reduce the computational complexity of the whitening transformation is to reduce the dimensionality of the transformation matrix. Since pulse-pair estimates of Doppler spectral moments and polarimetric variables utilize only a few lags of the correlation estimate, one would be tempted to move the whitening transformation one step further into the processing chain; that is, to whiten only the few correlation lags needed in the estimation process as depicted in Figure 5.8. Unfortunately, the whitening transformation does not do well preserving the mean of a sequence unless this mean is zero. To see this consider a non-zero mean process \mathbf{X} with correlation matrix

$\mathbf{C}_X = \mu^2 \mathbf{1}\mathbf{1}^T + \sigma_X^2 \mathbf{C}$, where $\mathbf{1} = [1 \ 1 \ \dots \ 1]^T$. The required transformation would have to operate on \mathbf{X} to generate a transformed sequence \mathbf{Y} with correlation matrix $\mathbf{C}_Y = \mu^2 \mathbf{1}\mathbf{1}^T + \sigma_Y^2 \mathbf{I}$. Therefore, as $\mathbf{Y} = \mathbf{W}\mathbf{X}$ and $\mathbf{C}_Y = E[\mathbf{Y}\mathbf{Y}^{*T}] = \mathbf{W}\mathbf{C}_X\mathbf{W}^{*T}$, the following two conditions for \mathbf{W} arise:

$$\begin{cases} \mathbf{W}\mathbf{W}^{*T} = \mathbf{I} \\ \mathbf{W}\mathbf{C}\mathbf{W}^{*T} = \frac{\sigma_Y^2}{\sigma_X^2} \mathbf{I} \end{cases}, \quad (5.45)$$

so \mathbf{W} is the unitary matrix that satisfies $\mathbf{W}\mathbf{C}\mathbf{W}^{*T} = \frac{\sigma_Y^2}{\sigma_X^2} \mathbf{I}$ or

$$\mathbf{C}\mathbf{W}^{*T} = \frac{\sigma_Y^2}{\sigma_X^2} \mathbf{W}^{-1} = \frac{\sigma_Y^2}{\sigma_X^2} \mathbf{W}^{*T}. \quad (5.46)$$

Hence, (5.45) can be satisfied only if $\sigma_Y = \sigma_X$ and \mathbf{C} is the identity matrix, which is not the case with correlation estimates. Therefore, whitening of correlation estimates is not feasible.

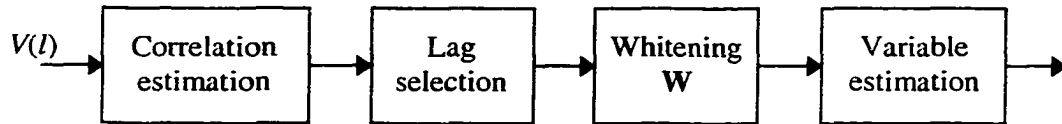


Figure 5.8. Block diagram depicting the process involving whitening of correlation estimates.

5.2.4. Whitening of Spectral Coefficient Estimates

Section 3.4 dealt with the estimation of the Doppler spectrum using two approaches, one of them employing whitened Fourier coefficients. Because complex Fourier coefficients of a zero-mean sequence have also zero mean, whitening of these coefficients is indeed feasible. Frequency-domain methods that estimate Doppler spectral parameters can, in

principle, reduce the amount of data involved in the estimation process by assuming a narrow Doppler spectrum and concentrating on those coefficients around the peak. This simplified method allows the estimation of Doppler velocity and spectrum width with an accuracy that depends on the number of coefficients employed in the process. However, power estimates are accurate only if the power contained in the skirts of the narrow spectrum can be neglected.

The whitening transformation for the Fourier coefficients can be obtained from their normalized correlation matrix along range time. By definition, Fourier coefficients are computed as

$$Z_v(l, k) = \sum_{n=0}^{M-1} V(l, n) e^{-j(2\pi/M)nk}, \quad 0 \leq l < L. \quad (5.47)$$

The correlation of these estimates along range time is

$$\begin{aligned} R_{Z_v}^{(R)}(m, k) &= E[Z_v^*(l, k) Z_v(l+m, k)] \\ &= E \left[\sum_{n=0}^{M-1} V^*(l, n) e^{j(2\pi/M)nk} \sum_{n'=0}^{M-1} V(l+m, n') e^{-j(2\pi/M)n'k} \right] \\ &= \sum_{n=0}^{M-1} \sum_{n'=0}^{M-1} E[V^*(l, n) V(l+m, n')] e^{-j(2\pi/M)(n'-n)k} \\ &= R_v^{(R)}(m) \sum_{r=-M+1}^{M-1} R_v^{(T)}(r) e^{-j(2\pi/M)rk} \\ &= \frac{\zeta_v(k)}{T_s} R_v^{(R)}(m), \end{aligned} \quad (5.48)$$

where $\zeta_v(k)$ is the usual power spectral density of V (k is a parameter). Because the normalized correlation matrices along range time of both time series and Fourier

coefficients are the same, namely $R_V^{(R)}(m)/R_V^{(R)}(0)$, a whitening transformation exactly like the one used on time series data can be applied to whiten Fourier coefficients.

Figure 5.9 depicts a block diagram for the scheme that employs whitened Fourier coefficients. Further study is needed to determine the trade-offs between data reduction and accuracy of estimates.

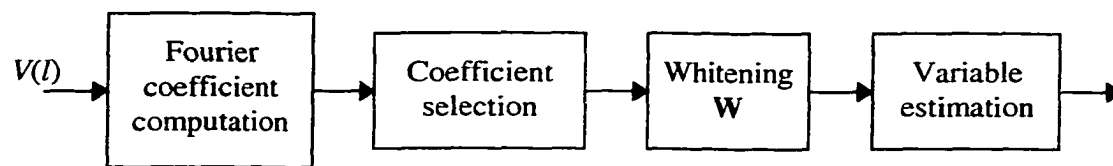


Figure 5.9. Block diagram depicting the process involving whitening of Fourier coefficients.

6. PRACTICAL EFFECTS AND IMPLEMENTATION ISSUES

Most of the analyses performed in previous chapters dealt with ideal systems, that is, systems that have a rectangular transmitter pulse and an infinite-bandwidth receiver filter. In this chapter, those assumptions are relaxed and the effects of non-rectangular transmitter pulses and limited-bandwidth receiver filters are studied. In addition, the derivation of the whitening transformation in Chapter 2 assumed that scatterers are uniformly distributed in the pulse volume. Therefore, it is important to investigate the effects of reflectivity gradients on the performance of WTB estimators. Finally, practical implementation issues are discussed, and the performance of the whitening transformation on real weather data acquired with a digital receiver is demonstrated.

6.1. Effects of Transmitted Pulse Shape

Although the envelope of the transmitted pulse shape on pulsed weather radars is ideally assumed to be perfectly rectangular, that is rarely the case in practice. Non-zero rising and falling times are unavoidable because finite transmission bandwidths smooth the sharp edges of the ideal rectangular shape. In this regard, it is useful to investigate the effects of non-ideal pulse shapes on the performance of the whitening transformation in terms of achieved variance reduction and noise enhancement.

Pulses deviating from the ideal rectangular shape tend to broaden on the tails, increasing the correlation of samples along range time. More correlated samples result in estimates with larger errors when left “untreated”. Hence, whitened samples derived from highly

correlated data lead to increased variance reduction factors. However, as data become more correlated, the decorrelation process turns out to be more difficult to accomplish. As an example, consider a set of fully correlated data. In such data set, only one sample conveys the information of the underlying process, and whitening or decorrelation of this data set is theoretically impossible. The difficulty in whitening a given set of samples is measured by the corresponding noise enhancement factor. Hence, in the following analysis the variance reduction and the noise enhancement factors are computed for different pulse shapes.

Pulse shapes can be modeled parametrically with the aid of sigmoid functions, where the parameter of the sigmoid determines the smoothness of the pulse. That is,

$$p(t) = f_{sig}(t) - f_{sig}(t - \tau), \quad (6.1)$$

where τ is the pulse length, and $f_{sig}(t)$ is the sigmoid function. Commonly referred to as “soft-limiting” functions (Zurada 1995), sigmoid functions are defined as

$$f_{sig}(t) = \frac{1}{1 + e^{-\gamma t}}, \quad (6.2)$$

where γ is the “smoothness” parameter that takes positive real values. For example, the ideal pulse is obtained in the limit as $\gamma \rightarrow \infty$. Figure 6.1 shows several pulse shapes using equation (6.1) for different values of γ .

Assuming an ideal receiver with infinite bandwidth, the correlation matrix $\mathbf{C}_V^{(R)}$ for the input signal V can be obtained as in (2.10), where the correlation coefficient is given by

$$\rho_V^{(R)}(m) = p(m) * p(-m), \quad (6.3)$$

and $p(m)$ is the discrete-time counterpart of the pulse envelope as defined in (6.1).

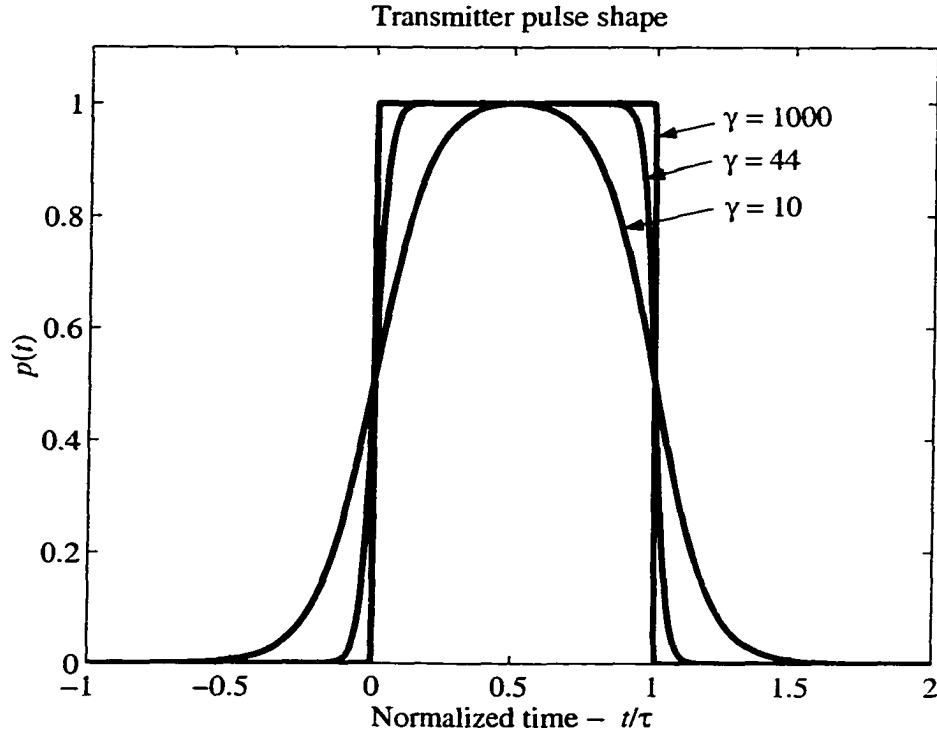


Figure 6.1. Transmitter pulse shape approximated with sigmoid functions for different values of γ . The ideal pulse is obtained as $\gamma \rightarrow \infty$. A pulse with a rise time of 10% of the pulse width (as the one in the WSR-88D weather radar) corresponds to $\gamma = 44$.

The variance reduction factor for power estimates was defined in Chapter 3 as

$$VRF = \frac{\text{Var}\{\hat{S}_{corr}\}}{\text{Var}\{\hat{S}_{whitened}\}} = \frac{\text{tr}\{[\mathbf{C}_v^{(R)}]^2\}}{L}, \quad (6.4)$$

and the noise enhancement factor was introduced in Chapter 2 as

$$NEF = \frac{\text{tr}\{[\mathbf{C}_v^{(R)}]^{-1}\}}{L}. \quad (6.5)$$

Thus, only the normalized correlation matrix $\mathbf{C}_v^{(R)}$ is needed to analyze the performance of the whitening transformation for different pulse shapes in terms of variance reduction

and noise enhancement. Figure 6.2 shows these parameters as a function of the pulse smoothness for an oversampling factor of eight.

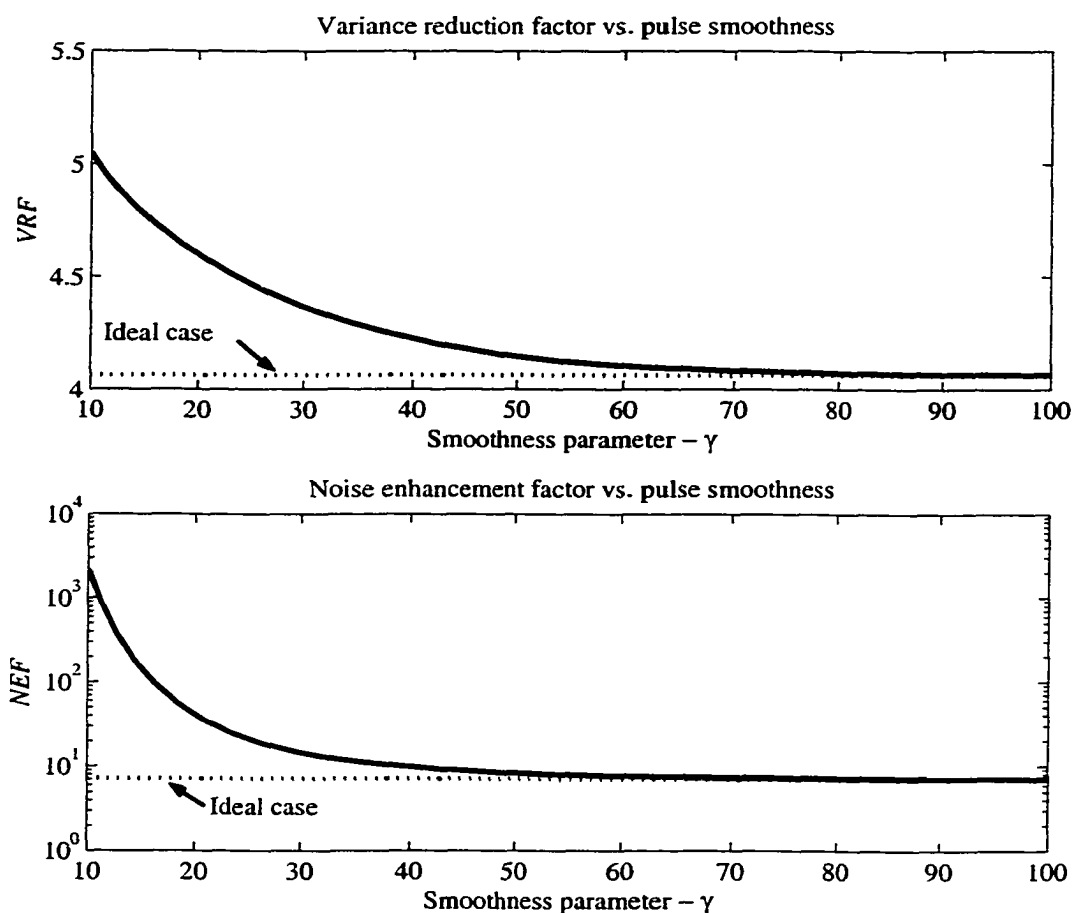


Figure 6.2. Effects of the transmitter pulse shape on the performance of the whitening transformation. (Top) Variance reduction factor vs. the pulse smoothness parameter γ , and (bottom) noise enhancement vs. the pulse smoothness parameter γ . In both cases the receiver filter is ideal and the oversampling factor L is 8.

As predicted, for smoother pulses (small γ) samples are more correlated and the variance reduction factor is larger. It is important to note that the larger variance reduction of a smooth pulse is not an improvement over a sharp pulse; rather, it is an improvement over the spoilage that the smooth pulse causes. In fact, it is more difficult to whiten the

samples corresponding to smooth pulses and this is corroborated by a considerable noise enhancement (about 20 dB). Conversely, for sharper pulses (large γ) samples are less correlated, and both the variance reduction and noise enhancement factors are smaller tending to the ideal case for values of γ larger than about 100. For values of γ greater than about 50, which corresponds to the pulse in the WSR-88D weather radars, the performance of WTB estimators is within 10% of the one observed in the ideal case.

6.2. Effects of Receiver Filter Characteristics

Analyses in previous chapters concerning an ideal system considered the bandwidth of the receiver filter to be very large, namely, larger than L/τ . In practice, the bandwidth of the receiver filter for weather radars should be as narrow as possible while keeping the desired range resolution that depends on the width of the filter characteristics and pulse shape (Doviak and Zrnic 1978). Then, it is important to investigate the effects of the receiver bandwidth on the performance of the whitening transformation in terms of achieved variance reduction and noise enhancement.

Equivalent to the effect of smoothing the pulse shape, reducing the receiver bandwidth results in more correlated samples. Therefore, variance reduction factors and noise enhancement should increase for whitened samples derived from heavily filtered data (Section 6.1). To test this hypothesis, a 5th-order, lowpass, Butterworth filter was selected to model a receiver filter with variable bandwidth. The bandwidth B_6 is specified as the band of frequencies where the filter power gain is within 6 dB of its highest level. Hence, following Doviak and Zrnic (1993), “matched” conditions are attained if the receiver-

bandwidth pulse-width product $B_6\tau$ is one. Figure 6.3 shows the variance reduction and the noise enhancement factors as a function of $B_6\tau$. As predicted, for narrower bandwidths (small $B_6\tau$) samples are more correlated and the variance reduction factor is larger. However, for very narrow bandwidths the noise enhancement creeps to unaffordable levels of up to 80 dB. Conversely, for broader bandwidths (large $B_6\tau$) samples are less correlated, and both the variance reduction and noise enhancement factors are smaller and tend to the ideal case for values of $B_6\tau$ close to L . Therefore, there is a tradeoff between the factors contributing to the total noise power after whitening. The narrower the receiver bandwidth, the lower the system noise power but the larger the noise enhancement factor. On the other hand, the broader the receiver bandwidth, the higher the system noise power but the smaller the noise enhancement factor. In a practical setting, the system would need to include a receiver filter with the optimum bandwidth in terms of SNR maximization.

In the standard Doppler weather radar the filters other than the “matched one” have a bandwidth of about 10 times the reciprocal of the pulse width (in the order of 10 MHz). These filters are needed to reject images and prevent interferences from contaminating the data. Further, filters with smaller bandwidths than about 10 MHz at RF frequencies are not readily available. Alternatively, in modern digital receivers the overall bandwidth is dictated by the antialias filter centered at the intermediate frequency (IF) with typical bandwidths of several MHz. Therefore, in a practical setting $B_6\tau > 7$, and from Figure 6.3 it can be concluded that the noise enhancement and variance reduction factor under typical working conditions would approach the ideal (infinite bandwidth) case.

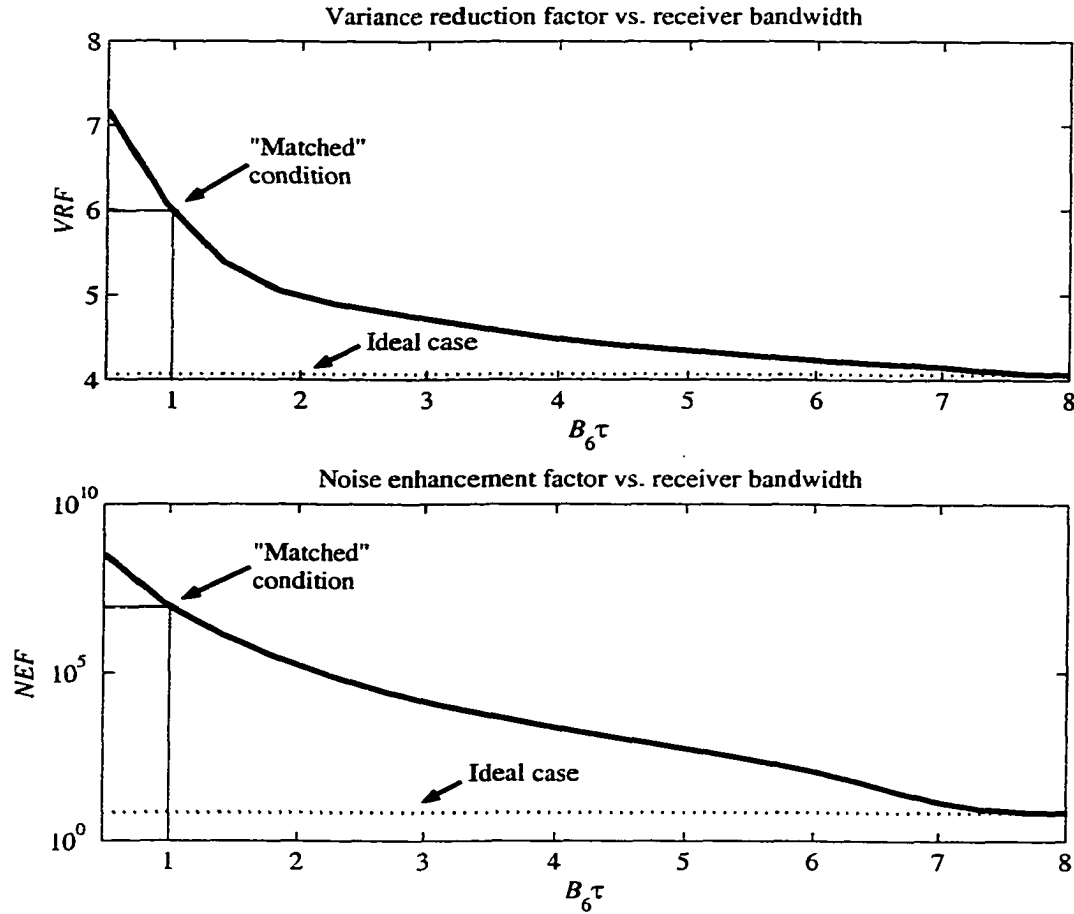


Figure 6.3. Effects of the receiver filter bandwidth on the performance of the whitening transformation. (Top) Variance reduction factor vs. the receiver-bandwidth pulse-width product $B_0 \tau$, and (bottom) noise enhancement vs. the receiver-bandwidth pulse-width product. In both cases the transmitted pulse is ideal and the oversampling factor L is 8.

6.3. Effects of Reflectivity Gradients within the Resolution Volume

Derivation of the whitening transformation on oversampled range data in Section 2.4 assumed that the pulse volume was uniformly filled with scatterers. That is, a uniform reflectivity profile is required for the theoretically predicted performance of WTB estimators. Therefore, it is important to analyze the sensitivity of WTB estimators to reflectivity gradients in the pulse volume. A comprehensive study of this effect would

include different types of “realistic” profiles that are typically encountered on weather phenomena. However, a thorough analysis goes beyond the scope of this dissertation, and only linear reflectivity profiles on decibel scale (constant reflectivity gradients) are studied in this section. This type of reflectivity profile has been used in the literature for various theoretical analyses (e.g., Scarchilli et al. 1999).

Assume that the pulse volume is filled with scatterers such that the backscattered power in range follows the exponential characteristic below:

$$\sigma_s^2(l) = \sigma_s^2 10^{gl/10}, \quad 0 \leq l \leq 2L - 2, \quad (6.6)$$

where g is the reflectivity gradient. The performance of WTB estimators is measured by the variance reduction and noise enhancement factors. However, noise enhancement is irrelevant in this case, because it depends solely on the whitening transformation matrix; this matrix is computed assuming a uniform reflectivity profile and therefore does not change. The variance reduction can be computed for the general case as

$$VRF = \frac{Var\{\hat{S}_{corr}\}}{Var\{\hat{S}_{whitened}\}} = \frac{tr\{[C_v^{(R)}]^2\}}{tr\{[C_x^{(R)}]^2\}}, \quad (6.7)$$

where the normalized covariance matrices can be expressed as

$$C_v^{(R)} = E\{V^{*T}V\}, \quad (6.8)$$

and

$$C_x^{(R)} = E\{X^{*T}X\} = W^{*T}C_v^{(R)}W. \quad (6.9)$$

In (6.9) W is computed as usual by assuming a uniform reflectivity profile. Using (2.5), $V(l)$ can be expressed in matrix form as

$$\mathbf{V} = \mathbf{P}\mathbf{s}, \quad (6.10)$$

where $\mathbf{V} = [V(0), V(1), \dots, V(L-1)]^T$ is the received signal vector, \mathbf{s} is the backscattered signal vector defined as $\mathbf{s} = [s(0), s(1), \dots, s(2L-2)]^T$, and \mathbf{P} is the “pulse matrix” defined in (5.35). Therefore, (6.8) becomes

$$\mathbf{C}_V^{(R)} = \frac{E\{\mathbf{P}^{*T} \mathbf{s}^T \mathbf{s} \mathbf{P}\}}{L} = \frac{\mathbf{P}^{*T} \mathbf{C}_s^{(R)} \mathbf{P}}{L}, \quad (6.11)$$

where $\mathbf{C}_s^{(R)} = E\{\mathbf{s}^* \mathbf{s}\}$ is the normalized correlation matrix for the backscattered signals.

Finally, the variance reduction factor is computed from (6.7) as

$$VRF = \frac{\text{tr}\{\mathbf{P}^{*T} \mathbf{C}_s^{(R)} \mathbf{P}\}^2}{\text{tr}\{\mathbf{W}^{*T} \mathbf{P}^{*T} \mathbf{C}_s^{(R)} \mathbf{P} \mathbf{W}\}^2}. \quad (6.12)$$

As argued in Chapter 2, the backscattered signals from different “slabs” are mutually independent, so $\mathbf{C}_s^{(R)}$ is just a matrix with diagonal entries $\{\sigma_s^2(0), \sigma_s^2(1), \dots, \sigma_s^2(2L-2)\}$.

Figure 6.4 shows the effects of reflectivity gradients on the performance of the whitening transformation versus the normalized gradient gL (gL indicates the total reflectivity variation on a range interval of $c\tau/2$ meters). The variance reduction factor was computed using (6.12), where $\mathbf{C}_s^{(R)}$ was generated according to (6.6). As expected, large reflectivity gradients deteriorate the performance of WTB estimators. However, small departures from uniform profiles seem to be tolerated. Figure 6.4 also depicts the normalized bias of power estimates versus gL . It is important to note that this bias is not caused by the whitening transformation but is due to the estimation algorithm that averages L power estimates assuming a uniform profile. Note that gradients of 10 dB/km (2.5 dB per 250 m for the WSR-88D pulse length) would create negligible performance deterioration.

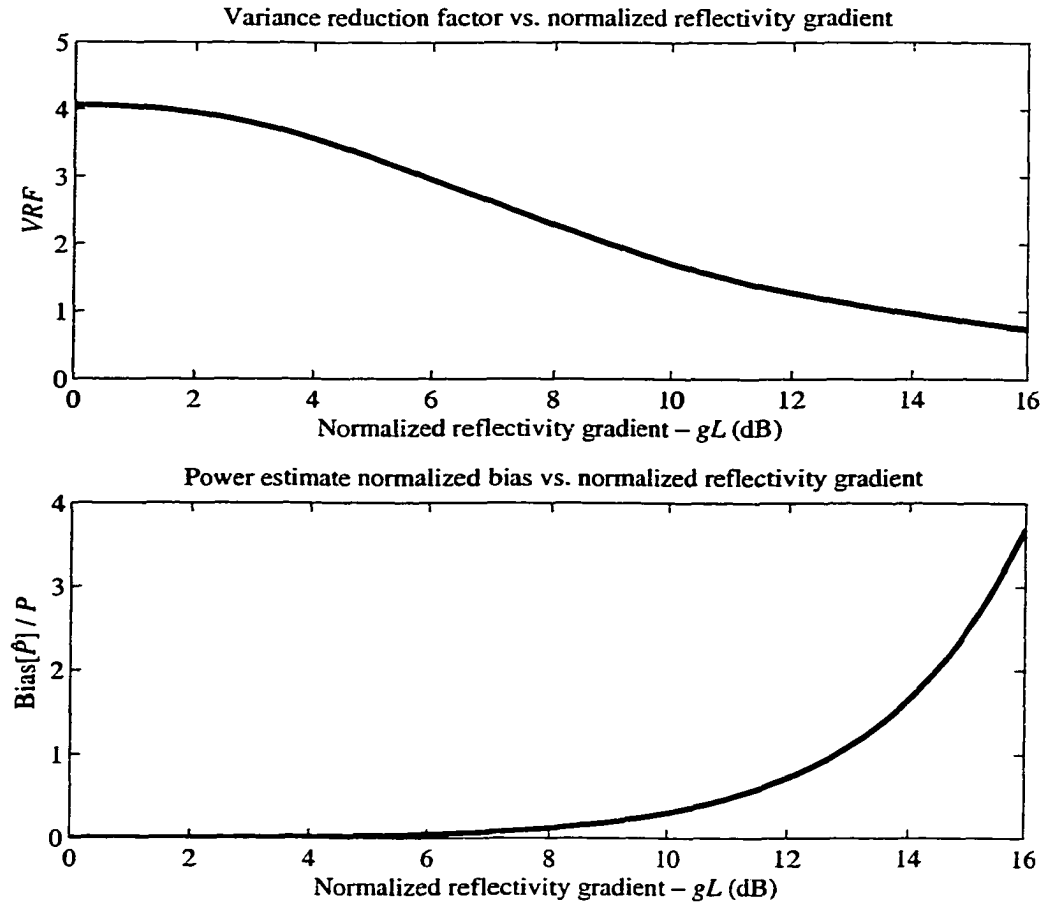


Figure 6.4. Effects of reflectivity gradients on the performance of the whitening transformation. (Top) Variance reduction factor vs. the normalized reflectivity gradient gL , and (bottom) normalized bias of power estimates vs. the normalized reflectivity gradient gL . In both cases, the reflectivity profile is linear on decibel scale and gL indicates the total reflectivity variation on a range interval of $c\tau/2$ meters.

6.4. Implementation Issues

Whitening-transformation-based estimators entail (1) whitening in range the oversampled signals, (2) processing time samples by any one of the well-known algorithms, and (3) combining in range intermediate results of these algorithms to yield significant reduction in the variances of estimates (see Figure 6.5 for a depiction of this process). Variance reduction occurs only if the signal-to-noise ratios are relatively large, as is usually the

case for most signals in weather surveillance radars. As shown in Chapters 3 and 4, at low SNR the variances increase so that there are crossover points (these are different for different estimates). Below the cross over SNR (SNR_c), the classical processing produces lower variances. An objective decision on which estimates to use for each variable, classical or the ones obtained from whitened samples in range, should be based on the SNR and the corresponding SNR_c . To avoid parallel computation, the choice of which channel to use can be made from a priori knowledge of the SNR, or data could be stored and processing in the appropriate channel could start after the SNR has been determined. Otherwise, both processing chains could proceed simultaneously and the decision on which one to use can be made at the end of the dwell time. This parallel processing and decision mechanism is illustrated in Figure 6.6.

As depicted in Figure 6.6, the classical processing includes a matched filter that maximizes the SNR of weather echoes. Because the actual SNR on the classical processing chain is about L times larger after the matched filter, it seems that the values of SNR_c computed in Chapters 3 and 4 need adjustment. In theory, the precise adjustment in SNR depends on the effective noise bandwidth of the matched filter (to compute the actual SNR enhancement for correlated samples) and on the behavior of the curves for variance of estimates vs. SNR (to compute the displacement of SNR_c due to the SNR enhancement). However, because the variance of estimates for correlated samples flattens for SNRs around the crossover point (see Figure 3.4), the adjusted SNR_c is practically equal to the SNR_c depicted in Figures 3.5, 3.8, 3.11, 4.3, 4.6, and 4.9. Therefore, the addition of a matched filter to the processing of correlated samples does not significantly change the relative performance of WTB estimates compared to classical estimates.

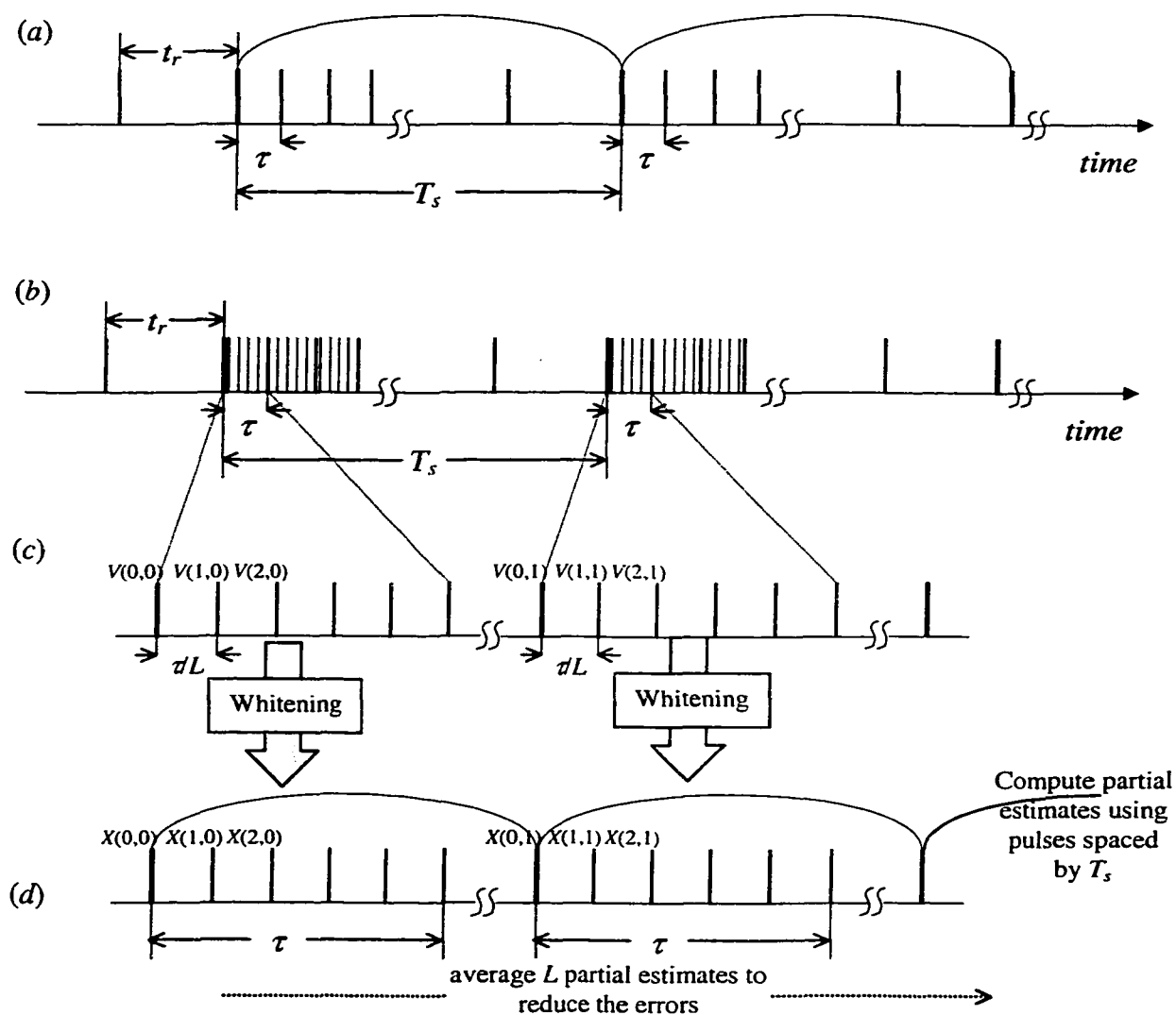


Figure 6.5. Depiction of sampling in range and processing of the signals. (a) Samples in range with spacing equal to the pulse length; standard processing to obtain the Doppler spectrum and its moments is indicated. (b) Oversampling in range. (c) Zoomed presentation of range locations (oversampled) at which meteorological variables (including spectra) are estimated. Range samples that are to be whitened are indicated. (d) Processing of whitened samples to obtain estimates of spectra, spectral moments, and polarimetric variables in range.

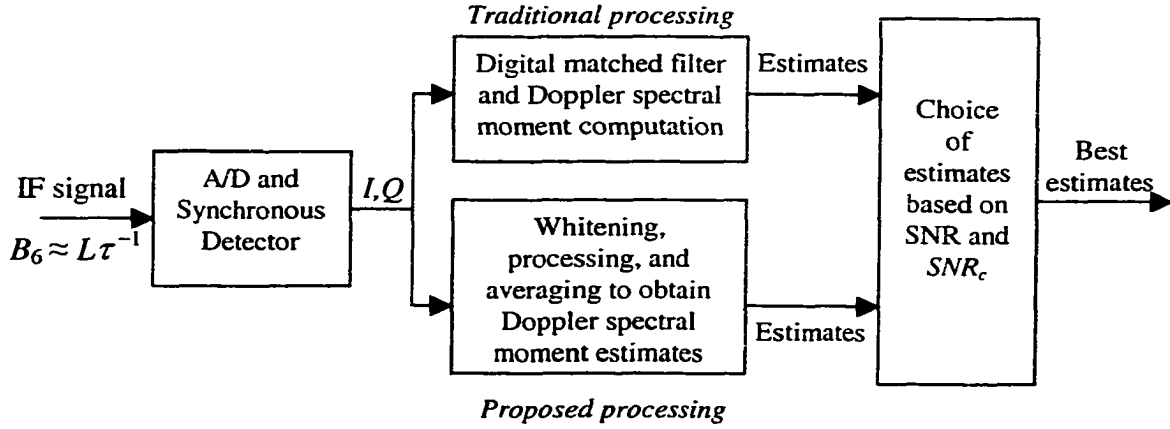


Figure 6.6. Schematic of the proposed processing that also retains the advantages of the traditional processing.

In addition to opening the bandwidth to accommodate the whitening transformation, oversampling increases the internal data rate for subsystems after the analog-to-digital converter. Consequently, practical implementation of the whitening transformation requires a digital signal processor with enough power to accept I and Q data at rates L times faster than with classical processing, and to process these samples for the computation of spectral moments and polarimetric variables within the dwell time (MT_s). Because the radar resolution is not increased the output of products remains the same. Processing of samples involves (1) a matrix multiplication of every block of L samples, (2) L times the classical processing for partial estimates, and (3) a final average of partial estimates to compute the meteorological variables of interest. It is believed from personal experience (Torres and Zahrai 2002) that implementation of this scheme on modern DSP boards will not present a major problem for oversampling factors of up to about 10.

Next, the performance of WTB estimators on real data is demonstrated. A digital receiver with an oversampling factor of $L = 3$ was used to acquire weather data, and an off-line

processing as the one shown in Figure 6.5 was employed to estimate total signal power and Doppler velocity. For a detailed description of the demonstration procedure refer to Ivic (2001).

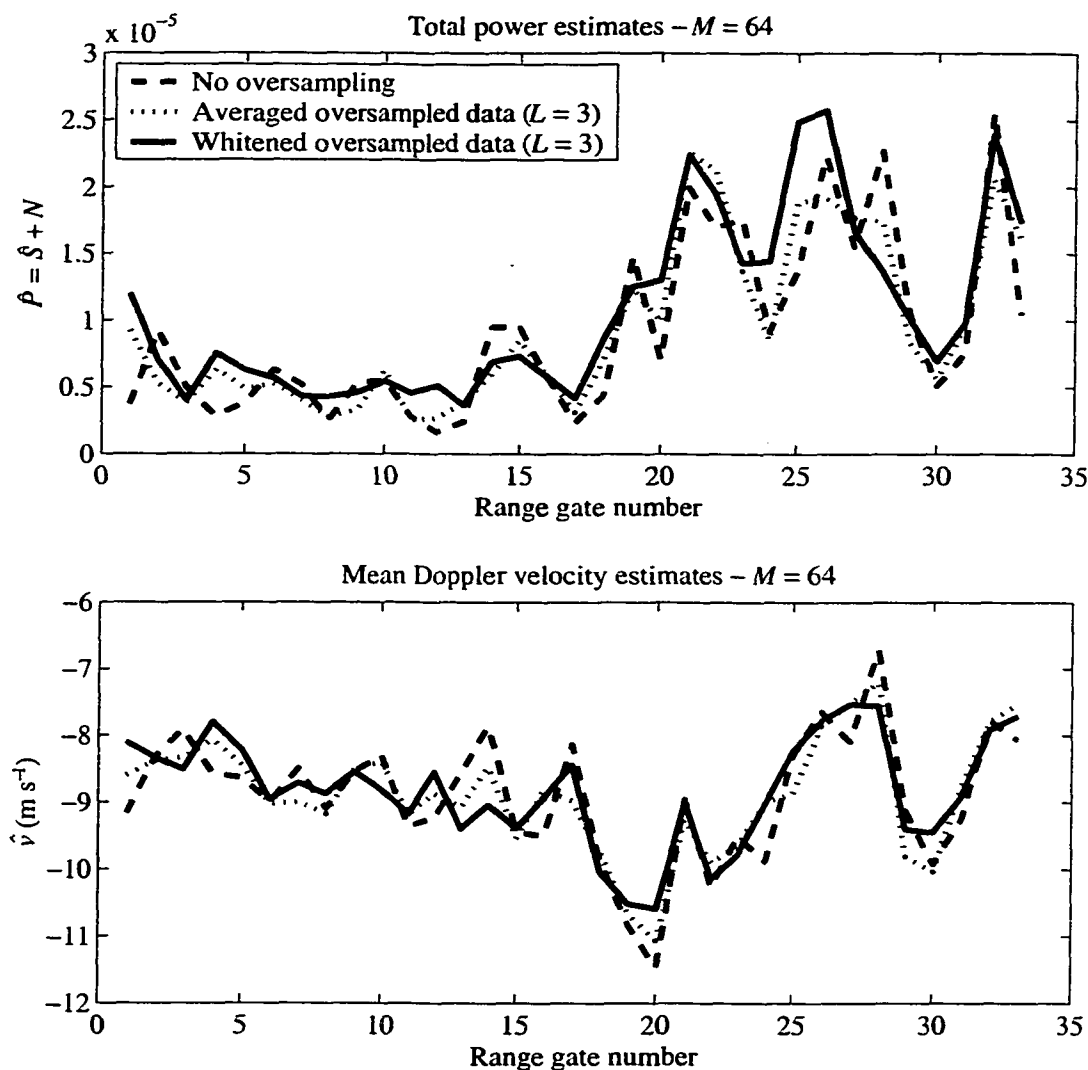


Figure 6.7. Performance of WTB estimators on real weather data. (Top) Total power estimates and (bottom) mean Doppler velocity estimates vs. range for whitened (solid line), correlated (dotted line), and non-oversampled data (dashed line). Data was acquired with a digital receiver and a stationary antenna. The oversampling factor is $L = 3$. Recorded data streams were processed off-line by the procedure described in Section 2.4 (see Figure 6.5). Results corroborate the accuracy of WTB estimators.

Figure 6.7 shows the power and velocity estimates on whitened and non-whitened data; classical estimates that do not employ oversampled data are also plotted. The agreement between the three types of estimators corroborates the predicted accuracy of WTB estimates. The variance reduction achieved through the whitening of range samples can be inferred from these curves by the smoothness observed in WTB estimates. A complete analysis to verify the performance of the whitening transformation on real data is very involved and left for future work (Ivic 2001). Still, this experiment confirms that the whitening transformation is indeed a viable candidate for future enhancements of polarimetric Doppler weather radars.

7. CONCLUSIONS AND FUTURE WORK

A method for estimation of Doppler spectrum and its moments as well as several polarimetric variables on pulsed weather radars was presented. This scheme operates on oversampled echoes in range, and the aforementioned radar variables are estimated by suitably combining weighted averages of these oversampled signals with usual processing of samples (spaced at pulse repetition time) at a fixed range location. The weights in range are chosen via a whitening transformation such that the oversampled signals become uncorrelated and consequently the variance of the estimates decreases significantly.

Whitening-transformation-based (WTB) estimators of spectral moments (Chapter 3) and polarimetric variables (Chapter 4) were introduced, and their performance was compared to that of classical estimators. The variance reduction achieved by WTB estimators under ideal conditions asymptotically tends to $L/2$ for large signal-to-noise ratios (SNR) and large oversampling factor L . For low signal-to-noise ratios there is a crossover point (SNR_c) for the variances of WTB and classical estimators. Analytical expressions that allow the computation of SNR_c for any variable and different conditions were derived. Above the SNR_c , WTB estimates are preferred over classical estimates. Below the SNR_c , the noise enhancement effect becomes more important and classical estimates are favored.

Methods that use range samples to reduce the estimation variance were compared in Chapter 5. Regular pulse with averaging is the simplest method, exhibits a good SNR, but has the worst statistical performance because range samples are not uncorrelated. Short

pulse with averaging genuinely obtains uncorrelated samples, but the transmission bandwidth is broadened and the average transmitted power is reduced. Therefore, the SNR is decreased. Pulse compression restores the SNR and achieves almost independent samples. However, as with a short pulse, it becomes impractical due to its increased transmission bandwidth requirements. The whitening transformation method deteriorates the SNR; however, it achieves independent samples without the need for a larger transmission bandwidth and with little sacrifice in range resolution. There are different trade-offs in this analysis, and the ultimate decision about the best method depends on several engineering factors such as transmission bandwidth, signal processor capacity, and transmitter peak power.

To avoid the effects of noise enhancement, minimum-mean-squared-error (MMSE) solutions were explored in Chapter 5. It was shown that MMSE schemes require detailed knowledge of the SNR for every range sample, making them impractical. As an alternative, pseudo-whitening methods achieve a compromise between whitening and noise enhancement in a more controlled fashion. They seem to be suitable candidates for practical implementation in future enhancements of the WSR-88D, and hence are worthy of further study.

Analysis of practical effects in Chapter 6 revealed that for typical parameters of a real system, performance of WTB estimators approaches theoretical limits of the ideal case. Parallel processing including whitened and classical estimators allows the selection of one or the other depending on current conditions such as SNR and spectrum width. Further, it was argued that addition of a matched filter in the classical processing chain

does not change the SNR_c for practical purposes. Therefore, the validity of WTB estimates is not affected.

Realistic simulations (see Appendix A) were performed using known statistical properties of signals reflected by passive scatterers in fluids. Further, simulations take the known properties of the probing pulse and receiver filter to reconstruct a composite signal from distributed scatterers illuminated by the pulse. In addition to the results obtained with simulated data, analyses on real weather data acquired with a digital receiver produced very encouraging outcomes. This work confirms that WTB estimators are indeed viable candidates for future enhancements of the WSR-88D radar network.

Summarizing, the whitening transformation allows increasing the speed of volume coverage by weather radar so that hazardous features can be timely detected. It also leads to better estimates of precipitation and wind fields. The application of this technique is possible because of two reasons:

- the correlation of samples in range is known exactly if the resolution volume is uniformly filled with scatterers (true over relatively short ranges), and the receiver bandwidth is large compared to the reciprocal of the pulse length.
- for all weather phenomena of interest, the SNR is relatively high (above the crossover SNR), so the increase of noise power is not critical and the method works well.

Several areas for future study can be derived from this work. For the interested researcher, below is a list with topics that deserve further investigation:

- Detailed analysis of implementation issues. If it is agreed that WTB estimators will be part of future WSR-88D enhancements, implementation issues will be of importance. The required processing power of digital signal processor (DSP) chips running the algorithms presented in this dissertation needs be established. In this regard, the feasibility of a parallel implementation to keep the current functionality as described in Chapter 7 has to be taken into account when performing such assessment. For a polarimetric radar transmitting alternate polarizations, changes in the estimation procedures need consideration, and their performance has to be reevaluated [a discussion on alternate transmission of horizontal and vertical polarizations can be found in Sachidananda and Zrnic (1989)].
- Comprehensive analysis of the effects of transmitter pulse shape, receiver filter impulse response, and reflectivity gradients within the pulse. Although Chapter 7 introduced these issues, a more thorough investigation is required. This is especially important when considering the characteristics of a practical system. In this regard, methods that accurately measure the correlation of echo samples in range need be devised so that WTB estimates can be correctly computed and the performance of the whitening transformation can be accurately predicted. The possibility to find an optimum receiver bandwidth in terms of SNR has to be explored as well.

- Study of the sensitivity of variance reduction factors (VRF) to the phase of the autocorrelation for range samples. It was discussed in Chapter 1 that the correlation of range samples includes a complex exponential term that depends on practical effects such as amplitude modulation-to-phase modulation (AM-to-PM) conversion within the pulse. Precise measurement of this phase is therefore required to achieve the predicted performance of WTB estimators. Even with a precise knowledge of the systematic phase term, the analysis in Chapter 1 neglected the phase contribution from propagation changes due to a non-homogeneous medium along the antenna beam. Still, it is expected that this kind of propagation effects will be minor compared with the systematic phase term (Ivic 2001). A deeper analysis will be required to evaluate the decay in variance reduction incurred either when the autocorrelation phase is not known precisely or when the propagation changes within the pulse are significant.
- Theoretical derivation of maximum likelihood estimates and the Cramer-Rao lower bound (CRLB). The computation of the CRLB would help to gain a deeper understanding of the advantages of using WTB estimators in a polarimetric weather radar. That is, the performance of WTB estimators can be evaluated against the theoretical limit given by the CRLB. On the other hand, maximum likelihood (ML) estimators usually achieve the CRLB but they are significantly more difficult to derive. This is especially true for the variables that depend on more than one estimate, as is the case for all polarimetric variables. In this regard, it is worthy to study the trade-offs between WTB estimators and their ML counterparts.

- Study of pseudo-whitening schemes. It is important to devise alternate and feasible methods that mitigate the noise-enhancement effect and do not require precise knowledge of the SNR. Two approaches for pseudo-whitening were introduced in Chapter 5. These require further investigation and new schemes need exploration. It is believed that some kind of pseudo-whitening would be the optimum solution with the best performance in a practical implementation.
- Application of the whitening transformation to increase the resolution of pulsed Doppler weather radars. It is suggested by the nature of the whitening transformation that if samples are not recombined through average, the resolution of weather radars in range could potentially be increased. Theoretical analyses are needed in order to prove the validity of this argument.
- Application of the whitening transformation to phased-array weather radars. The method of decomposing echo signals into their orthogonal components along the range-time axis could be applied to phased-array radars. Further research is required to determine the implementation and implications that this novel technique would bring to these sophisticated remote sensing devices.

REFERENCES

- Aydin, K., Y.M. Lure, and T. A. Seliga, 1990: Polarimetric radar measurements of rainfall compared with ground-based rain gauges during MAYPOLE'84. *IEEE Trans. Geosci. Remote Sens.*, **28**, 443-449.
- Bamler, R., 1991: Doppler frequency estimation and the Cramer-Rao bound. *IEEE Trans. Geosci. Remote Sens.*, **29**, 385-390.
- Brunkow, D.A., 1999: A new receiver and signal processor for the CSU-Chill radar. Preprints, 29th Conf. on Radar Meteorology, Montreal, Canada, Amer. Meteor. Soc., paper 2-29.
- Bruniquel, J., A. Lopes, J.G. Planes, F. Cazaban, and M. Deschaux-Beaume, 1996: On the use of the whitening filter and optimal intensity summation to produce multi-look SAR images. *International Geoscience and Remote Sensing Symposium*, Lincoln, NE, Institute of Electrical and Electronics Engineers, 387-389.
- Chandrasekar, V., and V.N. Bringi, 1986: Statistical properties of dual polarized radar signals. Preprints, 23rd Conf. on Radar Meteorology, Showmass, CO, Amer. Meteor. Soc., 193-196.
- Chornoboy, E.S., 1993: Optimal mean velocity estimation for Doppler weather radars. *IEEE Trans. Geosci. Remote Sens.*, **31**, 575-586.
- Doviak, R.J., and D.S. Zrnic, 1979: Receiver bandwidth effect on reflectivity and Doppler velocity estimates. *J. Appl. Meteor.*, **18**, 69-76.
- Doviak, R.J., and D.S. Zrnic, 1993: *Doppler radar and weather observations*. 2d ed. Academic Press, Inc., 562 pp.
- Doviak, R.J., V. Bringi, A. Ryzhkov, A. Zahrai, and D. Zrnic, 2000: Considerations for polarimetric upgrades to operational WSR-88D radars. *J. Atmos. Oceanic Technol.*, **17**, 257-278.
- Ebbini, E.S., P.C. Li, and J. Shen, 1993: A new SVD-based optimal inverse filter design for ultrasonic applications. *Proc. Ultrasonics Symposium*, Baltimore, MD, Inst. Electrical Electronics Engineers, 1187-1190.
- Faddeev, D.K., and V.N. Faddeeva, 1963: *Computational methods of linear algebra*, W.H. Freeman and Co., 621 pp.
- Fjortoft, R., and A. Lopes, 2001: Estimation of the mean radar reflectivity from a finite number of correlated samples. *IEEE Trans. Geosci. Remote Sens.*, **39**, 196-199.

- Frehlich, R., 1993: Cramer-Rao bound for Gaussian random processes and applications to radar processing of atmospheric signals. *IEEE Trans. Geosci. Remote Sens.*, **31**, 1123-1131.
- Frehlich, R., 1999: Performance of maximum likelihood estimators of mean power and Doppler velocity with a priori knowledge of spectral width. *J. Atmos. Oceanic Technol.*, **16**, 1702-1709.
- Galati, G., and G. Pavan, 1995: Computer simulation of weather radar signals. *Simulation Practice and Theory*, **3**, 17-44.
- Herrmann, G.F., and L.L. Kelley, 1989: Enhanced resolution in simple radars. *IEEE Trans. Aerosp. Electron. Syst.*, **25**, 64-72.
- Ivic, I.R., 2001: Demonstration of an efficient method for estimating spectral moments. M.S. thesis, Dept. of Electrical and Computer Engineering, Univ. of Oklahoma.
- Izquierdo, M.A.G., M.G. Hernández, O. Graullera, and J.J. Anaya, 2000: Signal-to-noise ratio enhancement based on the whitening transformation of colored structural noise. *Ultrasonics*, **38**, 500-502.
- Johnson, D.H., and D.E. Dudgeon, 1993: *Array signal processing: Concepts and techniques*. Prentice Hall, 533 pp.
- Kay, S.M., 1993: *Fundamentals of statistical signal processing: Estimation theory*. Prentice Hall, 595 pp.
- Koivunen, A.C., and A.B. Kostinski, 1999: The feasibility of data whitening to improve performance of weather radar. *J. Appl. Meteor.*, **38**, 741-749.
- Kostinski, A.B., and Koivunen, A.C., 2000: On the condition number of Gaussian sample-covariance matrices. *IEEE Trans. Geosci. Remote Sens.*, **38**, 329-332.
- Liu, L., V.N. Bringi, V. Chandrasekar, E.A. Mueller, and A. Mudukutore, 1994: Analysis of the copular correlation coefficient between horizontal and vertical polarizations. *J. Atmos. Oceanic Technol.*, **11**, 950-963.
- Lütkepohl, H., 1996: *Handbook of matrices*, John Wiley & Sons, 304 pp.
- Mohamed, A.H., and K.P. Schwarz, 1998: A simple and economical algorithm for GPS ambiguity resolution on the fly using a whitening filter. *Navigation: J. Inst. Navigation*, **45**, 221-231.
- Mudukutore, A.S., V. Chandrasekar, and R.J. Keeler, 1998: Pulse compression for weather radars. *IEEE Trans. Geosci. Remote Sens.*, **36**, 125-142.

- Nathanson, F.E., 1969: *Radar design principles; Signal processing and the environment*. McGraw-Hill, 626 pp.
- Novak, L.M., and M.C. Burl, 1990: Optimal speckle reduction in polarimetric SAR imagery. *IEEE Trans. Aerosp. Electron. Syst.*, **26**, 293-305.
- Papoulis, A., 1984: *Probability, random variables, and stochastic processes*. 2d ed. McGraw-Hill, 576 pp.
- Proakis, J.G., and M. Salehi, 2000: *Contemporary Communication Systems Using MATLAB*. Brooks/Cole, 428 pp.
- Reed, I.S., 1962: On a Moment Theory for Complex Gaussian Processes. *IRE Trans. on Inf. Theory*, **8**, 194-195.
- Rodríguez González, O.L., 1999: Independent samples in range averaged finite bandwidth log receivers outputs. Preprints, 29th Conf. on Radar Meteorology, Montreal, Canada, Amer. Meteor. Soc., paper 10A.7.
- Ryzhkov, A., and D.S. Zrníc, 1998: Polarimetric Rainfall estimation in the presence of anomalous propagation. *J. Atmos. Oceanic Technol.*, **15**, 1320-1330.
- Sachidananda, M., and D.S. Zrníc, 1985: ZDR measurement considerations for a fast scan capability radar. *Radio Sci.*, **20**, 907-922.
- Sachidananda, M., and D.S. Zrníc, 1986: Differential propagation phase shift and rainfall rate estimation. *Radio Sci.*, **21**, 235-247.
- Sachidananda, M., and D.S. Zrníc, 1989: Efficient processing of alternately polarized radar signals. *J. Atmos. Oceanic Technol.*, **6**, 173-181.
- Scarchilli, G., E. Gorgucci, and V. Chandrasekar, 1999: Detection and estimation of reflectivity gradients in the radar resolution volume using multiparameter radar measurements. *IEEE Trans. Geosci. Remote Sens.*, **37**, 1122-1127.
- Schulz, T.J., and A.B. Kostinski, 1997: Variance bounds on the estimation of reflectivity and polarization parameters in radar meteorology. *IEEE Trans. Geosci. Remote Sens.*, **35**, 248-255.
- Scott, R.D., Krehbiel P.R., and W. Rison, 2001: The use of simultaneous horizontal and vertical transmissions for dual-polarization radar meteorological observations. *J. Atmos. Oceanic Technol.*, **18**, 629-648.
- Seliga, T.A., and V.N. Bringi, 1978: Differential reflectivity and differential phase shift: Applications in radar meteorology. *Radio Sci.*, **13**, 271-275.

- Sirmans, D., and W. Bumgarner, 1975: Numerical comparison of five mean frequency estimators. *J. Appl. Meteorol.*, **14**, 991-1003.
- Sosulin, Y.G., and V.V. Kostrov, 1998: Whitening filter: Evolution and application. *J. Comm. Technol. and Electron.*, **43**, 1030-1043.
- Straka, J.M., D.S. Zrnica, and A.V. Ryzhkov, 2000: Bulk hydrometeor classification and quantification using polarimetric radar data: Synthesis of relations. *J. Appl. Meteor.*, **39**, 1341-1372.
- Therrien, C.W., 1992: *Discrete random signals and statistical signal processing*. Prentice Hall, 727 pp.
- Tong, L., 1995: Blind sequence estimation. *IEEE Trans. Commun.*, **43**, 2986-2994.
- Torres, S., and A. Zahrai, 2002: Migration of WRS-88D signal processing functionality to open systems. Submitted to 18th IIPS, Orlando, FL., Amer. Meteor. Soc.
- Urkowitz, H., and S.L. Katz, 1996: The relation between range sampling rate, system bandwidth, and variance reduction in spectral averaging for meteorological radar. *IEEE Trans. Geosci. Remote Sens.*, **34**, 612-618.
- Van Trees, H.L., 1968: *Detection, estimation, and modulation theory*. Vol. 1. John Wiley & Sons, 697 pp.
- Walker, G.B., P.S. Ray, D.S. Zrnica, and R.J. Doviak, 1980: Time, angle, and range averaging of radar echoes from distributed targets. *J. Appl. Meteor.*, **19**, 315-323.
- Zahrai, A., and D.S. Zrnica, 1997: Implementation of polarimetric capability for the WSR-88D (NEXRAD) radar. Preprints, 13th IIPS, Longbeach, CA., Amer. Meteor. Soc., paper 9.5.
- Zurada, J.M., 1995: *Introduction to artificial neural systems*. Reprint. West Publishing Co., 683, 57, 19 pp.
- Zrnica, D.S., 1975: Simulation of weatherlike Doppler spectra and signals. *J. Appl. Meteor.*, **14**, 619-620.
- Zrnica, D.S., 1977: Spectral moment estimates from correlated pulse pairs. *IEEE Trans. Aerosp. Electron. Syst.*, **13**, 344-354.
- Zrnica, D.S., 1979: Estimation of spectral moments for weather echoes. *IEEE Trans. Geosci. Remote Sens.*, **17**, 113-128.
- Zrnica, D.S., and A.V. Ryzhkov, 1999: Polarimetry for weather surveillance radars. *Bulletin of the Amer. Meteor. Soc.*, **80**, 389-406.

Zrníc, D.S., and R.J. Doviak, 1978: Matched filter criteria and range weighting for weather radar. *IEEE Trans. Aerosp. Electron. Syst.*, **14**, 925-930.

APPENDIX A. SIMULATION OF OVERSAMPLED WEATHER RADAR SIGNALS

Computer simulations of weather echoes are necessary to study the properties and behavior of whitening-transformation-based estimators. Theoretical results can be verified using perfectly known and controlled conditions, reassessing the effectiveness of the proposed processing scheme. In this appendix, a method for the efficient generation of simulated over-sampled dual-polarization data is presented. The method is based on a combination of the procedure for generating single-polarization time series (Zmic 1975) with a procedure for generating correlated time series (Galati 1995). The simulations use known statistical properties of signals reflected by passive scatterers in fluids. Further, they take into account the known properties of the probing pulse and receiver filter to reconstruct a composite signal from the distributed scatterers illuminated by the pulse. The constructed time series pair exhibits the required autocorrelation in range, autocorrelation in time, and cross-correlation between time series for horizontal and vertical polarizations.

A.1. Autocorrelation of Samples along Range Time

Signals received by a Doppler meteorological radar at any given time are due to the superposition of the waves backscattered by the hydrometeors that are present in the radar resolution volume. The range location r_s of the resolution volume with respect to the radar depends on the time delay between the transmitted pulse and the sampling time τ_s as given by

$$r_s = \frac{c\tau_s}{2}, \quad (\text{A.1})$$

where c is the speed of light.

The simulation procedure starts with oversampling in range (along the range-time axis) so that there are L samples during the pulse duration τ . The contribution of scatterers within the resolution volume is distributed among L "slabs," where each slab encompasses a large number of hydrometeors but is represented by its equivalent "scatterer center," which backscatters the voltage $s(l)$. This is reasonable because there are numerous scatterers in the resolution volume so that their contribution causes the voltage backscattered by each slab to be a Gaussian complex random variable. Thus, each element of the sequence $s(l)$ is an independent, identically distributed (iid) complex Gaussian random variable (rv) with zero mean and unit variance. It is assumed that the slab centers are separated in range by $c\tau/2L$ and that the weather signal is sampled at a rate L times faster than the reciprocal of the pulse width, i.e., $\tau_o = \tau/L$ seconds apart. Figure A.1 shows a simplified scheme of the basic elements involved in the simulation procedure.

The case of an ideal receiver is considered first. For such receiver, the impulse response $h(n)$ is given by the unit-sample sequence, i.e., $h(n) = \delta(n)$. If range time is indexed with l , a range sample of the weather signal is given by

$$V_1(l\tau_o) = \sum_{i=0}^{L-1} s\left(\frac{lc\tau_o}{2} + \frac{ic\tau_o}{2}\right) p[(L-1-i)\tau_o], \quad (\text{A.2})$$

or simply

$$V_1(l) = \sum_{i=0}^{L-1} s(l+i)p(L-1-i), \quad (\text{A.3})$$

where s is a $2L-1$ vector of iid Gaussian random variables with zero mean and unit variance, and p is the transmitted pulse envelope.

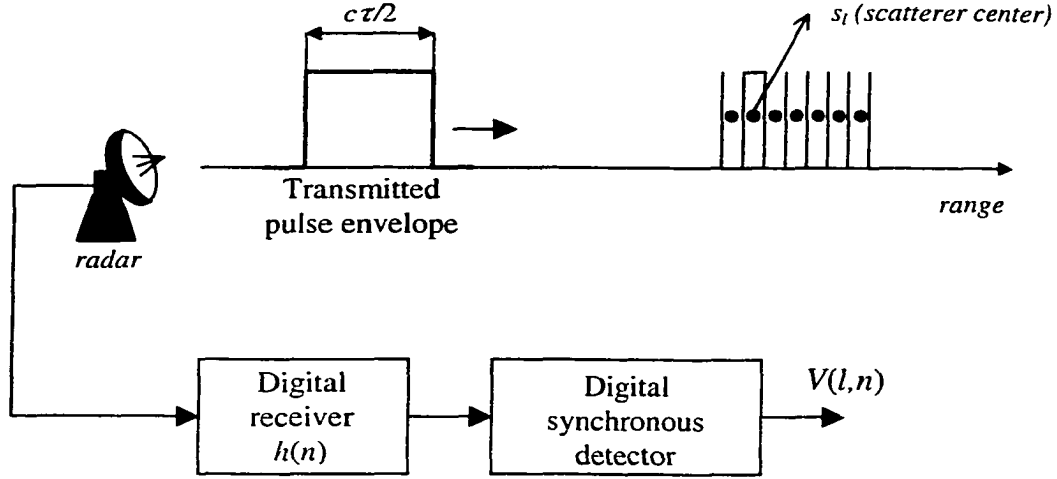


Figure A.1. Basic elements involved in the simulation of oversampled weather signals.

To verify the validity of (A.3), we can compute the correlation in range time of the set of samples $V_1(l)$ as

$$\begin{aligned} R_{V_1}^{(R)}(m\tau_o) &\equiv R_{V_1}^{(R)}(m) = E[V_1^*(l)V_1(l+m)] \\ &= \sum_{i=0}^{L-1} \sum_{j=0}^{L-1} p(L-1-i)p(L-1-j)R_s^{(R)}(m+j-i), \end{aligned} \quad (\text{A.4})$$

where the superscript (R) denotes “range time”. By the arguments presented above, the range-time correlation of $s(l)$ is given by

$$R_s^{(R)}(m) = \delta(m). \quad (\text{A.5})$$

Then,

$$R_{V_1}^{(R)}(m) = \sum_{j=0}^{L-1} p(j)p(j-m), \quad (\text{A.6})$$

which agrees with (4.39) of Doviak and Zrnic (1993). It is important to note from the previous equation that the mean power of the signal at the end of this stage is $\sum_{l=0}^{L-1} p^2(l)$.

To avoid unnecessary complications normalized powers (through a 1Ω resistor) are considered, so signals are voltages (or currents).

A non-ideal receiver channel can be modeled with the following block diagram:



Assuming that the receiver is a linear, shift-invariant system with impulse response given by h , the convolution operation can be used to obtain $V_2(l)$ as

$$V_2(l) = V_1(l) * h(l) = \left[\sum_{i=0}^{L-1} s(l+i)p(L-1-i) \right] * h(l). \quad (\text{A.7})$$

The power of this signal is now affected by the receiver's filter. The mean signal power after adding correlation in range is $G = \sum_{l=0}^{F+L-2} |(h * p)(l)|^2$, where F is the receiver's filter impulse response length. In addition, the length of the input data sequence V_1 in (A.7) need be adjusted to $L+F-1$ samples so enough convolution samples are computed in order to bypass transients and obtain a sequence V_2 with L samples.

A.2. Autocorrelation of Samples along Sample Time

For Doppler measurements the radar is pulsed at a sufficiently high rate so that the atmospheric phenomena produce correlated signal samples. Samples for every range location are taken at intervals of T_s seconds, giving origin to the “sample time”. It can be proved that the sample-time correlation of weather signals is Gaussian (Doviak and Zrnic 1993) and given by

$$\begin{aligned} R_V^{(T)}(mT_s) &\equiv R_V^{(T)}(m) = E[V^*(l, n)V(l, n+m)] \\ &= S \exp\{-8(\pi\sigma_v mT_s / \lambda)^2\} e^{-j4\pi\bar{v}mT_s / \lambda}, \end{aligned} \quad (\text{A.8})$$

where the superscript (T) denotes “sample-time”, λ is the radar wavelength, S is the weather signal mean power, \bar{v} the mean Doppler velocity of scatterers, and σ_v the associated spectrum width. Observe that V in (A.8) is a two-dimensional quantity where the first index corresponds to range time and the second one to sample time.

To assimilate the required correlation in sample time (A.8) proceed as follows. Repeat the simulation in (A.7) for M sample-time data points using independent realizations of s for each iteration. This generates a $(L+F-1)$ -by- M matrix V_3 given by

$$V_3(l, n) = \left[\sum_{i=0}^{L-1} s(l+i, n) p(L-1-i) \right] * h(l), \text{ for } 0 \leq l < L+F-1 \text{ and } 0 \leq n < M, \quad (\text{A.9})$$

where s is a $(2L+F-2)$ -by- M matrix of iid, zero-mean, unit-variance, Gaussian random variables. Transient removal can be accomplished by constructing a truncated version of V_3 as $V_4(l, n) = V_3(l+F-1, n)$, for $0 \leq l < L$ and $0 \leq n < M$. It can be observed that for a given time (fixed n) the samples $V_4(l, n)$ for $0 \leq l < L$ have a correlation given in (A.6),

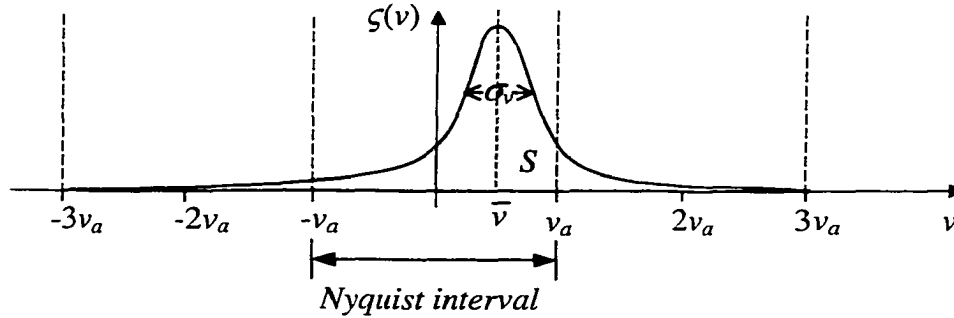
and for a given range (fixed l) they are iid complex Gaussian rv with zero mean and variance G (see previous section). Therefore, the usual coloring procedure can be applied along sample time.

Start by expressing the power spectrum (on a discrete Doppler velocity axis) of (A.8) as

$$\zeta(v_k) = \frac{S}{(2\pi)^{1/2} \sigma_v G} \exp\left[-(v_k - \bar{v})^2 / 2\sigma_v^2\right], \quad (\text{A.10})$$

$$v_k = -v_a + \frac{2kv_a}{M}, \quad k = -M, -M+1, \dots, 2M-1,$$

where v_a is the maximum unambiguous velocity. The next step is to alias this spectrum into the Nyquist interval (M samples) and then flip it to change the Doppler velocity axis to the frequency axis ($v = -\lambda f_d/2$). This “flipped” sequence will be referred to as $\zeta'(k)$, where $0 \leq k < M$.



Summarizing, the time series with sample-time correlation is obtained (for a fixed l) using discrete-time Fourier transforms (\mathcal{F}) as

$$V(l, n) = \mathcal{F}^{-1}\left\{\mathcal{F}\{V_4(l, n)\}\sqrt{\zeta'(k)}\right\}, \quad 0 \leq l \leq L-1; \quad (\text{A.11})$$

where V_4 is the truncated version of the time series with only range-time correlation, and V exhibits the required correlation in both range and sample time. Finally, note that since (A.10) is normalized, the mean power of V is S , as required.

A.3. Cross-correlation of Horizontally- and Vertically-Polarized Echoes

In the case of dual-polarized echoes two time series need be generated, V_H and V_V , each with the previous marginal structure, i.e., exhibiting correlation in both range and sample time. Simultaneously, it is required to specify the properties of the joint density through the cross-correlation coefficient ρ_{HV} . To accomplish this, we construct two independent time series (X and Y) with assigned range- and sample-time correlation following (A.9) and (A.11). Then, proceed as follows:

$$V_H(l, n) = X(l, n) \quad (\text{A.12})$$

and

$$V_V(l, n) = \alpha X(l, n) + \beta Y(l, n), \quad (\text{A.13})$$

where α and β are complex constants to be determined.

It is not difficult to verify that this transformation produces the desired result. In the case of V_H , it is obvious that the range- and sample-time correlations are the prescribed ones.

For V_V , it follows that

$$\begin{aligned} R_{V_V}^{(R)}(m) &= E[V_V^*(l, n)V_V(l + m, n)] \\ &= |\alpha|^2 R_X^{(R)}(m) + |\beta|^2 R_Y^{(R)}(m) = (|\alpha|^2 + |\beta|^2) R_V^{(R)}(m). \end{aligned} \quad (\text{A.14})$$

Therefore, to obtain the required correlation in range we must have $|\alpha|^2 + |\beta|^2 = 1$.

In a similar way,

$$\begin{aligned} R_{V_V}^{(T)}(m) &= E[V_V^*(l, n)V_V(l, n + m)] \\ &= |\alpha|^2 R_X^{(T)}(m) + |\beta|^2 R_Y^{(T)}(m) = (|\alpha|^2 + |\beta|^2) R_V^{(T)}(m) = R_V^{(T)}(m). \end{aligned} \quad (\text{A.15})$$

The cross-correlation between V_H and V_V is

$$R_{V_H V_V}^{(T)}(m) = E[V_H^*(l, n) V_V(l, n + m)] = \alpha R_V^{(T)}(m). \quad (\text{A.16})$$

In fact, Sachidananda et al. (1986) argued that $\rho_{HV}(m) = \rho_{HV}(0)\rho(m)$, where $\rho(m)$ is the correlation coefficient obtained from (A.8). Therefore, α in (A.16) is equal to $\rho_{HV}(0)$ and we can solve for $|\beta|$ to get $\sqrt{1 - |\rho_{HV}(0)|^2}$. Note that the argument (phase) of β is not constrained to any particular value. If β is chosen to have the same argument as α then

$$V_V(l, n) = \left[|\rho_{HV}(0)| X(l, n) + \sqrt{1 - |\rho_{HV}(0)|^2} Y(l, n) \right] e^{j\phi_{DP}}. \quad (\text{A.17})$$

As the last step in this stage of the simulation the differential reflectivity Z_{DR} must be incorporated to the signal pair. Z_{DR} is defined as P_H/P_V ; hence, the mean power of V_V , P_V , must be equal to P_H/Z_{DR} . Finally,

$$V_V(l, n) = \left[|\rho_{HV}(0)| X(l, n) + \sqrt{1 - |\rho_{HV}(0)|^2} Y(l, n) \right] \frac{e^{j\phi_{DP}}}{\sqrt{Z_{DR}}}. \quad (\text{A.18})$$

It is important to recall that for bivariate Gaussian processes, the auto- and cross-correlation functions (or their equivalent power spectral densities) provide a complete description of the underlying processes.

A different technique for generating dual-polarized echoes was introduced by Chandrasekar et al. (1986). This approach makes use of the structure of the covariance matrix of the spectral components of a bivariate Gaussian time series, and is intrinsically a frequency-domain method. Consequently, it is computationally more intensive than the procedure described by Galati (1995). Although both methods yield equivalent results, it

turns out that Chandrasekar's approach is more general because it can simulate bivariate Gaussian random processes with arbitrary auto- and cross-correlation functions. On the other hand, the method described by (A.12) and (A.13) requires that the two random processes exhibit the same autocorrelation and that the cross-correlation be proportional to the autocorrelation. In other words, the method works well only if $R_{V_v}^{(T)} = R_{V_H}^{(T)} = \kappa R_{V_H V_v}^{(T)}$, which is true for this case (Sachidananda et al. 1986).

A.4. Additive Noise

Under realistic conditions, the sky environment and the receiver always introduces some amount of additive noise to the weather signals of (A.12) and (A.18). It is customary to assume that this noise is white (at least when compared to the signal bandwidth) and Gaussian with zero mean and power (variance) N . To add noise to the weather signals two independent time series of iid complex Gaussian rv (N_H and N_V) are generated and added to $V_H(l, n)$ and $V_V(l, n)$, respectively. That is

$$V_H(l, n) = X(l, n) + N_H(l, n) \quad (\text{A.19})$$

and

$$V_V(l, n) = \left[|\rho_{HV}(0)| X(l, n) + \sqrt{1 - |\rho_{HV}(0)|^2} Y(l, n) \right] \frac{e^{j\phi_{DP}}}{\sqrt{Z_{DR}}} + N_V(l, n). \quad (\text{A.20})$$

A.5. Reflectivity Gradients

It was implicitly assumed in Section A.1 that the scatterers in the resolution volume were uniformly distributed along the pulse depth. This assumption, which holds true for

relatively narrow pulses, led to the construction of $s(l,n)$ as a sequence of iid rv. Reflectivity gradients are given by a non-uniform distribution of hydrometeors among the slabs within the pulse. To simulate this effect, the $s(l,n)$ sequence is multiplied with an arbitrary “gradient” function $g(l,n)$, which can be a time-varying function.

A.6. Simulation Procedure

The complete simulation procedure is summarized as follows:

- Input parameters
 - M : number of samples along sample-time (number of pulses)
 - L : number of samples along range-time (oversampling factor)
 - F : length of receiver filter’s impulse response
 - $g(l,n)$: (time-varying) reflectivity gradient
 - $p(l)$: transmitter pulse shape
 - $h(l)$: receiver channel impulse response
 - S : signal mean power
 - N : noise mean power
 - \bar{v} : Doppler mean velocity
 - σ_v : Doppler spectrum width
 - λ : transmitter wavelength
 - v_a : maximum unambiguous velocity

for dual-polarized echoes:

- $|\rho_{HV}(0)|$: magnitude of the cross-correlation coefficient for lag zero
- ϕ_{DP} : differential phase
- Z_{DR} : differential reflectivity

- Procedure

$$\circ \quad \bar{V}_q(l, n) = \left[\sum_{i=0}^{L-1} s_q(l+i, n) g(i, n) p(L-1-i) \right] * h(l),$$

where

$s_q(l, n)$ is a $(2L+F-2) \times M$ matrix of complex iid Gaussian random variables with zero mean and unit variance

$$q = \begin{cases} 1 & \text{for single polarization} \\ 1, 2 & \text{for dual polarization} \end{cases}$$

$$l = 0, 1, \dots, L+F-2; \quad n = 0, 1, \dots, M-1$$

$$\circ \quad V_q(l, n) = \bar{V}_q(l+F-1, n)$$

$$l = 0, \dots, L-1; \quad n = 0, \dots, M-1$$

$$\circ \quad v(k) = -v_a + 2(k+1)v_a/M, \quad k = -M, \dots, 2M-1$$

$$S_{unf}(k) = \exp[-(v(k) - \bar{v})^2 / 2\sigma_v^2]$$

fold, flip, and normalize to obtain $S_f(k)$

$$S'(k) = \sqrt{\frac{S}{G}} S_f(k), \quad 0 \leq k \leq M-1$$

$$\text{where } G = \sum_{l=0}^{F+L-2} |(h * p)(l)|^2$$

$$\circ \quad X_q(l, n) = \mathcal{F}^{-1} \left\{ \mathcal{F} \{ V_q(n, l) \} S'(k) \right\}, \quad 0 \leq l \leq L-1$$

$$q = \begin{cases} 1 & \text{for single polarization} \\ 1, 2 & \text{for dual polarization} \end{cases}$$

$$\circ \quad Y_1(l, n) = X_1(l, n)$$

for dual polarization:

$$Y_2(l, n) = \left[|\rho_{HV}(0)| X_1(l, n) + \sqrt{1 - |\rho_{HV}(0)|^2} X_2(l, n) \right] \frac{e^{j\phi_{br}}}{\sqrt{Z_{DR}}}$$

- for single polarization: $V(l, n) = Y_1(l, n) + \eta_1(l, n)$
- for dual polarization: $V_H(l, n) = Y_1(l, n) + \eta_1(l, n)$
 $V_V(l, n) = Y_2(l, n) + \eta_2(l, n)$

where $\eta_q(l, n)$ are matrices of complex iid Gaussian random variables with zero mean and variance N

$$q = \begin{cases} 1 & \text{for single polarization} \\ 1, 2 & \text{for dual polarization} \end{cases}$$

- Outputs
 - For single polarization: V
 - For dual polarization: V_H and V_V

Note: rows correspond to range times and columns to sample times.

A.7. Simulation Results

To illustrate the performance of the procedure described in Section A.6 a dual-polarized, oversampled, weather echo was simulated with the following set of parameters: $M = 256$, $L = 10$, $g(l) = 1$, $p(l) = 1$, $h(l) = \delta(l)$, $S = 10$ dBm, $N = -10$ dBm, $v = 5$ m s⁻¹, $\sigma_v = 2$ m s⁻¹, $v_a = 32$ m s⁻¹, $\lambda = 10$ cm, $|\rho_{HV}(0)| = 0.99$, $\phi_{DP} = 30$ deg, and $Z_{DR} = 5$ dB. The results are shown in Figure A.2 and Figure A.3.

By observing Figure A.2 and A.3 it is evident that the simulated signals exhibit the same range-time correlation, mean Doppler velocity, spectrum width, SNR, and cross-correlation as specified. More precisely, it was verified that by applying spectral moment and polarimetric variable estimation algorithms, the original set of parameters was retrieved within the expected estimation errors.

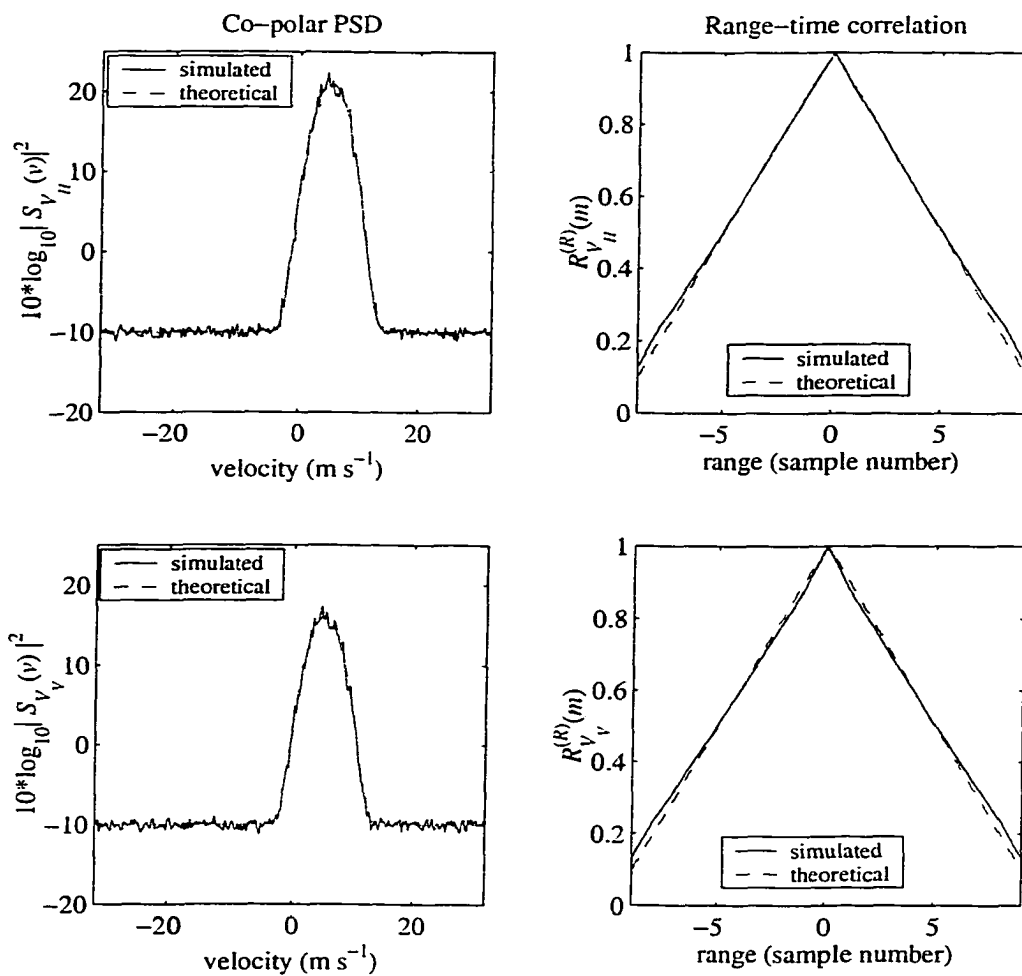


Figure A.2. Dual-polarized weather signal simulation. (Left column) Theoretical and simulated sample-time power spectral density (PSD) for both channels. (Right column) Theoretical and simulated range-time autocorrelation for both channels.

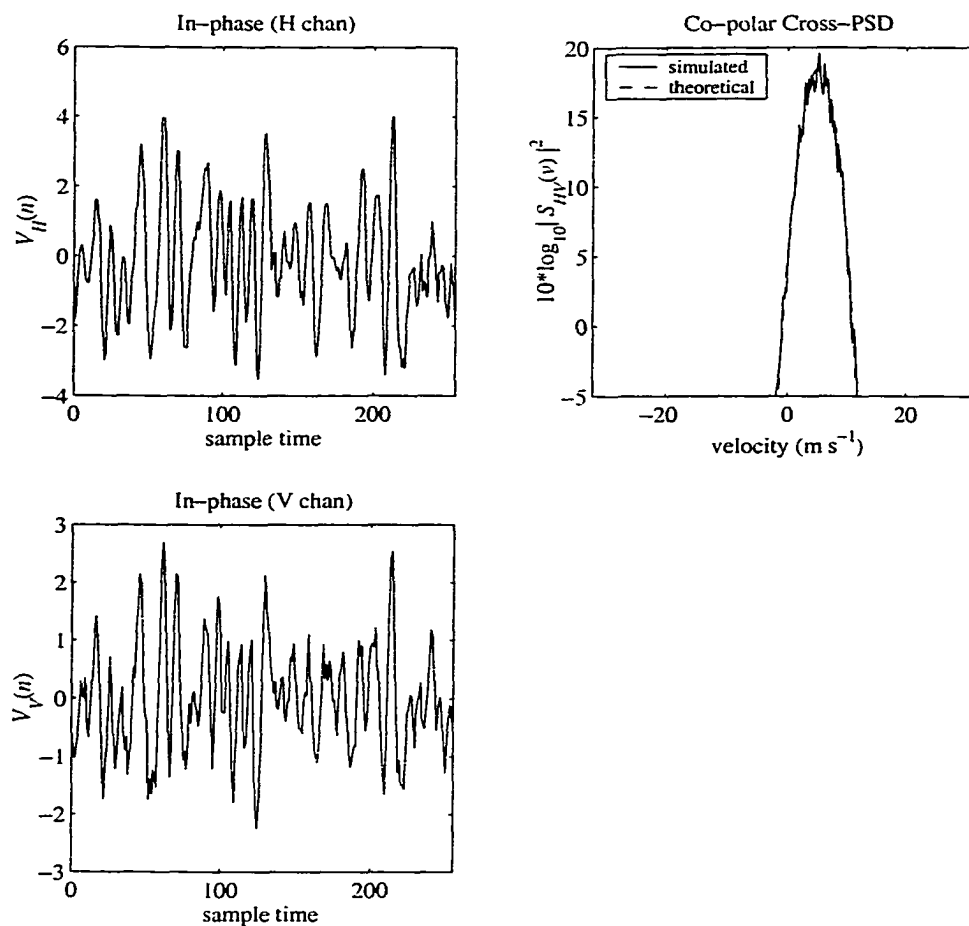


Figure A.3. Dual-polarized weather signal simulation. (Left column) Time-series on a sample-time axis for both channels. (Right column) Theoretical and simulated cross-power spectral density (PSD).